Department of Industrial Engineering
University of Stellenbosch

Additive Manufacturing Enabled Drug Delivery Features for Titanium-Based Total Hip Replacement Cementless Femoral Stems

Martin Botha Bezuidenhout

Thesis presented in partial fulfilment of the requirements for the degree MEng(Research) in Industrial Engineering at the University of Stellenbosch

Supervisor: Prof D.M. Dimitrov

Co-supervisor: Prof L.M.T. Dicks

Co-supervisor Prof A.F. van der Merwe

March 2015

Declaration

By submitting this thesis (electronically), I, Martin Botha Bezuidenhout, declare that the entirety of the work contained therein is my own, original work, that I am the sole author thereof (save to the extent explicitly otherwise stated), that reproduction and publication thereof by Stellenbosch University will not infringe any third party rights and that I have not previously in its entirety or in part submitted it for obtaining any qualification.

Date: February 2015

Abstract

Bacterial colonisation and biofilm formation onto total hip replacement femoral stems remain a serious complication detrimental to the success of total hip arthroplasty. Current treatment procedures are accompanied by a heavy financial burden and morbidity for the patient while failing to guarantee a successful outcome with no reinfection. In fact, infection rates after revision surgeries are typically higher than those for primary hip arthroplasties.

This study investigates conceptual drug delivery channels to be incorporated within cementless femoral stems by applying additive manufacturing as enabler technology. Drug delivery from these features is aimed at both prophylaxis and treatment of infection, with the latter emphasising the concept of creating a reinforceable antimicrobial depot inside the implant. The novelty lies in facilitating the administration of multiple drug dosages from within the implant instead of the once-off implant-based release strategies currently employed.

Samples containing internal channels were designed based on analogies to drug delivery studies reporting on the commercial antibiotic loaded bone cement, Palacos R+G loaded with gentamicin. These samples were manufactured by LaserCUSING® from Ti-6Al-4V ELI powder. For prophylactic proof of concept, testing the channels were filled with Palacos R+G and challenged with two clinical isolates of *Staphylococcus aureus* in a bacterial growth inhibition study. Gentamicin-susceptible *S.aureus* Xen 36 was prevented from colonising for a minimum of 72 hours, whereas gentamicin resistant *S.aureus* Xen 31 reached the material within 24 h, signifying the importance of drug selection according to pathogen. Hence, a solution of vancomycin in phosphate buffered saline pH 7.4 was used during *in vitro* reservoir release testing. Three dosage injections were made into each of six samples during a cumulative incubation period of 100 h. A biocompatible 5,000 Da molecular weight cut off polyethersulfone nanoporous membrane was employed as release rate-controlling device. Released vancomycin was quantified with reversed phase high performance liquid chromatography. The resulting release profile was characterised by means of the Korsmeyer-and-Peppas model for diffusion based drug delivery. Constraint diffusion was identified as the mechanism controlling release, implying interplay between Fickian diffusion and polymer relaxation for effecting vancomycin release from within the reservoir.

The concept created in this study provides a basis towards the development of full scale intelligent implants with multiple dose *in situ* drug delivery capabilities. Implants incorporating this concept could aid in the perpetual struggle against infection by providing a new strategy for delivery of high level antibiotics directly to the site of infection.

Opsomming

Kolonisering van bakterieë en die vorming van biofilms op totale heupvervanging femorale stamme bly ŉ ernstige komplikasie tot die sukses van ŉ totale heupvervanging. Huidige behandelingsprosedures gaan gepaard met ŉ swaar finansiële las en infeksies vir die pasiënt sonder versekering van ŉ suksesvolle uitkoms. Die voorkoms van infeksie is tipies hoër vir revisie prosedures as vir primêre heupvervangings.

Hierdie studie ondersoek konseptuele dwelmvoorsieningskanale wat in sementvrye femorale stamme geïnkorporeer kan word deur middel van toevoegingsvervaardiging as bemagtigingstegnologie. Dwelmtoediening deur hierdie strukture is gemik op beide voorkoming en behandeling van infeksie met ŉ klem op die konsep van ŉ herlaaibare antimikrobiese depot in die implantaat. Die nuwigheid lê in die fasilitasie van toediening van veelvuldige dwelm dosisse vanaf binne die implantaat in plaas van die huidige eenmalige implantaatgebaseerde toedieningstrategieë.

Die ontwerp van monsters wat interne kanale bevat is baseer op vergelykings met literatuur op kommersiële beensement, Palacos R+G, wat met gentamisien belaai is. Hierdie monsters is vervaardig met LaserCUSING® van Ti-6Al-4V ELI poeier. Kanale is gevul met Palacos R+G en uitgedaag met twee kliniese isolate van *Staphylococcus aureus* in ŉ bakteriële groei inhibisie studie. Gentamisien-sensitiewe *S.aureus* Xen 36 is verhoed tot kolonisasie vir ŉ minimum van 72 uur, terwyl gentamisien-weerstandige *S.aureus* Xen 31 die materiaal binne 24 uur bereik het. Vervolgens was ‘n oplossing van vankomisien in fosfaatbuffer soutoplossing pH 7.4 gebruik tydens *in vitro* vrystellingstoetse. Drie dosisse inspuitings is in elk van ses monsters oor ŉ inkubasietydperk van 100 uur toegedien. ŉ Biokompatibiele 5,000 Da molekulêre massa afsnypunt polietersulfoon nanoporeuse membraan is as vrystellingskoers regulerende apparaat gebruik. Vrygestelde vankomisien is gekwantifiseer met omgekeerde fase hoë verrigting vloeistof-chromatografie. Die vrystellingsprofiel is gekarakteriseer met die Korsmeyer-en-Peppas model vir diffusie gebaseerde dwelmtoediening. Beperkte diffusie is geïdentifiseer as die meganisme wat vrystelling beheer. Dit impliseer ŉ tussenspel in Fickiaanse diffusie en polimeer verslapping vir die tot stand bring van vankomisien vrystelling vanaf binne die reservoir.

Hierdie konsep van die studie verskaf ŉ basis vir die ontwikkeling van volskaalse intelligente implantate met ŉ veelvuldige *in situ* dwelmtoedienings vermoë. Implantate met hierdie konseptuele strukture kan steun gee aan die voortdurende stryd teen infeksie deur ŉ nuwe strategie daar te stel vir die toediening van hoë vlak antibiotika direk by die infeksie area.

Acknowledgements

I would sincerely acknowledge the following people and institutions and express my gratitude towards the essential impacts and contributions they made during the project:

Professor D.M. Dimitrov for supervising the study with an active interest in the progress and results of the experiments, for having patience during times of literature study, and for taking time to provide thorough guidance and insightful inputs.

Professor L.M.T. Dicks for valuable inputs and insights, the enthusiasm towards collaboration, and for the availability of his laboratory for microbiological testing procedures.

Professor A.F. van der Merwe for acting as co-supervisor and insightful input during the planning phase of the reservoir release study.

Du Preez van Staden for all his time and effort in the preparation of the Modifed Kirby-Bauer experiments, use of laboratory space, assistance and operating of the HPLC unit, and providing very insightful inputs from a microbiologist's perspective.

Johan Du Plessis for his contribution and work during his Bachelor's thesis.

Dr N. de Beer for initially acting as co-supervisor and liaison between the currently involved parties.

Samantha Buitendag at Heraeus South Africa (Pty) Ltd for sponsoring Palacos R+G gentamicin loaded bone cement.

Philip Hugo and Xola Madyibi at the Institute for Advanced Tooling (IAT) for insightful inputs during the concept development phase and for operating the LaserCUSING machine during the manufacturing phase.

The Technology and Human Resources for Industry Programme (THRIP) for funding the research.

To my parents, Johan and Louise, and partner, Elizabeth Swartz for their continuous motivation, support and patience throughout the study.

Table of Contents

List of Figures

List of Tables

List of Abbreviations

3DP	Three Dimensional Printing
ALBC	Antibiotic Loaded Bone Cement
AM	Additive Manufacturing
BHI	Brain-Heart Infusion
CT	Computed Tomography
DMLS	Direct Metal Laser Sintering
DNA	Deoxyribonucleic Acid
EBM	Electron Beam Melting
FDA	United States Food and Drug Administration
MIC	Minimum Inhibitory Concentration
MRSA	Methicillin Resistant Staphylococcus Aureus
MWCO	Molecular Weight Cut-off
NIH	National Institutes of Health
OA	Osteoarthritis
OECD	Organisation for Economic Cooperation and Development
PBS	Phosphate Buffered Saline
PES	Polyethersulfone
PJI	Prosthetic Joint Infection
PMMA	Poly(methyl methacrylate)
mRNA	Messenger Ribonucleic Acid
RP-HPLC	Reversed Phase High Performance Liquid Chromatography
SLA	Stereolithography
SLM	Selective Laser Melting
SLS	Selective Laser Sintering
STL	Standard Triangulation Language
THA	Total Hip Arthroplasty
THR	Total Hip Replacement
TKA	Total Knee Arthroplasty
USP	United States Pharmacopoeia
ZOI	Zone of Inhibition

Glossary

Aseptic	The absence of infectious microorganisms
Biocompatibility	Ability to not evoke an immune response when placed inside the human body
Biofilm	An extracellular matrix encapsulating bacterial communities
Biomaterial	Material that does not evoke an immune response
Chromophores	Structures within a molecule which absorb light
Chronic infection	Long term persisting infection
Colonisation	Bacterial adhesion in large numbers onto a surface
Comorbidity	Secondary diseases or disorders to a primary disease
Culturing	Process during which bacteria from an infectious wound is identified
Cutaneous	Pertaining to the skin
Cytotoxicity	Level of toxicity towards living cells
Debridement	Removal of all infected and dead tissue
Drug-carrier	Substance into which a drug is loaded for release
Exogenous	From outside of the body
Extracellular matrix	A protective structure consisting of biopolymers such as proteins, DNA, and polysaccharides
Femoral stem	The part of a total hip replacement system that is implanted into the femur
Glycosidic bond	Bond between a carbohydrate and another group
Gram-positive bacteria	Bacteria that retains the crystal violet of a Gram-stain due to the presence of a thick multilayered peptidoglycan
Gram-negative bacteria	Bacteria that do not retain the Gram-stain due to the presence of an outer lipopolysaccharide membrane

Hematogenous	Present in the bloodstream
Hydrophilic	Affinity for water
Hydrophobic	Aversion for water
In situ	In the actual place of origin
In vitro	Outside of a living organism
In vivo	Inside a living organism
Intraosseous	Inside the bone
Isotopic cluster	Cluster of similarly charged molecules on a mass spectrum consisting of different isotopic arrangements of its constituent elements
Minimum inhibitory concentration	Concentration of antimicrobial below which a bacterium can survive
Mobile phase	Transportation medium of samples in liquid chromatography
Monoisotopic mass	Mass of a molecule consisting only of its most abundant elemental isotopes
Osseointegration	Direct bond between the biomaterial surface and host bone
Osteoarthritis	Gradual degradation of the articular cartilage
Osteoinductive	Enhancing the bone growth process
Palacos R+G	Commercial antibiotic loaded bone cement used in this project
Pathogen	Disease causing microorganism
Pathogenesis	The mechanisms by which a disease develops
Peptidoglycan	A structural part of the bacterial cell wall
Phenotype	Specific characteristics of a microorganism due to the interaction of its genetic constitution with its surrounding environment
Phosphate buffered saline	A saline buffer often employed in microbiological research
Planktonic	Floating unattached in the blood or body fluid

Poly(methyl methacrylate)	Polymer used as bone cement for cemented fixation of femoral stems
Primary stability	Stability of the femoral stem and the measure of micro-motions after implantation
Prophylaxis	Preventative measures against infection
Quorum sensing	Process that regulates gene expression and cell to cell communication amongst bacteria
Resection	Removal of bone, tissue or organs during surgery
Retention	To keep the implant in place during treatment
Stationary phase	Separation medium of compounds in liquid chromatography
Virulence	Measure of the ability to cause disease
Zone of inhibition	Area in a disc diffusion test in which all bacteria are killed

1. Introduction

1.1 Background

The human hip, a synovial ball-and-socket joint, functions as the human body's primary connection between the lower limbs and the trunk [1]. Consequently, the hip joint is constantly subjected to heavy loadings, supporting almost two thirds of the body weight during static conditions [2]. Furthermore, the hip joint is also responsible for facilitating everyday mobility such as walking, running and stair climbing, during which the hip has to sustain dynamic forces up to nearly five times that of the person's body weight [2, 3]. A frequent ailment of the hip joint is the gradual degradation of the articular cartilage, which is symptomatic of osteoarthritis (OA) [2]. OA is the most frequent diagnosis for patients to undergo total hip replacement [4-7]. Although different theories exist, the exact etiology of OA is still under dispute [2, 8].

A reconstructive surgical procedure termed total hip arthroplasty (THA) or total hip replacement (THR) is typically performed to replace a problematic hip joint that does not respond to normal medical treatment, with a prosthetic substitute [9]. It is regarded as the most effective procedure for relieving the pain, disability and frustration attributed to OA [10]. Not only does this result in an enhanced quality of living for patients but can also reduce the psychological burden accompanying pain and disability. Furthermore, the number of annual THA surgeries performed is on the increase [10-12]. With an average functional lifetime of 10 – 15 years for hip replacement implants, emphasis can be placed on the need for the enhancement on certain properties in order to increase implant longevity, especially in younger patients, and reduce the risk of implant failure [13].

The two most prevalent failure modes of hip replacement implants, not presented in any specific order, is the occurrence of aseptic loosening due to an increase in micromotions between the implant and bone interface in cementless fixation and the bone cement mantle and bone interface in cemented fixation [14]. It is argued that micromotions and consequently aseptic loosening, is attributed to an inadequate primary mechanical stability of the fit that the surgeon could achieve during surgery, and the stress shielding phenomenon at a later time after surgery [15-17].

A second, very serious obstacle, which is at the core of this study, is the prevalence of implant infection. Implant infection currently poses one of the greatest challenges in orthopaedic surgery [18-20]. It occurs in both cementless (implant surface is in direct contact with bone), and cemented (implant is embedded in bone cement which forms a mantle between the implant and the bone) femoral stems [21, 22]. The infection rate for primary hip replacement surgeries is generally acctepted to be around 1% and infection rates for revision surgeries can be significantly higher [18, 19, 23]. This seemingly low percentage of primary THA infection is, however, significant because of the high (1,832,931 hip replacements in the Organisation for Ecomnomic Co-operation anf Development (OECD) countries alone for 2009) and increasing amount of THA procedures performed annually [10]. Furthermore, an increase in revision suregeries due to infection is also reported [12, 24].

Immediately following a THR surgery, a process dubbed “race to the surface” initiates, during which a race exist between tissue integration and the adhesion of bacterial cultures onto the implant to create a biofilm [25]. A biofilm is a specialized extracellular matrix which envelops the bacterial strain and is resistant to the human immune system as well as antibiotics [26-28]. Thus, one of the most probable ways of currently removing a biofilm based infection is through surgical procedures and removal of the implant [29-32].

Even though various surgical interventions and protocols exist for the treatment of infected THR femoral stems, an optimal treatment strategy still remains an area of debate [33-35]. Giulieri *et al.* [36] proposed an algorithm as a guideline for deciding upon surgical and antibiotic procedures in the treatment of infected hip replacements. The main surgical procedures for treatment of infection usually are either debridement with retention, one-stage or two-stage exchange arthroplasty [36]. The choice between which depends on factors such as the type of infection, time after surgery, damage to tissue and bone, condition of the implant, and miscellaneous factors which are situation specific [36]. Due to the nature of biofilm infection, whichever treatment procedure the surgeon in question chooses to follow cannot completely guarantee that there will be no re-infection [30, 35]. In some cases of serious and persistent deep infection, amputation might even be required to eradicate the infecting organism [37]. Even cases of mortality have been reported as a consequence of deep and chronic infection [38]. It is therefore argued that infection prevention is an extremely important strategy in ensuring implant success.

1.2 Problem Statement

Amongst possible THR complications, prosthetic joint infection (PJI) is one of the most difficult and serious conditions to diagnose and manage [36, 39]. One strategy to prevent bacterial colonisation is the prophylactic utilisation of antibiotic-loaded bone cement (ALBC). Drugs elute from the ALBC into the surrounding environment with the aim to kill surrounding pathogenic bacteria to prevent colonisation onto the biomaterial [40]. It is already a well-established and accepted practice in the case of cemented arthroplasties; however, it has been reported that typically less than 10% of the total loaded amount of antibiotic in the cement is effectively released during the first week [41]. Therefore debates exist about the dangers of this strategy to elute antibiotics at sub inhibitory concentrations that can cause bacteria to mutate and become resistant [40]. An appealing aspect of ALBC is that a range of clinically approved and commercially available products already exist.

Recent research has shown the possibilities of customising cementless implant surfaces with alternative coatings containing nanotechnology [42]. The problem is however, that due to the limitations of the current manufacturing processes for cementless hip implants, the focus remained on coatings on the exterior of the implant. This results in a once-off type of release without the possibility of administering more doses or drugs different from the ones originally used for surface coating.

A type of hybrid femoral stem which ensures cementless fixation and is functionally customised for amtimicrobial elution from within the biomaterial in order to aid in the prevention of bacterial colonisation, could thus be useful in supporting the ongoing struggle against infection in the femoral canal. Conventional manufacturing processes of hip replacement prostheses, however, do not allow for the intricate geometries and features that would accompany such customisation. In fact, THR femoral stems are largely manufactured from wrought material by subtractive processes. Custom designing and manufacturing for specific cases with short lead times is not yet readily applied in clinical practice [43].

A novel idea has been presented by Mueller *et al.* [44] to utilise additive manufacturing (AM) technologies in order to manufacture a femoral stem with internal channels, which can be used for a number of applications. Figure 1.1 shows an adapted and recreated abstraction of the concept model manufactured at the Fraunhofer Institute for Machine Tools and Forming Technology (IWU) and is used here as an example to illustrate the concepts of Mueller *et al.* [44]. With the emergence of generative processes such as selective laser melting (SLM) and electron beam melting (EBM), complex geometries as presented in Figure 1.1 can be produced in THR femoral stems [44].

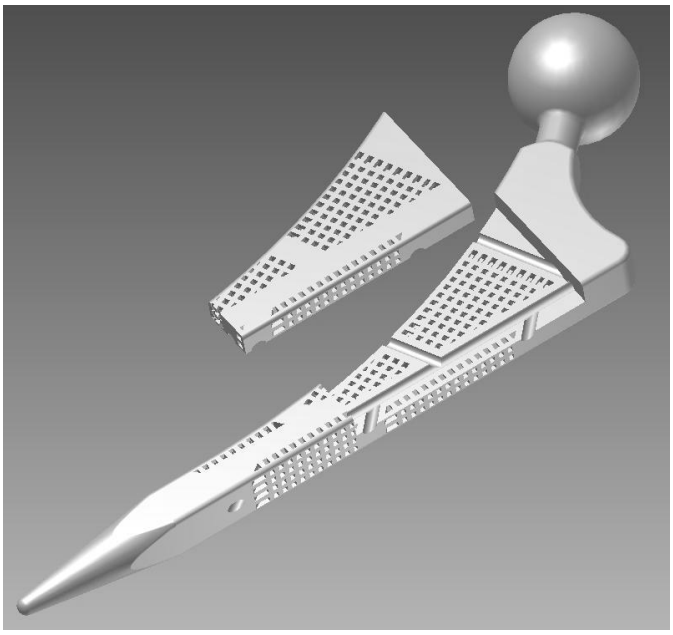

Figure 1.1: Total hip replacement femoral stem with internal channels (adapted from [44])

An important aspect to notice is that these developments are as of yet mostly conceptual and prototypes. Although EBM acetabular cups have been granted regulatory clearance [45], heavy load bearing prostheses, for example, femoral hip stems, manufactured by AM technologies seem to lack evidence of being officially approved for clinical use through regulatory boards such as the United States Food and Drug Administration (FDA) [46]. Extensive testing and clinical trials are required in order to first prove the feasibility and the efficacy of these concepts [47, 48]. It is therefore necessary to investigate these aspects.

In this study, the validity of the concept of bacterial colonisation prevention by having an antimicrobial drug delivery substance embedded within the biomaterial is investigated. Also investigated is the possibility of local drug delivery from within reservoir samples for multiple doses of an antibiotic typically used in the treatment of infection.

The successful incorporation of such strategies in the future can potentially not only prove to have personal benefits for patients and medical staff, but also economical benefits for medical aid companies. In the case of chronic infection, the complex two-stage procedure, which involves the interim implantation and removal of a temporary spacer, could possibly be substituted with a procedure in which an antimicrobial infiltrated, fully functional implant is inserted after debridement as a one-stage replacement. Eventually, this could potentially reduce hospitalisation and operating theatre occupation time for many cases of chronic infection, leading to a reduction in cost for both the patient and medical aid companies.

In summary, the problem statement is that bacterial colonisation onto the femoral stem and subsequent biofilm formation is a serious complication in orthopaedic surgery. Strategies for cementless stems to deliver multiple doses of antibiotics for either prophylaxis or treatment locally to the site of infection do not yet exist. Although concepts to address this situation by utilising AM for fabrication of internal channels from which antibiotics can be delivered have been presented, they still need to be evaluated with regard to the actual enabling of local drug delivery of antibiotics from within a femoral stem.

1.3 Research Question and Objectives

The overall objective of this study is to contribute to the field of infection prevention and treatment strategies for cementless femoral stems. This is to be achieved by investigating the prevention of bacterial colonisation onto and local drug release through AM titanium alloy samples containing conceptual drug delivery features that can be incorporated into cementless femoral stems. Therefore, the research question is presented as:

Can bacterial colonisation prevention onto, and controlled local drug release of multiple doses through Ti-6Al-4V ELI samples be achieved by embedding a drug delivery substance within samples containing conceptual drug delivery features manufactured by Selective Laser Melting?

Subsequent issues to support the investigation of the main research question are summarised as follows:

- What is the pathogenesis and mechanisms of chronic PJI?
- What type of drugs and carriers are already clinically accepted and can be used to ensure clinical feasibility with regard to the antimicrobial products used?
- What analogies can be made with drug elution studies to identify possible geometries for the features in which to embed the drug in order to effectively test the concept?
- Can the concept of embedding antimicrobial drugs for the prevention of bacterial colonisation be expanded from prophylactic use to treatment of an already established infection?
- Where does the strategy currently fit into the field of infection prevention and treatment?

The following objectives have been identified and need to be achieved in order to answer the main research question:

- Establishment of suitable conceptual drug delivery features based on literature
- Additive manufacturing of samples with conceptual features for drug delivery on a suitable SLM machine
- *In vitro* evaluation of prophylactic activity against susceptible *S.aureus*
- *In vitro* evaluation of reinforcing reservoir controlled local drug delivery through passive diffusion across a commercial membrane.

1.4 Research Approach

A comprehensive literature review will be performed to elucidate the relevant themes from different interacting scientific disciplines that combine to form the background for the experimental phase of the project. The experimental phase is divided into three stages. Stage 1 is the establishment of sample geometries followed by the utilisation of SLM for additive manufacturing of reservoir samples. Stage 2 is the evaluation of the strategy towards prophylaxis and Stage 3 is the evaluation of reservoir drug release from within the samples for an antibiotic typically to be used in treatment of gram-positive bacterial infection scenarios.

A computer aided design (CAD) concept model is to be developed in order to convey the message visually to any interested parties. Since such implants do not yet exist, the concept will mainly focus on analogies to ALBC cement release studies in literature. The zone of inhibition (ZOI) is the area in a two dimensional plane where no bacteria can survive due to the concentration of antimicrobial drug eluted from the drug carrier [49]. It is also important to note that the concept model will serve as a visual aid in conveying the ideas and the strategy of preventing colonisation from within the implant. It is not claimed to be an optimised or commercially feasible design, but is meant to serve as a foundation for evaluating this novel drug delivery possibilities from within cementless hip stems, enabled by AM technologies. However, once the concept is proven as an effective strategy, subsequent research projects can follow in order to optimise various aspects such as, but not limited to, design geometries, drug carrier and drug combination, as well as diagnostic procedures and process chain optimisation towards achieving a high value, quick to market transition to patient- or diagnose-specific THR femoral stems.

Once a concept model with analogy to relevant literature has been developed, a sample of the feature can be isolated in order to test the concept. These samples are then to be manufactured by SLM using default machine process parameters stored in the machine control software. The build orientation of the part is also important, since the channels should be free of supports, placement should be at angles not exceeding the geometric process capabilities of the machine.

Stage 2 will initiate with the identification and procurement of an appropriate drug-carrier combination to use in prophylactic testing. To incorporate clinically relevant materials, an applicable commercially available ALBC is to be incorporated. With collaboration from the Microbiology Department, the prophylactic efficacy is to be evaluated. This will be done through

a modified Kirby-Bauer test procedure. For this experiment, two clinical isolates of *Staphylococcus aureus* (*S.aureus*), one methicillin sensitive (Xen 36), and one methicillin resistant *S.aureus* (MRSA) (Xen 31), will be used. It is expected to see very little activity against the resistant strain from the commercial ALBC bone cement.

Stage 3 entails the evaluation of the application towards the local release of a reinforcement antibiotic, a vancomycin saline solution, from within the reservoirs inside the samples. The means of release will be passive diffusion across a commercial nanoporous membrane with appropriate material and pore characteristics. Samples will be filled with the vancomycin solution and placed within a phosphate buffered saline (PBS) buffer. At specific time intervals aliquots will be taken and the concentration of vancomycin in the buffer quantified.

The concentration of vancomycin will be quantified using reversed phase high performance liquid chromatography (RP-HPLC), a widely used separation technique for the analysis of a variety of solutions and mixtures, especially pharmaceuticals. A release curve will then be constructed to describe the elution of the antibiotic from within the reservoir sample. The efficacy of the antibiotic release depends on the ability of the mechanism to maintain concentrations of antibiotic released sufficiently above the minimum inhibitory concentrations (MICs) for pathogens the antibiotic is directed against.

Together the three stages endeavour to evaluate a foundation for the release of drugs for infection prevention and treatment from within conceptual features aimed at cementless femoral hip stems enabled by AM technologies, SLM in particular.

1.5 Limitations and Exclusions

This study focuses on the femoral stem part of a complete THR system and excludes the acetabular cup, because emphasis is placed on infection which develops postoperatively in the femoral canal. Another reason for the exclusion of the acetabular component is that the objective is to test whether a strategy of embedding or loading an antibiotic inside the stem can prevent bacterial colonisation on the implant surface.

For manufacturing of the samples, SLM in the proprietary form of LaserCUSING® by means of a M2 cusing system from Concept Laser will be utilised. Other AM technologies such as EBM are

also recognised and reviewed in section 2.3. LaserCUSING®, however, can produce parts with remarkable geometrical accuracy and enables the fabrication of a wide range of complex geometries with near full density. Heart stents with strut dimensions as thin as 300 μm have previously been manufactured for demonstration purposes in house at the Rapid Product Development Laboratory (RPD), showcasing the capabilities of the machine.

The material to use in the study is Ti-6Al-4V ELI (Grade 23) (medical grade) powder from Concept Laser. Certain concerns about this alloy with regards to Aluminium attributing to diseases such as Alzheimer's and cytotoxicity from possible excessive Vanadium-ion release has been raised in literature [50, 51]. There are however, diamond-like carbon (DLC) films that have been developed to prevent the release of ions from alloys used in biomedical applications [52]. Thus, for the purpose of *in vitro* testing, the biomaterial Ti-6Al-4V ELI was deemed feasible.

For purposes of proof of concept *in vitro* antimicrobial testing, it is important to utilise clinically approved products to reduce the amount of ambiguity with regard to clinical relevance. Therefore, a commercial PMMA ALBC, Palacos R+G (sponsored by Heraeus Medical), loaded with gentamicin, is to be used. Similarly, an appropriate solution of the antibiotic vancomycin in, used in treating MRSA infections, in phosphate buffered saline (PBS) will be used for reservoir release testing. The membrane to use for release testing were identified and procured through another in house study. It is a 5000 Da molecular weight cut off (MWCO) non-biodegradable polyethersulfone (PES) ultrafiltration flat sheet membrane.

The Bacterial strains for investigation were selected for both its clinical relevance and its ability to quickly colonise biomaterials to form biofilms [53, 54]. Although a variety of bacteria species can be found growing together in a biofilm, the use of two clinical isolate *S.aureus* strains will already reveal the efficacy of such colonisation prevention and future treatment strategies.

The antimicrobial experiments will be performed under *in vitro* conditions at the Department of Microbiology at Stellenbosch University.

2. Integrated Approach to Total Hip Replacement, Infection Prevention and Additive Manufacturing – An Overview

This chapter presents the literature reviewed in order to gain an understanding of the various disciplines which each form an integral part in the investigations of the study. A holistic view of the issues surrounding the problem situation is sketched. In order to achieve this, the sections have been arranged sequentially to incorporate and elaborate on the different significant processes that combine to each form part of the problem statement. Figure 2.1 graphically presents the layout of the chapter. According to the scope of the study, limits and exclusions with regard to the extent of the review are stated where necessary.

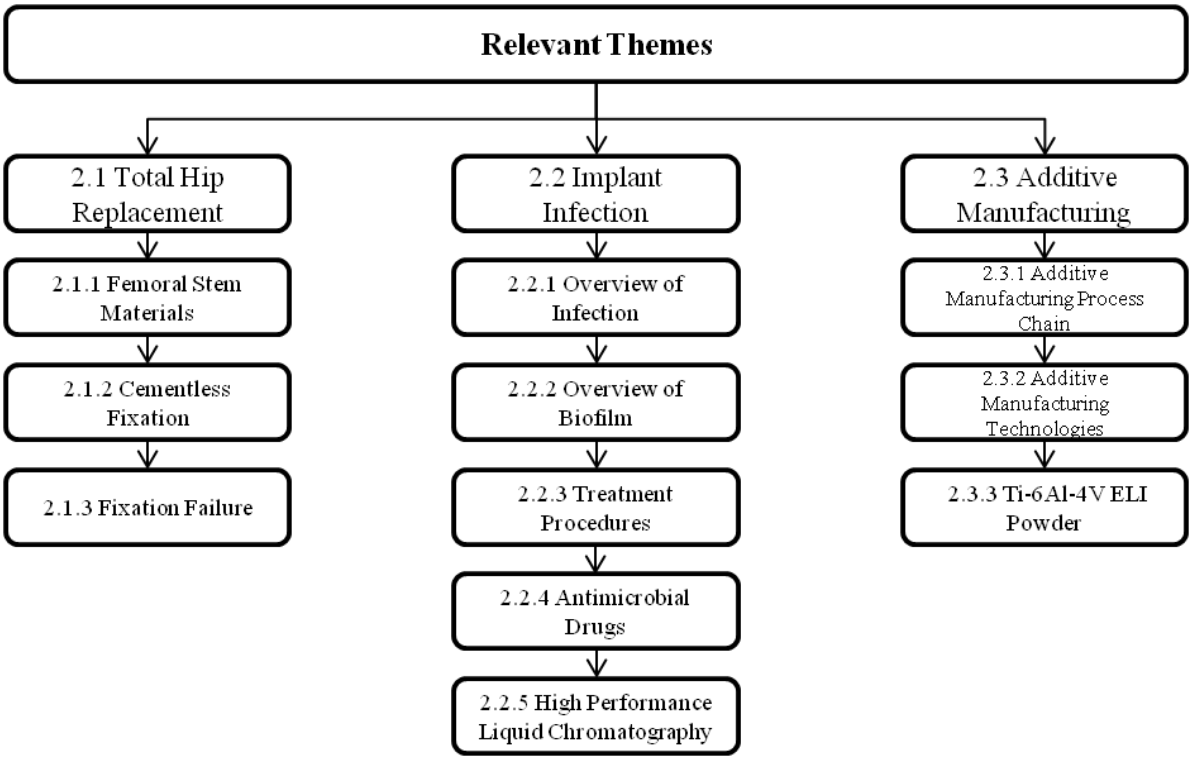

Figure 2.1: Schematic representation of the structure and sequence (left to right) in which the literature review is presented

2.1 Total Hip Replacement

In the 1994 National Institutes of Health Consensus Statement for Total Hip Replacement, the following excerpt can be found, *"Total hip replacement is an option for nearly all patients with diseases of the hip that cause chronic discomfort and significant functional impairment* [55]*."* Thus, one would expect the amount THAs performed annually to be high, and it is indeed reflected as such in the OECD 2011 "*Health at a Glance"* publication [10].

Figure 2.2 shows the amount of THR surgeries performed per 100,000 inhabitants of OECD countries in 2009, or that of the closest year where data for 2009 was not readily available [10]. It is evident that the average amount of annual procedures for these selected countries is about 150 per 100,000 inhabitants, which, when using the 2009 OECD population average of 1,221,954,000 amounts to 1,832,931 THA surgeries performed in the OECD countries alone [56].

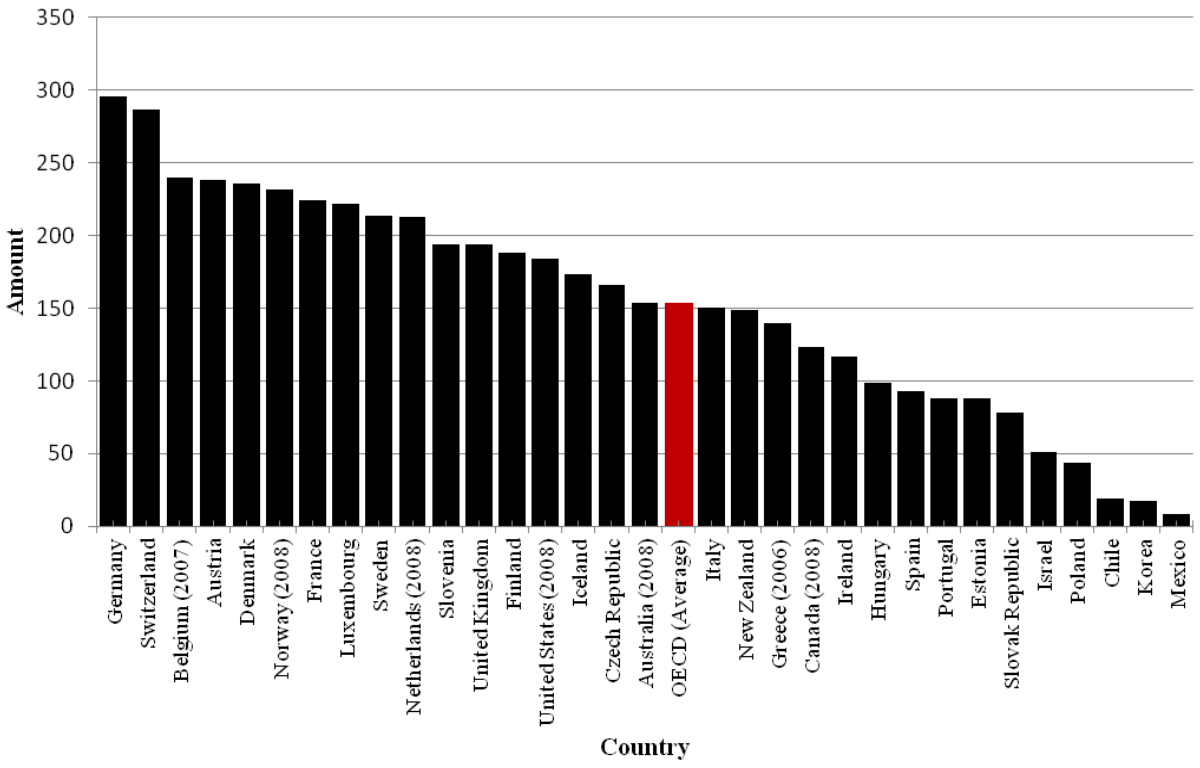

Figure 2.2: Amount of Total Hip Replacement surgeries per 100 000 inhabitants of OECD countries in 2009 (or nearest year), [10]

A high variability in the rate of THR occurrences exist between these countries. Although specific explanations for this do not yet exist, Pabinger and Geissler [57] found significant

correlation between the number of THRs with economic indicators of health care expenditures- and gross domestic product per capita, which can account for some of the possible multitude of factors influencing this variability.

The average estimated cost for hip replacements in 2007 is around 14,000 United States Dollars (USD) per procedure [10]. This means that, when applying the 2007 price, the annual monetary value of these procedures (1,832,931 multiplied by 14,000) is in the order of USD 256.6 billion. Furthermore, the already high occurrence of THA is on the increase [10]. Some of the suggested reasons for the increase in surgeries is the increase in life expectancy, yielding a greater number of people in the ageing population [58] as well as an increase in younger patients with developing hip problems [59].

2.1.1 Femoral Stem Materials

Femoral stems are manufactured from biomaterials. Geetha *et al.* [60] defines a biomaterial to be either a natural or synthetic material, utilised in producing implants or any type of structure, that is utilised to treat or replace any damaged and diseased part of the body with the objective to restore it to a functional state. A very wide range of biomaterials therefore exists [61, 62]. For primary cementless femoral stems, however, metal alloys, and more specifically titanium alloys, can be regarded as the biomaterial of choice [60-62] (Table 2.2). This is due to the excellent biocompatibility, corrosion resistance, high strength, ductility and fatigue behaviour of titanium alloys [60, 62, 63]. Furthermore, titanium alloys have a much lower elastic modulus than cobalt alloys or stainless steels, resulting in a reduction of stress shielding [64, 65]. Stress shielding is a phenomenon that occurs due to the mismatch between the elastic modulus of bone and implant material. Most of the natural load is transferred by the stiffer implant and not anymore by the bone, which according to Wolff's law causes the bone to remodel and resorb [17]. Figure 2.3 displays the elastic modulus of a wide variety of titanium alloys in relation to that of human bone.

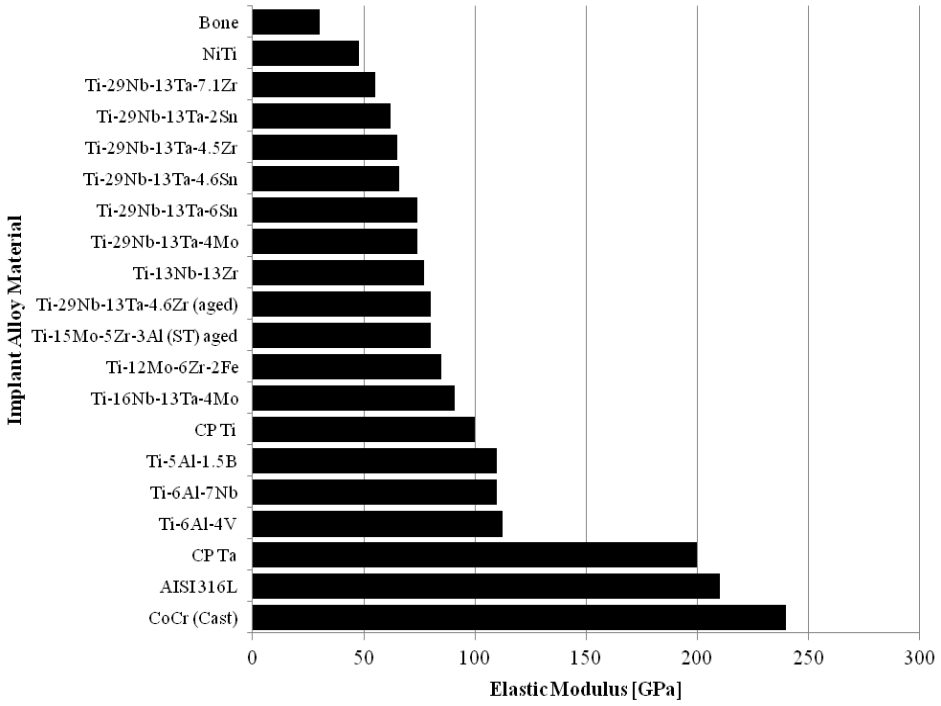

Figure 2.3: Different elastic moduli of various wrought implant alloy materials (adapted from [60])

Figure 2.3 encompass both so-called 'first generation' and 'second generation' biomaterials. They are distinguished by their crystal structure which can consist of α-phase (hexagonal close packed) and or ß-phase (body centred cubic) crystallographic configurations. One of the advantages of these second generation alloys is their lower elastic modulus, which will also lead to a reduction in stress shielding. Table 2.1, which is extracted and adapted from Geetha *et al.* [60] shows some of the mechanical properties of both first and second generation biomedical titanium alloys.

Table 2.1: Selected details regarding titanium biomedical alloys (adapted from [60])

Material	**Standard**	**Elasticity Modulus [GPa]**	**Alloy Type**
First generation (1950-1990)			
Commercially pure Ti (CpTi)	ASTM 1341	100	*α*
Ti-6Al-4V ELI (Grade 23)	ASTM F136	110	*α + ß*
Ti-6Al-4V (Grade 5)	ASTM F1472	112	*α + ß*
Ti-6Al-7Nb Wrought	ASTM F1295	110	*α + ß*
Second generation (1990-present)			
Ti-13Nb-13Zr Wrought	ASTM F1713	79-84	Metastable *ß*
Ti-12Mo-6Zr-2Fe	ASTM F1813	74-85	*ß*
Ti-35Nb-7Zr-5Ta		55	*ß*
Ti-29Nb-13Ta-4.6Zr		65	*ß*
Ti-15Mo-5Zr-3Al		82	*ß*

Although *ß*-alloys with much lower stiffness are currently under development with great interest, the Ti-6Al-4V ELI (α + *ß)* remains one of the most utilised titanium alloys among commercially available cementless femoral stems [60, 66]. This is also evident from Table 2.2, which lists some of the more often reported on in literature, commercial primary cementless femoral stems, along with their constituent materials.

Table 2.2: Noteworthy primary cementless THR femoral stems

Manufacturer	Model	Material(s)
Biomet [67]	*Taperloc*	Ti-6Al-4V
Zimmer [68]	*M/L Taper*	Ti-6Al-4V
Zimmer [69]	*Fitmore*	Ti-6Al-4V
Zimmer [70]	*Trabecular Metal*	Ti-6Al-4V/Ta-TM[a]
Zimmer [71]	*Alloclassic Zweymüller*	Ti-6Al-7Nb/Ti-6Al-4V
Zimmer [72]	*VerSys Epoch*	CoCrMo/PEEK[b]/Ti-FM[c]
DePuy [73]	*Summit*	Ti-alloy[d]
DePuy [74]	*S-ROM*	Ti-6Al-4V
DePuy [75]	*TRI-LOCK*	Ti-alloy[d]
DePuy [76]	*Corail*	Ti-alloy[d]
Corin [77]	*MetaFix*	Ti-6Al-4V
Corin [78]	*TriFit TS*	Ti-alloy[e]/CpTi

[a] *'TM' refers to the Zimmer proprietary name of Trabecular Metal*

[b] *'PEEK' refers to the polymer polyetheretherketone*

[c] *'FM' refers to Fiber Metal, indicating titanium in a very thin, fibrous physical state*

[d] *Ti-alloy is the material referred to in the DePuy documents, however likely this is to be Ti-6Al-4V, it cannot be assumed without proper confirmation, therefore the entry is kept similar to the original manufacturer's documents.*

[e] *The same as for (c), but since this is a different manufacturer, it has its own designation.*

From the materials specified in the manufacturer's brochures (Table 2.2) it is evident that the Ti-6Al-4V alloy is still predominantly used, despite concerns about the long term implications on Alzheimer's disease from aluminium and cytotoxicity of the vanadium alloying elements [50, 51, 60]. Consequently, Ti-6Al-4V ELI (extra low interstitial) is deemed an appropriate material to utilise for AM of the samples with the M2 cusing system.

2.1.2 Cementless Fixation of Femoral Stems

Cementless femoral stems are designed to establish a secure fixation via osseointegration and eventual bone ingrowth [21, 79]. It is important to distinguish between the terms *osseointegration*, *bone ingrowth*, and *bone ongrowth*. Albrektsson *et al.* [21] and Brånemerk [80] have used the term *osseointegration* to describe the direct bond that is formed between the biomaterial surface and host bone. The result of the bone remodelling process itself, by which new bone is formed to secure the implant in place is, depending on the surface morphology, referred to as either *ongrowth* or *ingrowth* [61, 81]. Therefore osseointegration can be regarded as the enabler, and its importance in achieving secure fixation underlined.

The difference between bone ingrowth and ongrowth is depicted in Figure 2.4. Ingrowth (left hand side schematic in Figure 2.4) describes the generation of new host bone and the growth of this bone into a porous layer on the biomaterial, securing the implant in place by means of physical integration [81]. Ongrowth (right hand side schematic in Figure 2.4) is also a means of implant fixation, but in this case, the surface of the biomaterial is roughened and without a porous layer with interstices into which host bone can grow [82]. Therefore, the host bone can only proliferate onto the roughened surface and is termed as such. According to Black, ongrowth yields much less tensile support than ingrowth [61].

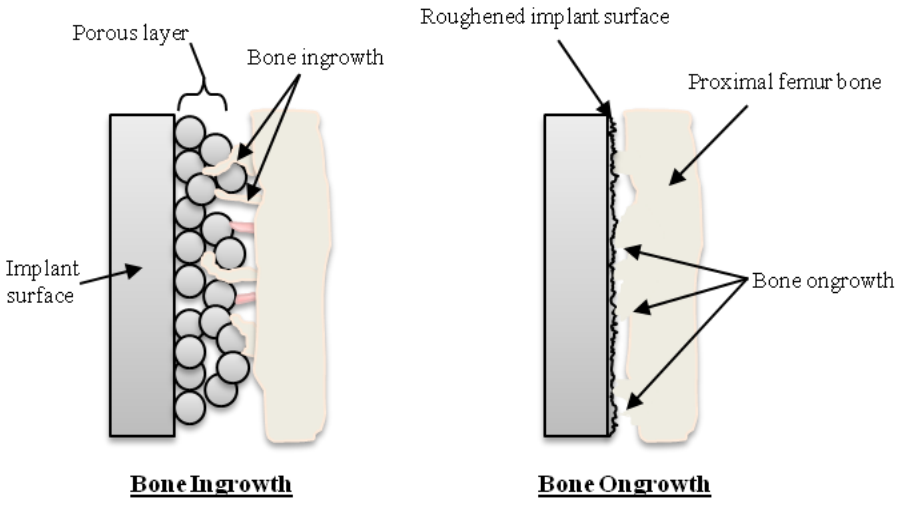

Figure 2.4: Schematic representation of the difference between bone ingrowth (left) and bone ongrowth (right)

2.1.3 Fixation Failure Modes of Cementless Femoral Stems

The loosening of cementless femoral stems is typically classified as either aseptic (in absence of any infectious pathogens) or septic (presence of infection) [83]. Aseptic loosening occurs typically due to mechanical phenomena. It includes the prevalence of excessive micromotions (in excess of 150 μm) between the implant surface and bone interface as a result of an insufficient primary stability of the stem and the stress shielding phenomenon during which bone remodels and resorbs due to a lack of load bearing stimulation [14-17].

The emphasis in this study is, however, on reducing the risk of septic failure by addressing the issue of bacterial colonisation onto the biomaterial. In Section 1.1 the process "race to the surface" was briefly mentioned, during which the biomaterial becomes conditioned with host proteins and a "race" initiates between osseointegration and the adhesion of bacteria [25]. If the implant surface is colonised by bacteria, they can enter biofilm mode of growth during which they encapsulate themselves in an extracellular matrix which is highly resistant to antibiotic penetration [26-28]. Therefore, extensive and expensive multiple stage surgical procedures during which the implant is removed and, after vigorous antibiotic regiments, a new one is eventually introduced have become a clinical standard for attempting the eradication of an established prosthetic infection [20, 29-32].

The negative influence of infection on prosthesis success and the patient's quality of life, together with the expensive financial implications only emphasises the need for effective infection prevention and treatment strategies [18, 84].

2.2 Implant Infection after Total Hip Arthroplasty

Infecrion can be described as an absence of a homeostatic balance between microorganisms and the tissue cells of the host [85]. Surgical intervention is required in order to attempt the eradication of an established infection, and despite best practices, some cases of serious and persistent infection can lead to implant removal, disfigurement, and even amputation or mortality [37, 38, 86, 87].

Various attempts and advances have been made through history in the struggle against surgical wound infection. In 1865 Sir Joseph Lister, a British surgeon, first introduced an antiseptic method for reducing wound infections [88]. Other major breakthroughs in reducing infections include the utilisation of rubber gloves in 1890 by W.S. Halsted and the introduction of a "Clean Air Operating Enlcosure" by Sir J. Charnley. In 1964 Sir J. Charnley correlated the intensity of bacterial contamination in the operating theatre air with infections after surgery [89]. By filtering the air of the surgical theatre, he achieved a reduction in infection rate from 9.5% to 1.1%. This was a major milestone for infection control in hip surgeries, and it revealed the importance of preventative aseptic conditions as to the earlier antiseptic paradigm [88].

In this section, the mechanisms of infection after hip replacement surgery are briefly reviewed. It is important to note that many themes with regard to the pathogenesis and persistence of infection, microbial behaviour and communication, are expert fields of science and research regarding the immense detail and complexity on cellular and gene expression level [90-92]. Therefore, the review is presented at a level of detail as to keep relevance to the main theme of the current study.

2.2.1 Overview of Infection

The infection of a THR femoral stem can be classified into two main categories, depending on the duration after surgery before its onset. They are termed exogenous and hematogenous respectively. Pathogens responsible for exogenous infection would typically intrude the implantation site during surgery, or shortly after, while the surgical wound is still healing. In hematogenous infections, the pathogen finds its way to the biomaterial by means of the host's blood system. There is no limit as to the time after surgery for the occurrence of hematogenous infection [93].

Despite the time after surgery and the pathogen's means of reaching the femoral stem, infection starts with the adherence of pathogens to the implanted biomaterial. According to Darouiche [94] this process is dependent on the complex interaction between the femoral stem, the human host, and the pathogens.

In order to further distinguish between the durations after surgery before manifestation of the infectious organism, exogenous infection can further be classified as 'early', occurring less than

two months after surgery, or 'delayed', occurring between three and twenty four months after surgery [11]. Pathogen sources include the operating theatre air, medical staff's clothing, surgical tools, cutaneous bacteria, and bacteria already in the host [95].

The wide variety of pathogenic sources is also reflected in the number of different infecting bacterial species that can be found in PJI sites, such as in the study of Berbari *et al* [96]. In their study, data about patients with THA and total knee arthroplasty (TKA) performed at the Mayo Clinic in Rochester, Minnesota, were obtained for the period of 1969 to 1991, during which 462 cases of PJI have been identified in 460 patients. A summary of the frequency of infecting organism from their study is presented in Table 2.3. *S.aureus* was found to be one the main infecting species. Similar findings with regard to staphylococcal species, and specifically *S.aureus,* as most frequent offending organisms have been published by both Pulido *et al.* [97] and Montanaro *et al*. [98]. It also reveals the high prevalence of *S.aureus* and the relevance of investigating antimicrobial efficacy against strains from this pathogen.

Table 2.3: Infecting organisms found in 462 prosthetic joint infections between 1969 and 1991 after THA and TKA at the Mayo Clinic, Minnesota (adapted from [96])

Infecting Organism	***Number***	***Percentage (%)***
S. aureus	101	22
Polymicrobial etiology	88	19
Coagulase-negative staphylococci (CNS)	86	19
Negative culture	57	12
Streptococci	42	9
Gram-negative bacilli	38	8
Anaerobes	29	6
Other	21	5

2.2.2 Overview of Biofilm

A biofilm is a collection of surface-adhering microorganisms, often from a variety of genera, embedded in an organic extracellular matrix, which is constituted from both the microorganisms' secretions as well as compounds from the surrounding environment [29, 90]. The typical sequence of biofilm formation is presented in Figure 2.5. The ability of bacteria growing in a biofilm to utilise these secretions, enable them to become resistant to various antibiotics and allows them to persist, leading to, amongst other, chronic prosthetic joint infections. Furthermore, the extracellular matrix also plays a pivotal role in establishing structural stability and a measure of protection for the bacteria growing as biofilm [28]. These types of infections can persist, showing very little response to host innate immune and inflammatory responses as well as antibiotic treatment [49].

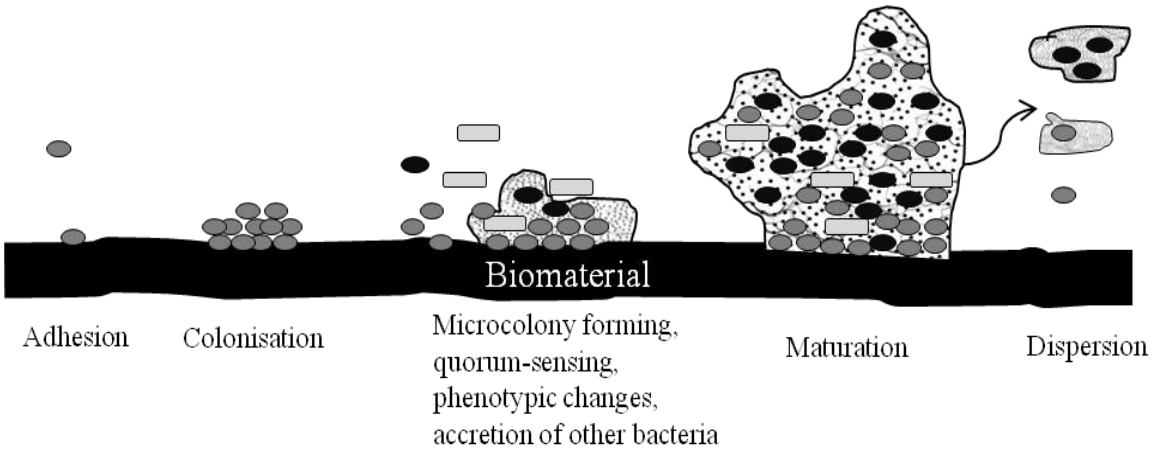

Figure 2.5: A sequential representation of the biofilm formation process (adapted from [90])

The mechanism of biofilm formation is discussed with reference to Figure 2.5, which represents a schematic of the sequential steps during biofilm formation. A biofilm typically begins with the reversible adhesion of a single species of planktonic bacteria onto the biomaterial surface via a variety of possible adhesive forces [29, 90, 93]. If the biomaterial is absent of protein conditioning, these bonds can typically include electrostatic processes, Van der Waals forces, hydrophobic processes, and hydrogen-bonds [26, 42]. *In vivo*, however, it becomes more complicated, since the biomaterial substrate is swiftly covered with proteic film, which then forms the new means of interaction with the bacteria [42].

It is important to note that the first stage of adhesion is reversible, and during this stage, bacteria are still susceptible to antibiotics. The administering of prophylactic antibiotics strives to eliminate planktonic and reversibly attached bacteria, prohibiting them from reaching the state of irreversible adhesion. If adhesion by a single species is successful, a rapid increase in the number of adhering bacteria follows. This process is known as colonisation of the substratum.

Once this has occurred, the bacteria can divide into daughter cells, which also bind to the surface. This results in a community of microcolonies, consisting of the original adhering bacteria as well as daughter cells from those that already began to multiply. Amongst the adhering bacteria, a secretion of various polymers and acidic polysaccharides takes place. The adhering bacteria, together with the produced extracellular compounds can then turn into a new substratum for other accreting bacteria species [90]. Typically, *in vitro*, the thickness of the biofilm grows to be around 50 μm, with the prevalence of vertical protrusions as the biofilm reach maturity [28]. A maximum resistance towards antibiotics appear in the mature stage of the biofilm. The final stage is the dispersion stage, where certain areas of the biofilm becomes dissolved and some of the encased bacterial cells are set free to seed on other locations of the substratum and form new biofilms [90].

The mechanisms behind metabolic changes, mutation and communication amongst bacteria in biofilm mode of growth, are being studied continuously and are highly specialised fields respectively. Therefore, only an overview of these concepts is presented in this document [28, 93, 99, 100].

According to Francolini & Donelli [26], areas of importance with regards to the prevention and controlling of biofilms are, firstly, the need to inhibit any microbes from successfully colonising the material, the interference of cell-to-cell communications and the separation of an already established biofilm matrix, emphasising the need for the evaluation of effective colonisation preventing and drug delivery strategies [26].

2.2.3 Treatment Procedures

The goal of treatment for each case of an infectious hip replacement is the complete eradication of all present offending microorganisms and subsequent restoration of proper functionality to the implant [30]. These procedures include:

- early debridement with retention
- one-stage exchange
- two-stage exchange,
- permanent removal of the implant,
- Girdlestone resection arthroplasty,
- and chronic antibiotic suppression [11, 30, 101].

The procedure of interest here is the two-stage exchange arthroplasty. It has yielded some of the most satisfying results (>90% success rate in some cases [30, 102, 103]) and is typically the procedure regarded as the standard treatment for patients with developed abscesses and sinus tracts [11, 35, 103]. The first stage procedure involves the removal of the implant, a thorough debridement, followed by a minimum 4 week period of antibiotics during which patients have very little mobility and are also instructed to use non-weight bearing mobility methods [31, 33].

A temporary spacer, constituted from antibiotic loaded bone cement, is often implanted to help eradicate infection by eluting antibiotics locally at the site of infection and to allow a certain measure of mechanical support. Only after antibiotic treatment and evidence of satisfying eradication of the infecting microorganisms, the second stage where a new functional implant is inserted can be performed [103]. This is where the interim period can be extended significantly, when screening of a joint aspirate turns out positive for cultures, the antibiotic treatment needs to be repeated before reimplantation of a functional prosthesis can occur [103].

2.2.4 Antimicrobial Drugs for Infection Prevention and Treatment

An extensive range of antibiotics available to treat orthopaedic infections exist. Zilberman and Elsner [85] summarised a collection of these antibiotics with regard to some of their respective properties. Their full summary is presented in Appendix C. When selecting an antimicrobial for prophylaxis, the antimicrobial should have a broad spectrum, whereas the antibiotic selection for treatment should be specific to the offending pathogen. Gentamicin has been selected for prophylactic testing and vancomycin for sustained drug release from within the samples.

2.2.4.1 Gentamicin

Gentamicin is an aminoglycoside antibiotic which is derived from the fermentation of the bacterial species *Micromonospora purpurea* and *Micromonospora echinospora* [104]. It is a combination of three different main occurring chemical structures, gentamicins C_1, C_2, and C_{1a} [105, 106]. Although more minor components have been discovered, these three are considered the main constituents of the gentamicin aminoglycoside. It is recognised by the bonding of at least two amino monosaccharides via glycosidic bonds to a central structure which is termed an aminocylitol [106]. In the case of gentamicin, this aminocyclitol is 2-deoxystreptamine, to which amino saccharides, garosamine and purpurosamine, have each glycosidically bonded at carbon atoms 4 and 6 respectively [106, 107]. It is utilised inside ALBCs in the form of gentamicin sulfate, which has the physical appearance of a white to yellowish white powder [105].

Gentamicin exhibits various properties that make this a very suitable antibiotic for prophylactic administration, especially via addition to bone cement. One such property is that it is relatively heat stable and therefore able to withstand the temperatures reached during polymerisation in PMMA bone cement. Table 2.4, lists some of the notable physicochemical properties of the three major gentamicins that collectively exist as the gentamicin part of gentamicin sulfate [104, 105]. The molecular weight in Table 2.4 is for each respective gentamicin only, and is exclusive of the molecular weight of sulphuric acid.

Table 2.4: Selected physicochemical properties of gentamicins [104, 105]

Generic name	***Empirical Formula***	***Molecular Weight [g/mol]***	***Melting Point ºC***	***Water Solubility***	***pH (4% solution in water)***
Gentamicin C_1	$C_{21}H_{43}N_5O_7$	477.6	218-237	50 mg/ml	3.5 - 5.5
Gentamicin C_2	$C_{20}H_{41}N_5O_7$	463.6	218-237	50 mg/ml	3.5 - 5.5
Gentamicin C_{1a}	$C_{19}H_{41}N_5O_7$	449.5	218-237	50 mg/ml	3.5 - 5.5

Gentamicin also exhibits a wide antibacterial spectrum. It also acts synergistically against microbes along with a number of other antibiotics and is often used in bone cements as a combination with other antibiotics such as clindamycin or vancomycin [105, 108]. The antibacterial spectrum of gentamicin is listed in Table 2.5.

Table 2.5: Antimicrobial spectrum of gentamicin [105]

Gram-positive	***Gram-negative***	***Naturally Resistant***
S. aureus	*Pseudomonae*	anaerobes
CNS	*Enterobacteriaceae*	streptococci
Staphylococcus epidermidis		others

Gentamicin exerts its bactericidal effect through the inhibition of prokaryotic protein synthesis by binding within the 30*S* subunit of the ribosome [106, 107]. It disrupts the translation process of the codons transcribed onto mRNA, the sequence of which was originally specified by the organism's DNA for protein synthesis [105, 109]. Consequently, the polypeptide chain of the protein cannot be correctly synthesised and adequate protein synthesis does not occur.

2.2.4.2 Gentamicin Release from PMMA

The process of antibiotic elution from the PMMA matrix has been extensively studied in the past four decades [110-112]. The release typically occurs in two definitive stages, an initial burst release of gentamicin into the surrounding fluid (typically within the first 24 hours [113]), followed by a steady sustained release which can last for an extensive period of time [110]. The exact mechanisms, however, by which antibiotics elute from PMMA bone cements currently still remains an area of debate and authors have expressed different opinions to the finer details of the process with regard to it being mainly a surface effect or a dissolution effect by which fluid slowly penetrates the PMMA matrix through imperfections such as cracks and pores [110]. Van de Belt *et al.* [41] have argued the release to be a combination of both, by which the initial burst release is mainly a surface dependent effect and the sustained release being a dissolution effect. This concept is illustrated in Figure 2.6.

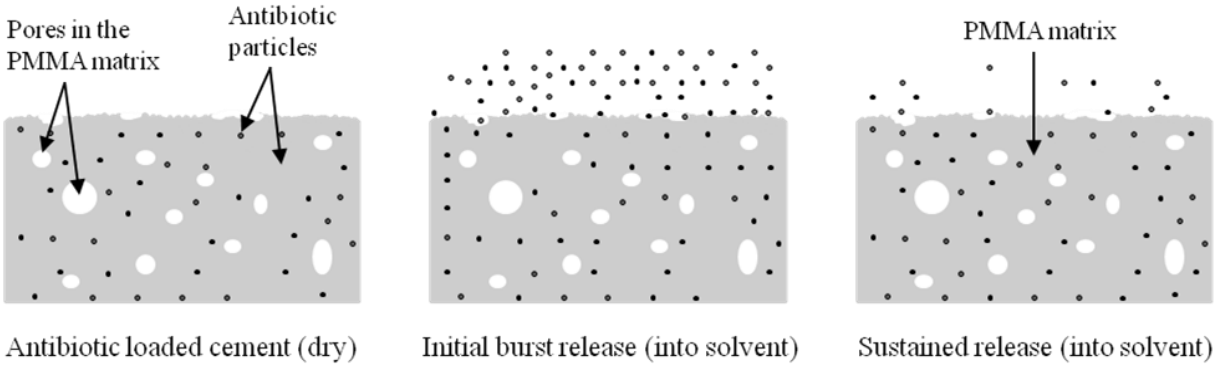

Figure 2.6: Schematic representation of different stages of antibiotic release from the PMMA matrix [41]

A generic curve created from the results of various reports in literature representing the typical cumulative release behaviour of gentamicin over time is presented in Figure 2.7 [110, 114-116]. In an ideal situation, the cumulative amount of drug release should reach a sufficiently high level in a short period of time and then either cease to elute or maintain effective concentrations, instead of continuing with a sustained slow and ineffective release [41].

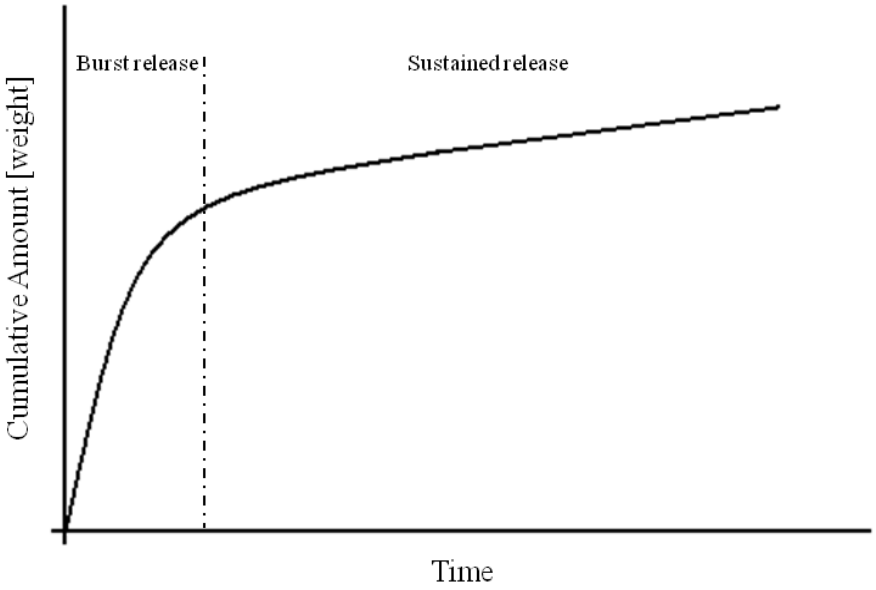

Figure 2.7: Generic curve representing typical cumulative release of gentamicin from PMMA [110, 114-116]

Various efforts to propose a mathematical model for describing the release of a drug randomly dispersed in a matrix have been reviewed by Lewis and Torrado *et al*. [113, 115]. Some of these models do not account for hydrophobicity of polymers such as PMMA and therefore cannot be assumed to be an accurate description of the real world process [113]. Modifications have however been made to some of these models and have been proved to be able to describe the process when parameters have been determined empirically [110, 115]. A standardised model, however, seems to remain elusive, which is evident in the studies of Cabanillas *et al.* [110] and Torrado *et al.* [115] who each used the same bone cements (CMW1 Gentamicin), but found differing best fit models to their measured data.

Due to these differences, and the apparent study specific variability in fitting equations to the released concentrations, the concept within this study is to be tested with the Modified Kirby-Bauer procedure described in Chapter 4. This test gives direct information regarding the colonisation prevention capacity of the concept, from which the duration of released concentrations above the therapeutic limit can be deduced.

2.2.4.3 Vancomycin

Vancomycin is a glycopeptide antibiotic obtained from fermenting the bacterial species *Streptomyces orientalis* [117]. It is used in treatment regimens against resistant Gram-positive bacterial infections and specifically MRSA infections [118]. Also known as a "drug of last resort", vancomycin is utilised with utmost care and specificity to prevent further development of resistance [119]. Vancomycin is distributed for laboratory use in the form of vancomycin hydrochloride, a white and odourless powder. The molecular structure of vancomycin is presented in Figure 2.8. Of particular importance are the aromatic carbon rings and carbonyl groups, which enable the molecule to be detected and quantified via UV absorption methods.

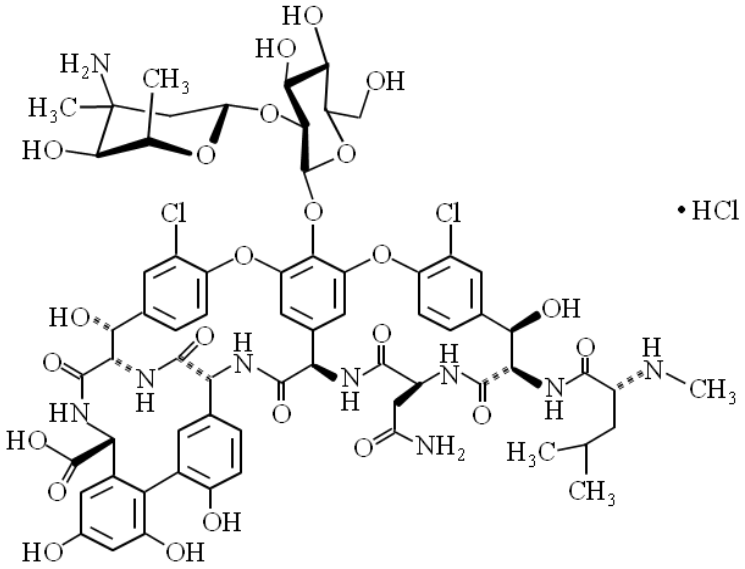

Figure 2.8: Molecular structure of vancomycin (adapted from [120])

Selected physicochemical properties of vancomycin are presented in Table 2.6. Similar to Table 2.4, the presented molecular weight is only for the vancomycin molecule and exclusive of hydrochloric acid.

Table 2.6: Selected properties of vancomycin [85, 120]

Generic name	*Empirical Formula*	*Molecular Weight [g/mol]*	*Melting Point ºC*	*Water Solubility*	*pH (5% solution in water)*
Vancomycin	$C_{66}H_{75}Cl_2N_9O_{24}$	1449.25	185-188	> 100 mg/ml	2.5 - 4.5

Vancomycin exerts its antibacterial properties by interfering with the synthesis of peptidoglycan (a structural polymer consisting of sugars and amino acids) in the cell walls of Gram-positive bacteria. It specifically binds to the D-alanyl-D-alanine termini where it prevents cross linking of peptidoglycan monomers, which significantly weakens the cell wall and results in bacterial death through lysis [117, 121]. The relative large molecular mass of vancomycin prevents it from crossing the outer layer (consisting of phospholipids, proteins and lipopolysaccharides) of the Gram-negative bacterium and is therefore inactive against it [117, 118]. The antibacterial spectrum of vancomycin is presented in Table 2.7. Since vancomycin is only used as a last resort and only against certain pathogens, Gram-positive bacteria typically treated with less severe antibiotics are omitted from Table 2.7 to maintain relevance to vancomycin application

Table 2.7: Gram-positive antibacterial spectrum of vancomycin [122, 123]

Susceptible	***Resistant***	***Intrinsically Resistant***
MRSA	VRSA	*Leuconostoc*
MRSE	VISA	*Pediococcus*
PRSP	VRE	*Lactobacillus*
VSE		*Erysipelothrix*

MRSE – Methicillin resistant Staphylococcus epidermidis; PRSP – Penicillin resistant Streptococcus pneumoniae; VSE – Vancomycin susceptible enterococci; VRSA – Vancomycin resistant Staphylococcus aureus; VISA – Vancomycin intermediate Staphylococcus aureus; VRE – Vancomycin resistant enterococci

For the purpose of this project, however, the main interest is its activity against MRSA. The MIC for vancomycin of MRSA is 2 μg/ml for 90% of tested isolates. The antibacterial activity of vancomycin is reported to be maximised at a concentration to MIC ratio of four [117]. This means that ideally the concentration of vancomycin at the infected site should not drop below 8 μg/ml but should also not reach levels that will evoke systemic toxicity. Currently, vancomycin is mainly administered intravenously with a dose of 1 g over 12 hours. Adverse effects include red man syndrome due to overproduction of histamine in the body upon too rapid infusion. The main toxic effects include possible nephrotoxicity at serum levels greater than 30 μg/ml and ototoxicity at concentrations greater than 50 μg/ml.

2.2.4.4 Local Controlled Vancomycin Release

The ultimate goal of controlled drug delivery is to "*deliver the therapeutic dose of the drug to the site in need for the necessary amount of time"* [124]. Controlled drug delivery differs from conventional medications (such as oral tablets) in the sense that instead of only controlling the total mass of the drug to administer, the rate of drug delivery is also controlled. The concept of controlled release versus conventional release is graphically presented in Figure 2.9 as a generic plot of drug concentration at the target site over time. It illustrates the cyclic fluctuating levels of drug concentration after each dosing time of conventional administration [125]. When the difference between minimum effective and toxic concentrations is small, conventional release has an increased risk of leading to both detrimental situations during the dosage cycle, also presented in Figure 2.9. Controlled release, on the other hand strives to ensure that the therapeutic effective concentration is quickly reached, and then maintained for an extended period.

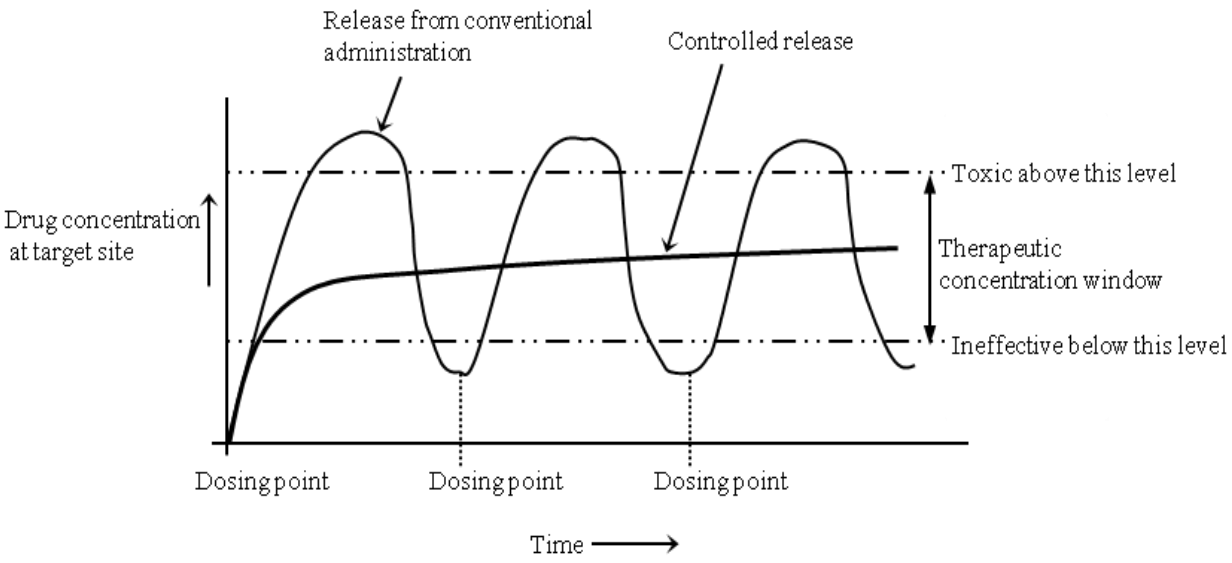

Figure 2.9: Generic drug release curve indicating the difference between conventional and controlled release (adapted from [125])

The therapeutic benefits of controlling the rate of release have been summarised by Baker [125]:

- Problems regarding drug overdosing and underdosing can be avoided
- High local concentrations can be achieved directly to the site of need without risking levels that would prove systemically toxic

- The therapeutic efficacy of the drug is improved by avoiding the large fluctuations in concentration that is characteristic of oral administering of tablets
- With controlled delivery, much less quantity of the drug is necessary to achieve the same local concentrations as would be with systemic delivery.

The last point has also been confirmed in a study by Young *et al.* [126]. By comparing 250 and 500 mg intraosseous bolus injections of vancomycin locally to 1 g of intravenous administration, they found much higher concentrations of vancomycin in bone and subcutaneous fat samples for both doses delivered locally. This implies that that the upper boundary is shifted greatly when drugs are delivered intraosseously. Since these high local concentrations of vancomycin did not produce systemic values close to the toxic limit, the focus is to maintain a minimum concentration higher than 4 times the MIC of MRSA (8 μg/ml).

2.2.4.5 Drug Release through Synthetic Membranes

Three main drug release profiles for local drug delivery are defined in literature. They are:

- diffusion according to Fick's law when the pores allow free movement of molecules,
- constraint diffusion as the pore size starts to restrict the movement of the molecules,
- single file diffusion when the pore size is smaller than two times the molecule size [127].

All three release profiles are therefore governed mostly by the membrane pore- to solute molecule size ratio. The three different models are depicted in Figure 2.10.

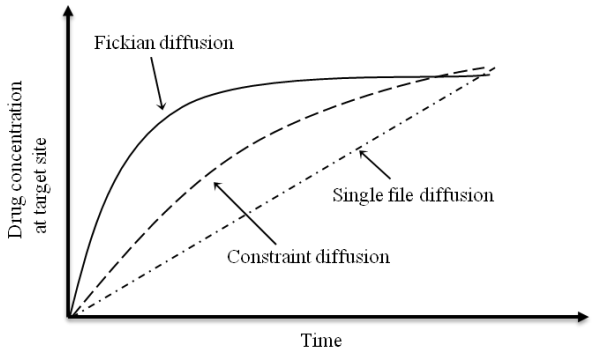

Figure 2.10: Different diffusion models resulting from the membrane pore to solute molecule size ratio (adapted from [127])

An appealing aspect of zero- or near order release is that the release rate of the drug becomes more or less constant without any influence from the reservoir drug concentration [128]. Where an initial burst release is good for the immediate reduction of bacteria, a sustained, near zero-order released would provide prolonged drug release for as long as the drug remains stable in the employed formulation. These two effects could also be combined by a bolus injection during one stage exchange, supplemented with constraint or single-file diffusion from within the implant reservoir to maintain a therapeutic drug concentration at the site of infection.

To empirically evaluate the mechanism of release, Fickian, constraint, or zero-order, the Korsmeyer-and-Peppas model can be applied [129, 130]. It accounts for the first 60% release of the loaded drug to determine the mechanism of release. The model is based on the released percentage of total loaded drug as follows,

$$\frac{M_t}{M_\infty} = Kt^n \qquad (2.1)$$

where M_t and M_∞ are the respective cumulative masses released at time t and infinity, K is the release rate constant (units t^{-n}) which takes into account geometrical and structural properties of the drug and polymer system, and n is the diffusion exponent that defines the mechanism of release in the obtained profile. The intervals and accompanying interpretations of n for release from slabs are summarised in Table 2.8.

Table 2.8: Values and accompanying interpretation of diffusion exponent *n* [129, 130]

Value of Diffusion Exponent n	***Diffusion Mechanism***
≤ 0.5	Fickian diffusion
$0.5 < n < 0.1$	Anomalous non-Fickian diffusion (constraint release)
1	Case-II transport (zero-order release)
>1	Super Case II transport

Therefore, if n is smaller or equal to 0.5 the release is controlled by Fickian diffusion alone, whereas for n = 1, the mechanism is controlled by relaxation in the polymer matrix. For n-values between the extremes, release occurs through a combination of a possibility of various effects,

typically amongst which is considered to be both diffusion and polymer relaxation resulting in a pseudo first order, constraint release profile [131].

For detection of vancomycin, reversed phase high performance liquid chromatography (RP-HPLC) is specified in the British Pharmacopoeia [132]. It is also the most precise method for concentrations in the μg/ml range [133].

2.2.5 Overview of High Performance Liquid Chromatography (HPLC)

HPLC is a widely used separation method that enables both the identification and quantification of different solutes within a solution or dispersion, in this case vancomycin. The process enables a sample solution containing vancomycin to be separated by passing it through a chromatographic bed, also referred to as the stationary phase. The medium which transports the sample through the solid phase is termed the mobile phase [134].

2.2.5.1 Process Apparatus

The fundamental components of an HPLC system are presented in Figure 2.11. Meyer lists these as the "*solvent reservoir(s), transfer line with frit, high-pressure pump, sample injection device, column, detector, and data acquisition"* [134].

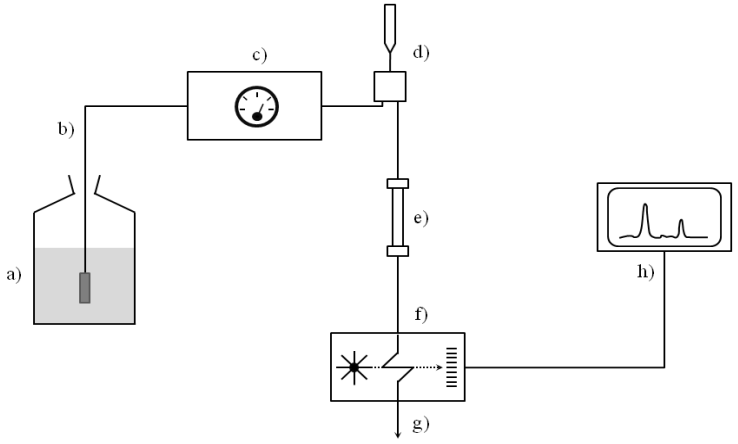

Figure 2.11: Simplified schematic of HPLC apparatus a) solvent reservoir, b) transfer line with frit, c) high pressure pump, d) sample injector, e) column, f) detector, g) waste, h) data acquisition and processing (adapted from [134])

In Figure 2.11 the mobile phase is contained in the solvent reservoir(s), which is transported through the transfer lines by means of a high-pressure pump. The sample injector then injects a specific volume of sample in to the mobile phase and is transported to the chromatographic column, where the separation takes place. Solutes elute at different retention times depending on their properties and are then transported to the detector before they exit the system through the waste transfer line. The signal from the detector is continuously fed to the data acquisition unit throughout the process where it is analysed.

A wide range of system components exists, the details of which each are applied to a variety of scientific fields and therefore, this section is limited to the configuration utilised in this project. This is the application of reversed phase HPLC (RP-HPLC) for vancomycin quantification by means of ultraviolet-visible light (UV-vis) detection.

2.2.5.2 Reversed-phase High Performance Liquid Chromatography (RP-HPLC)

RP-HPLC is regularly applied for the analysis of pharmaceuticals. It describes the chromatographic process in which the mobile phase is more polar than the stationary phase, and in which the stationary phase is hydrophobic [134, 135]. The hydrophobicity is due to the surface modification of normal silica with n-alkyl silanes, most notably those with 18 carbons, C_{18} [135]. Solutes elute at different rates through the column according to their degree of hydrophobicity and polarity [136]. Water is the weakest eluent in RP-HPLC, allowing the direct injection of samples with the only required pre-treatment being centrifugation or filtration. The “strength” of the interaction between solute and stationary phase requires the use of organic solvents to transport solutes through the column to the detector [134].

2.2.5.3 UV-Vis Absorbance Detection

UV-Vis detectors are among the most common used detectors. These detectors are stable during small changes in temperature and also exhibits linearity in their detection (signal value is linearly proportionate to the concentration of solute). Molecules for UV detection need to contain chromophores [134]. When the vancomycin passes the detector, it records the variations in concentration within the mobile phase as deviations from the baseline and outputs it as an electrical signal to the interface software where it is graphically displayed as a chromatogram.

2.2.5.4 Chromatogram

The signals from the detector are displayed as Gaussian curves, also termed peaks. A chromatogram is the complete set of peaks recorded during the entire analysis period of the sample [134]. A generic simplified chromatogram revealing the presence of two distinct solutes is presented in Figure 2.12.

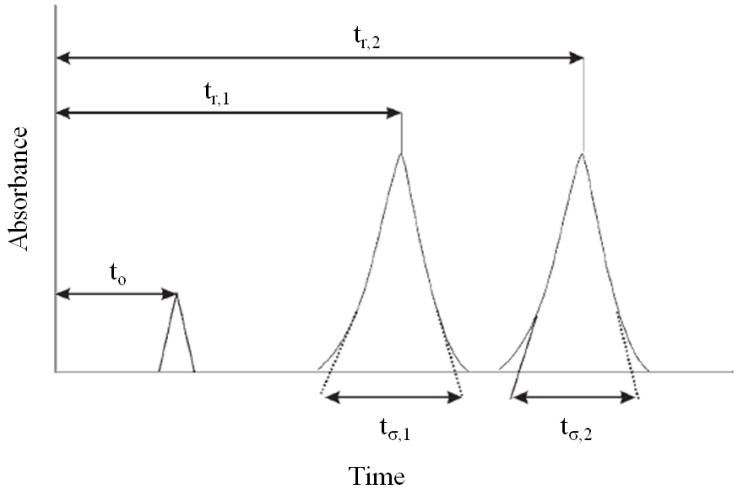

Figure 2.12: Simplified representation of a chromatogram with two solutes [137]

The elapsed time between sample injection and detection of the compound of interest is known as the retention time, $\boldsymbol{t_r}$, for that compound. In Figure 2.12 the retention times of the two compounds are denoted as $\boldsymbol{t_{r,1}}$ and $\boldsymbol{t_{r,2}}$ respectively, whereas $\boldsymbol{t_0}$ represents the retention time for a solute that is not retained in the system. Total absorbance for a compound is obtained by the integral across the base width of its peak, denoted by $\boldsymbol{t_{\sigma,1}}$ and $\boldsymbol{t_{\sigma,2}}$ for two arbitrary analytes in Figure 2.12.

2.2.5.5 Quantification of Vancomycin Concentration

For quantification it is necessary to first establish a calibration curve for the specific analyte and method in use. This is done by analysing the absorbance of the drug in injection volumes from a specific predetermined dilution series of the antimicrobial and fitting a straight line to the dataset with simple linear regression analysis (absorbance on the y-axis as the response variable and concentration on the x-axis). The concentrations of drug eluted from the implant samples are then determined by substituting y in the resulting linear regression model with the measured absorbance to find the corresponding value for x, the concentration.

2.3 Additive Manufacturing

Modern layer AM technologies are based on the paradigm developed in the late 1980's with the well-known liquid based stereolithography (SLA), a cornerstone of Rapid Prototyping (RP) technologies [138, 139]. Initially they were mainly utilised for creating parts for visualisation purposes only, but in recent years, RP has evolved into technologies that allow the manufacturing of functional parts. These technologies are today collectively referred to as AM [140]. Therefore, metal powder based AM technology entails the fabrication of functional products in a layer-by-layer addition of material approach instead of the conventional subtractive processes during which a product is machined or cut from a larger volume of stock material [141]. Consequently, this enables the manufacturing of a wide variety of unusual and intricate geometries, leaving the designer with much more freedom and possibilities than with conventional design for manufacture [142]. AM technologies are especially of interest in the aerospace and biomedical sectors. The process in total also seems to bear significant economic advantages, since conventional manufacturing by subtractive processes during which great percentages of the bulk material goes to waste, can be very expensive and time consuming in comparison to AM [143, 144].

Cronskär *et al*. [143] determined that, under suitable circumstances, a cost reduction of 35% can be achieved for the manufacture of femoral hip stems with AM (EBM) in comparison to conventional manufacturing. Similarly, Dehoff *et al*. [144] published that AM technologies pose the opportunity to reduce the manufacturing cost by more than 50% for a thin walled aerospace bracket.

A generic process chain of the basic steps applicable to nearly all AM processes is presented and each of the different steps in the process chain is discussed. In order to gain an understanding of the paradigms and underlying concepts of AM, it is necessary to present an overview of the different technologies as is applicable to the eventual development of metallic powder bed fusion. Due to the large variety of AM technologies on the market, the scope of the discussion on AM has been shifted in order to maintain relevance to the main theme of the study. With the exception of stereolithography (SLA), the focus is placed on the technologies in which a layer of powder is distributed over a building table and cured or fused according to a specified layer thickness (slice) of the cross sectional geometry of the 3D CAD input file.

2.3.1 Generic Additive Manufacturing Process Chain

The different AM processes each exhibit certain specific technical characteristics in terms of the actual machines that distinguish them from each other. In the process of part creation, however, many similarities exist between most of the processes. Therefore, a general process chain can be presented to apply to most, if not all, AM processes.

The process primarily consist of the following five steps, Standard Triangulation Language (STL) file generation, file verification and repair, build file creation, part construction, and part cleaning and finishing [145]. Although it is argued that 3D CAD modeling of the part is not inherently part of the actual AM process, it is included in the generic process chain diagram of Figure 2.13 because all digital manufacturing parts have to start with the CAD modeling thereof. The CAD model is of importance since it is the input data to the AM manufacturing process, and as with all processes, the quality of the output is directly linked to the quality of the input data.

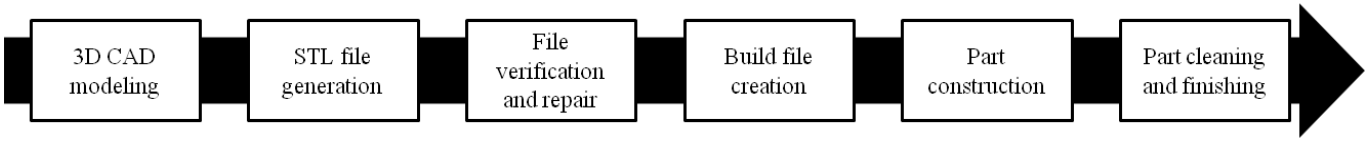

Figure 2.13: Generic AM process chain

Figure 2.13 shows the first step after creating a satisfying CAD model to be the generation of an Standard Triangulation Language (STL) file, which is a neutral file format utilised for AM. All commercial CAD software packages have the ability to export the part to STL format, but not all produce STL files with the same accuracy and quality. It is an important factor to consider when selecting the software package. An STL file is a mesh of triangles that approximates the geometry of the part. The file can be exported in either binary or ASCII format and consist of all the coordinates of the vertices of the triangles which collectively approximate the original 3D CAD model [145]. An example of this concept is presented in Figure 2.14, with the original 3D CAD model on the left and the exported STL approximation of the original model on the right.

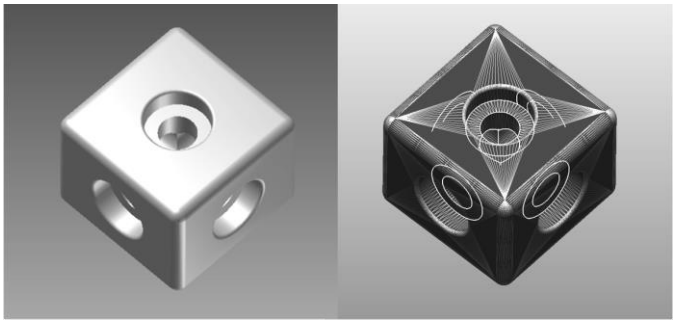

Figure 2.14: 3D CAD model on the left with STL approximation on the right

Once an STL file has been generated it needs to be verified and repaired if any defects are present. Common triangulation defects can typically be overlapping triangles, near flat triangles and non-coincident triangles [145]. To ensure a valid file, two vertices must be shared by adjacent triangles and the direction of surface normals must be outward. Although commercial software packages such as *Magics* (Materialise) have STL repair and refining toolsets, in some cases it can be necessary to revise the CAD model in order to ensure a functional STL part for the AM process.

The next step is the creation of the build file, which encompass some sub-steps and concepts to regard. The first is part orientation. Due to the layer-by-layer nature of AM, all parts will inherently have 'stair-stepping' (Figure 2.15) with the exception if all features are completely vertical or horizontal [146]. This effect can be minimised with decreasing layer thicknesses, which in turn will lead to more layers and an increase in build time. It is therefore important to decide upon this trade-off in preparing the build file.

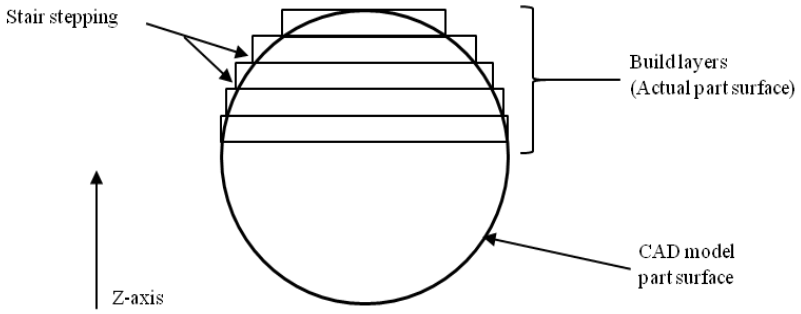

Figure 2.15: Representation of the stair stepping effect due to slicing for finite layer approximation of the original CAD geometry (adapted from [145])

Another aspect to consider is whether or not support structures are needed. Support structures provide a means of attachment for the part to the base plate, ensure that any overhanging geometries are kept in place and also contributes to heat dissipation during the build process. These structures can also be placed within part features to assure proper support for the structure in order to warrant for geometrical accuracy. It is important to keep in mind that these structures need to be removed after the built, typically with aggressive mechanical processes such as manual removal or machining, and should be specified so as to not cause any damage to the part surface during removal. Figure 2.16 shows the support structures utilised for building cylinders on an M2 cusing system. The supports can be removed manually by chiselling them away from the part surface or by wire cutting if they are more bulky.

Figure 2.16: Support structures for attaching cylindrical parts to the build plate of a Concept Laser M2 cusing machine

The next step is to decide on the layers, 'slicing', of the part according to available range of layer thicknesses permissible by the AM system in question. Each slice includes the cross sectional two dimensional geometry of a specific height of the part. This is in essence the *X-Y* tool path in which the control system guides the laser (or other system for creating layers) to create each layer [145]. As mentioned with regard to the stair effect, an appropriate trade-off must be made between build time and part integrity when selecting the slice or layer thickness.

The part placement on the build plate can now be specified and the build file created. In compiling the build file, parameter selection is very important. Many AM systems have default processing parameters as specified by the manufacturer, but varying these parameters can near optimise the process to the specific user's needs [147]. Two of the main parameters are laser

power and laser travel velocity (scanning speed), but different AM processes inherently have different parameters that can be varied. When the build file is created it is sent to the machine control software to begin the build.

Parts are built from the bottom up, one slice at a time. Once the part is finished it can be removed from the machine, support structures removed and cleaned. Some parts require post processing such as wax or bronze infiltration in order to ensure better structural integrity. Other processes can be sand-blasting, grinding or polishing, but the important point is that the operator should identify and thoroughly execute the necessary post processes to ensure functionality and applicability of the part for its intended use. An overview of selected relevant AM processes is presented in the following sections.

2.3.2 Additive Manufacturing Technologies

2.3.2.1 Stereolithography

SLA is a liquid based AM process commercialised by 3D Systems in 1987, and is argued to be one of the fundamental technologies developed with an additive based paradigm [139]. A photosensitive polymeric resin is selectively scanned and cured by a stationary ultraviolet (UV) laser which is directed by scanning mirrors according to two dimensional, *X*-*Y* plane, cross sectional slices from a 3D CAD model [145]. The energy from the UV laser penetrates into the photopolymer and causes it to solidify. Figure 2.17 displays a simplified schema of the process.

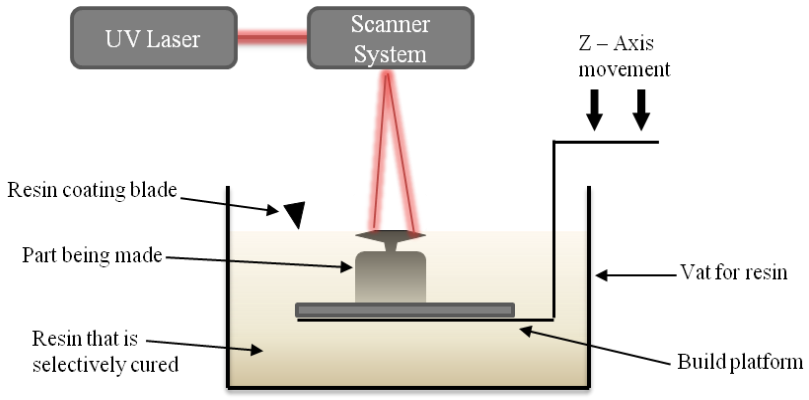

Figure 2.17: Schematic representation of the SLA process (adapted from [148])

After the cross section in question has been fully scanned by the UV laser, the build platform lowers in the Z-direction into the resin by the preset layer thickness, typically 100 μm [139]. A coating blade then ensures the even dispersal of a fresh layer of resin onto the build platform after which the next cross section is scanned and cured. This process is repeated until all the slices are completed and the 3D part is finished. All parts produced by SLA are placed in either a thermal or UV oven in order to ensure that any uncured resin is cured.

2.3.2.2 Three Dimensional Printing

The three dimensional printing (3DP) process, as currently commercialised by Z Corporation, originated out of research conducted at the Massachusetts Institute of Technology (MIT) in the early 1990s [149]. A process called drop-on-demand jetting technology, which closely resembles that of inkjet printing, selectively delivers droplets of binder fluid onto a powder bed. The binder then solidifies, creating the *X*-*Y* cross sectional geometry of the 3D CAD model in question [145]. A simplified schema of the process is presented in Figure 2.18.

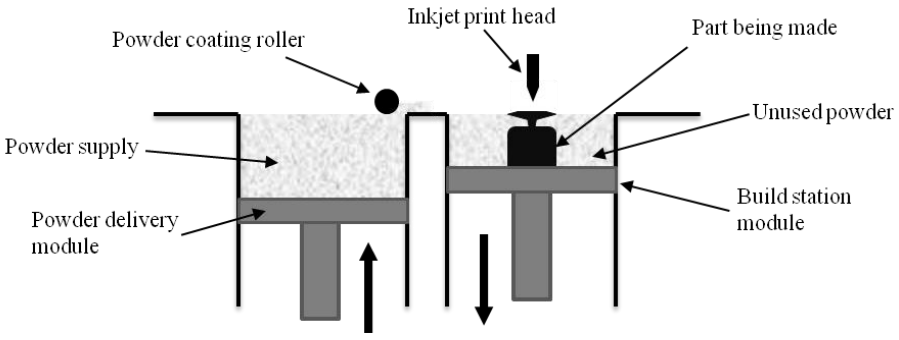

Figure 2.18: Schematic representation of the 3D Printing process (adapted from [139])

At the start of the build, the build station module lowers by the preset layer thickness which is typically in the region of 0.080 – 0.250 mm [150]. The powder delivery module rises to supply a fresh layer of powder which is evenly spread over the build chamber by a roller. A modified inkjet print head selectively traverse the powder bed, delivering binder droplets onto the profile of the layer in question. This process is repeated until all the layers, and consequently, the part is finished. Adequate time is then given for the binder to dry and harden before the part is extracted [145]. To add structural stability to the part, it can be infiltrated with various epoxies or wax material as part of post-processing [151].

2.3.2.3 Selective Laser Sintering

Selective laser sintering (SLS) was first patented by Ross Householder in 1979, but the process was only commercialised in the late 1980's as a result of development work at the University of Austin in Texas [139]. Similarly to 3D Printing, SLS produces three dimensional parts in a layered fashion. The SLS process, however, is capable of processing polymers, polymer coated-ceramics and metals. A simplified schema of the process is presented in Figure 2.19.

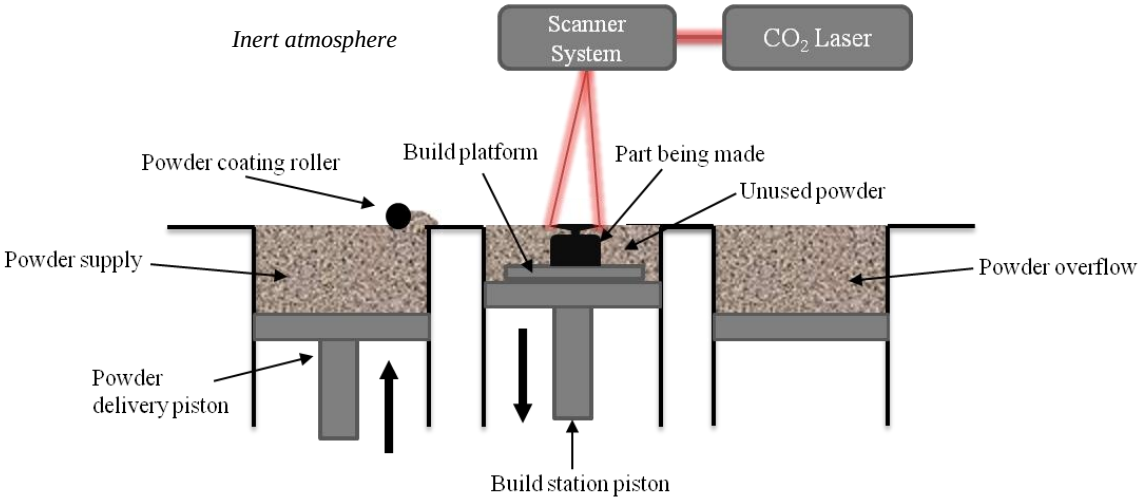

Figure 2.19: Schematic representation of the SLS process (adapted from [139])

Thermal energy supplied by a carbon dioxide (CO_2) laser is used to fuse powder particles together within a highly controlled environment. A system of scanning mirrors controls the focal points of the laser and guides it to selectively traverse the powder bed in order to fuse together the 2D profile of the layer in question. The build station then lowers by the preset layer thickness (typically 0.020 – 0.15 mm) and a powder coating roller evenly spreads a fresh layer of material before the next layer profile is scanned [152]. This process repeats until the full 3D CAD model is built. The powder is preheated inside the build chamber to just below the sintering temperature of the working material. This reduces the otherwise high thermal gradients between the non-sintered and sintered powder particles. Non-sintered powder particles serve as supports for the part. After build completion, the build station rises and the chamber needs to cool down uniformly before the part can be removed [145]. Metal parts however, are not fully dense after processing, and are similar to powder metallurgy parts in the green state. Post processing in a furnace is necessary to burn away the polymer coating, followed by bronze infiltration to complete the metallic part [139].

2.3.2.4 Electron Beam Melting

In contrast to 3D Printing and SLS, fully functional and nearly fully (> 99%) dense metallic parts can be created through EBM without the need for additional binder materials [153, 154]. An electron beam in a vacuum is utilised to melt the metal powders layer-by-layer [142]. A simplified schema of the EBM process is presented in Figure 2.20.

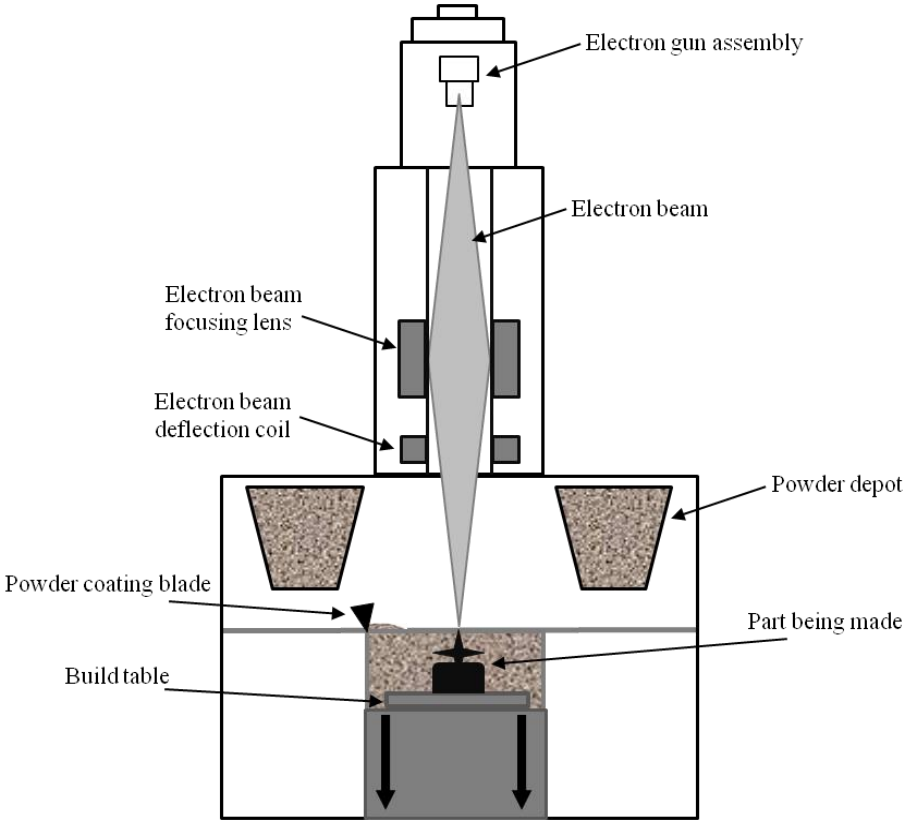

Figure 2.20: Schematic representation of the EBM process (adapted from [142])

In EBM, an electron gun supplies a focused electron beam. This is achieved through the emission of electrons when heating a tungsten filament in excess of 2500°C and the acceleration of these electrons by means of a high voltage difference [153]. The nominal operating voltage for the electron gun is 60 kV. The electron beam is positioned and controlled by the deflection coils in order to scan and melt the powder on a preheated table in order to fuse and create the specific slice in question [142]. Layer thicknesses for EBM can typically vary between 0.05 to 0.2 mm [153].

Energy for fusing the metal powder stems from the heat generated from loss in kinetic energy as the electrons crash into the metal powder [153]. Once a layer is completely scanned, the build table lowers by the layer thickness and a fresh supply of powder is deposited from the powder depots. A powder coating blade then moves across the build table to ensure an even spread of powder. The layer in question is again scanned by the electron beam and the process repeats for all layers until the part is complete. The whole build process is executed in a vacuum [142].

Depending on the needs and requirements of the intended use, various post processing operations can be performed on EBM parts. These can typically include, amongst others, both machining and heat treatment processes such as drilling, high speed milling, annealing [155] and hot isostatic pressing (HIP) [156].

2.3.2.5 Selective Laser Melting

Selective laser melting (SLM) is a relatively young manufacturing technology through which complex three dimensional near net shape metallic parts can be produced in a layer-by-layer approach [157]. During this process, thermal energy from a focused fiber laser beam is utilised to selectively scan, melt, and fully fuse metallic powder particles on a powder bed, creating near full density (> 99%) parts [158, 159]. In house studies have reported an achievable part density of up to 99.81 ± 0.1% for SLM processed Ti-6Al-4V ELI [160]. Figure 2.21 shows a simplified schema of the SLM process.

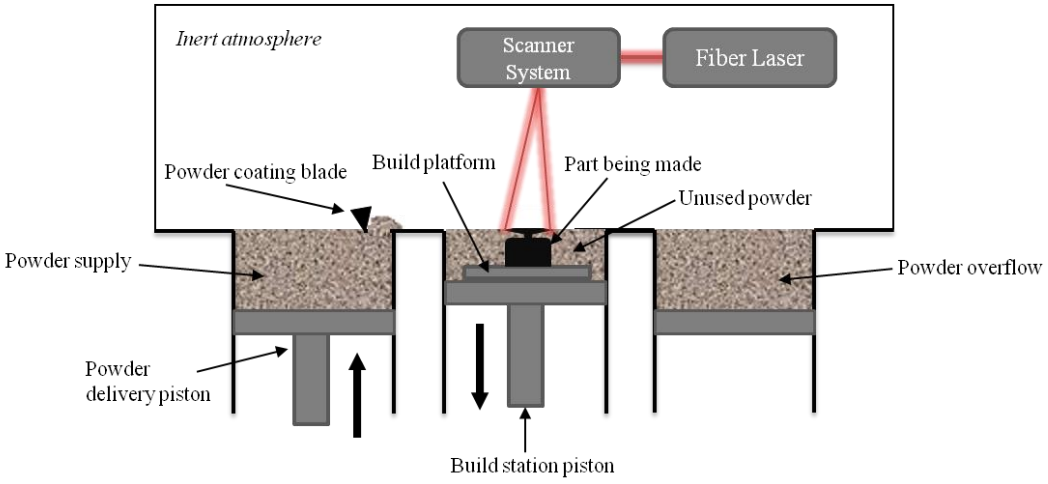

Figure 2.21: Schematic representation of the SLM process (adapted from [161])

The SLM process itself, utilises the same sequence as SLS for the basic principles of the layer wise, bottom-up building process (Figure 2.19), but in SLM, however, full melting of the metal powder is the goal [152]. This is achieved by heating the metal powder to beyond its melting temperature, in order to secure the full consolidation of the powder for creating the geometry of the two dimensional layer in question. The build platform then lowers by the preset layer thickness (typically 30 to 70 μm) [161]. A fresh layer of powder is deposited and evenly spread by the coating blade after which the next layer is scanned until all layers are consolidated and the part completed. An attractive characteristic of SLM is that the unused powder can be recycled and used in future builds [162].

To avoid oxidation of the metals, SLM needs a controlled, inert environment. This is achieved by flooding the build chamber with Nitrogen or Argon gas, depending on the metal alloy powder used. By doing so, the Oxygen content in the build atmosphere can be reduced to below 0.1% [146].

Post processing includes the removal of support structures, usually by mechanical means such as machining or manual chiselling (Figure 2.16). Depending on the specified requirements and intended application of the parts, further machining can be necessary in order to reduce surface roughness and heat treatment to tailor the microstructure and further reduce porosity [162, 163].

For the remainder of the document, the SLM process shall be referred to by the specific technology utilised in the study, which is the Concept Laser proprietary LaserCUSING®. The name stems from combining the words ‘fusing’ with the ‘C’ from ‘Concept Laser’ [164]. More specifics regarding to this process are discussed in Chapter 3 with accordance to manufacturing of the samples.

From Table 2.2 it was evident that a very significant percentage of the current commercial cementless stems are made from the Ti-6Al-4V alloy. Therefore, a Concept Laser Ti-6Al-4V ELI powder alloy is to be used for manufacturing of the samples.

2.3.3 Ti-6Al-4V ELI Powder

Grade 23 Ti-6Al-4V ELI is a material widely used for the manufacture of medical implants and devices. The acronym ELI stands for Extra Low Interstitial and it refers to a reduction in specified amounts of interstitial impurities in the lattice structure, specifically with regard to elements such as Iron (Fe), Carbon (C), and Oxygen (O) than the well known Grade 5 Ti-6Al-4V [142]. In this section the composition and some of the mechanical properties, as is applicable to the respective international standards on femoral stems, of the material are reviewed.

The international standard specifications for the chemical composition of Ti-6Al-4V ELI powder for powder bed fusion manufacturing processes is published by ASTM with designation F3001-13 [165]. The specified composition is presented in Table 2.9.

Table 2.9: ASTM standard specification for the composition of Ti-6Al-4V ELI for Powder Bed Fusion [165]

Element	***min***	***max***
Aluminium	5.50	6.50
Vanadium	3.50	4.50
Iron	...	0.25
Oxygen	...	0.13
Carbon	...	0.08
Nitrogen	...	0.05
Hydrogen	...	0.012
Yttrium	...	0.005
Other elements, each	...	0.10
Other elements, total	...	0.40
Titanium	remainder	remainder

2.4 Concluding Remarks

This chapter presented an integrated review of the different disciplines encompassed within the focus of the study. Some of the research sub-questions have also been addressed. These include the pathogenesis and mechanisms of chronic PJIs, some of the clinically approved drugs and commercially approved drug delivery products, and the positioning of the current study within the larger field of infection prevention strategies.

The multidisciplinary nature of the project is also evident, concerning medical, microbiological, pharmaceutical and additive manufacturing sciences. Combining elements from these sciences towards evaluating a new concept for infection prevention and treatment in cementless femoral hip stems is central to this study. It is especially important since a product, service or strategy cannot be developed without proper knowledge regarding the extent, conditions and environments surrounding its intended use. The relationships between the disciplines are summarised below in Figure 2.22.

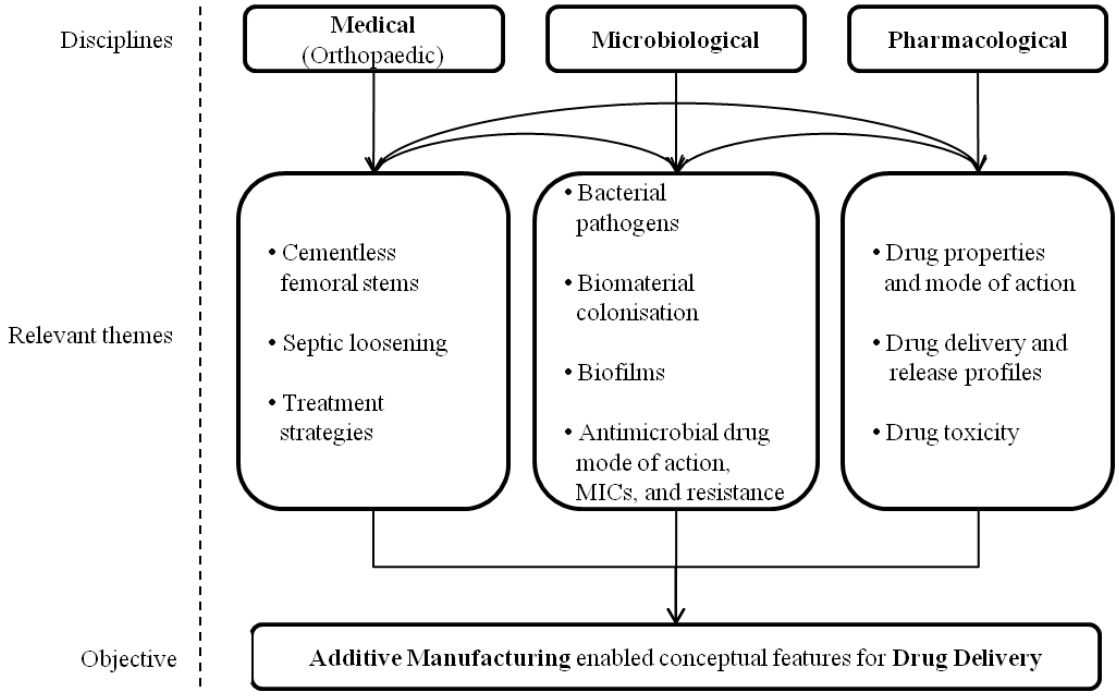

Figure 2.22: Schematic of interdisciplinary relationships

Further interactions within these relationships are also apparent in the remaining chapters during which the additive manufacturing and testing of the concept are evaluated and discussed.

3. Fabrication of Drug Delivery Samples

This chapter presents the establishment of the samples and conceptual features together with the manufacturing thereof samples by LaserCUSING®. The AM process chain as discussed in Section 2.3.1 was applied throughout the manufacturing phase.

3.1 Establishment of Conceptual Features

For the design of these conceptual features, different zone of inhibition (ZOI) studies, which all included Palacos R+G, were used as guidelines and are summarised in Table 3.1. ZOI values have been converted to area for application to the current study, with the zone widths of the respective studies in parentheses. It is important to note that the reported results are specific to the conditions present in each respective laboratory which cause variability.

Table 3.1: Reference studies on Palacos R+G ZOI testing

Reference	*Disc Dimensions (Ø x h) [mm]*	*Disc Surface Area [mm²]*	*S.aureus Strain*	*ZOI after 24 hours [mm²] (width [mm])*
Ensing *et al* [108]	6.0 x 3.0	113.10	7323	≥ 587.48 (11.0)
Meyer *et al.* [166]	9.6 x 3.25	242.78	ATCC 6538P	500.17 (8.7)
Miola *et al.* [167]	10.0 x 5.0	314.16	ATCC 29213	776.76 (13.5)
Thompson *et al.* [168]	9.7 x 3.3	248.36	ATCC 6538P	469.36 (8.3)
Ferraris *et al.* [169]	10.0 x 4.0	282.74	ATCC 29213	628.32 (10.0)

It was deduced from Table 3.1 that the size range of the discs tested did not have a large effect on the antibacterial efficacy. One would have to scrutinise the details and differences in mixing techniques, elution protocols, environmental conditions and *S.aureus* strains to better account for the variability, which was not the purpose here. Rather, the features to utilise in this study should be based on dimensions that would typically fit into an actual femoral stem. To this extent, the most suitable geometry for analogy and subsequent incorporation was found in the study by Ensing *et al.* [108] who reported on the antimicrobial efficacy of discs with 6mm diameter and 3mm thickness. Based on this, a revised concept model to the one in Figure 1.1 was developed. The main feature from the concept model was isolated for samples to be manufactured. This process is depicted in Figure 3.1.

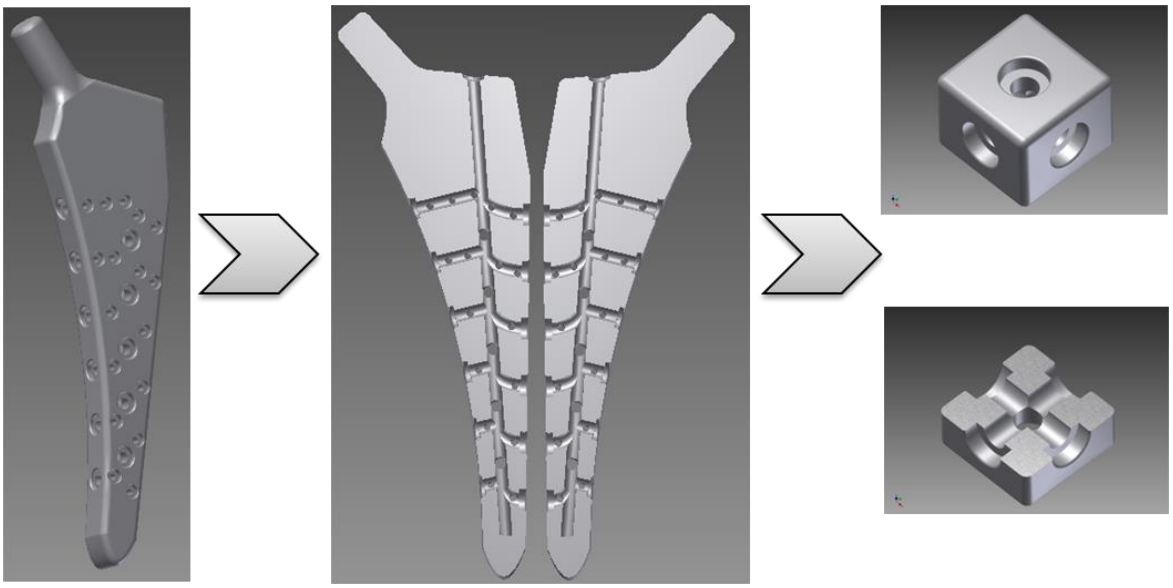

Figure 3.1: Isolation of main conceptual feature from the larger stem

The extracted samples are 15 mm by 15 mm by 12 mm with 3.5 mm diameter internal channels centred on and perpendicular to each of the six surfaces. These details regarding the sample are presented in Figure 3.2. Since the burst effect of ALBC elution is mainly a surface phenomenon, each channel opens at the surface of the sample with a 6mm diameter by 2mm deep disc geometry to avail a larger surface area for gentamicin elution [41].

Channel openings of these dimensions enable the possibility for expected results. Since Palacos R+G is a highly standardised product, the ZOI should be at least 587.48 mm^2 after 24 hours, but is expected to be greater due to the higher amount of gentamicin that should release in the burst phase because of the six release surfaces in the concept instead of only one as in the literature.

Towards maintaining a conservative design, the size of the sample had to be such that the bacterial growth boundary of the lower limit of the widths of ZOIs reported by Ensing *et al.* [108] after 24 hours (11 mm) would not traverse any of the edges. This is shown in Figure 3.3. In a full scale prototype the channel openings should also be spaced such that the entire surface area between the openings would be accounted for in preventing bacterial colonisation.

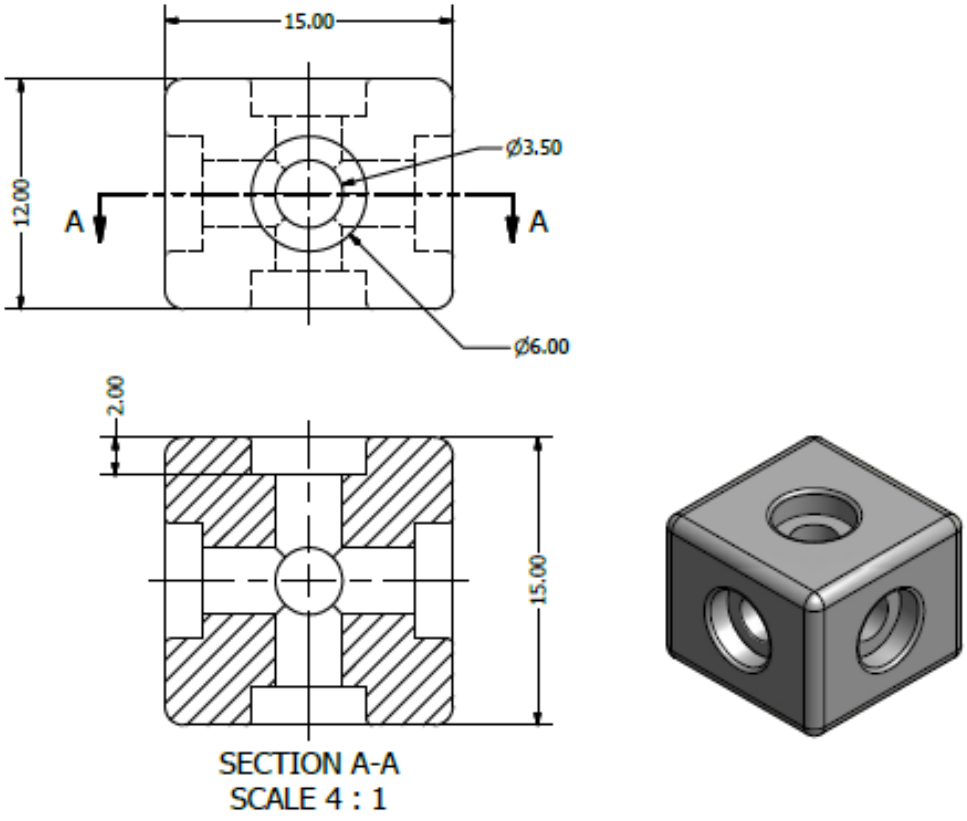

Figure 3.2: Detailed drawing of the samples with the conceptual features

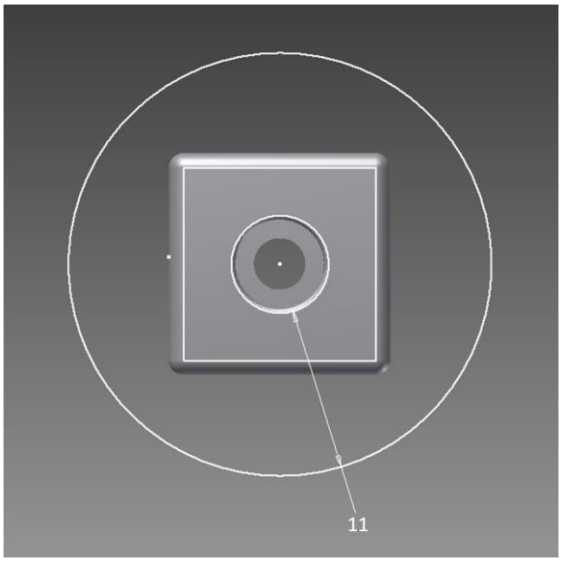

Figure 3.3: Sample size in relation to a reported lower limit of ZOI width of 11 mm after 24 hours from Palacos R+G discs with similar dimensions

3.2 Manufacture of Samples

All samples were manufactured on the Concept Laser M2 cusing system (Figure 3.4) from Ti-6Al-4V ELI powder (Concept Laser designation CL 41TI ELI). The powder has a rated particle size distribution of 38 μm to 55 μm and is specified by Concept Laser to meet the ASTM requirements

Figure 3.4: Concept Laser M2 cusing system

Conceptual 3D models were developed in *Inventor Professional 2011* (Autodesk) and exported as a STL file with the built in STL generator. The file was imported into *Magics 15.0* (Materialise) for pre-processing and build file creation. The STL file was generated accurately and no errors were present that needed repair. Part orientation was set directly on the build plate at an angle of 45 degrees to reduce the number of channels that would have to be built parallel to the build plate. No support structures were necessary within the channels as they are all less than 8 mm in diameter as specified in the machine manual. The build file was created with a slice thickness of 30 μm. The build file was loaded onto the machine software for part placement and process parameter selection. Parts were placed at an angle towards the coating blade to ensure an even spread of powder over the geometry of each two dimensional slice. Figure 3.5 a) shows the 45° orientation of the samples towards the horizontal and Figure 3.5 b) shows the part angled towards the coating direction which is indicated with the black arrow.

(a) **(b)**

Figure 3.5: Manufactured samples on build plate with a) revealing the 45° part orientation towards the horizontal and b) the angular orientation of the parts towards the coating direction of the powder coating blade, indicated by the arrow (parts other than the reservoir samples were built for a different study)

Default processing parameters for Ti-6Al-4V ELI were used for LaserCUSING® of the samples. These parameters are 100 W laser power, 600 mm/s scanning speed, and 30 μm layer thickness, were used for the processing of the samples. A screen shot of the parameters are presented in Figure 3.6.

The layers of powder are scanned by the laser in 5 mm x 5 mm islands oriented perpendicular to each other. The hatching pattern is set to single vectors parallel to one another inside the island with spacing between the vectors (indicated as 'a1' in the 'fill vectors exposure' section of Figure 3.6) fixed at 0.7 of the laser diameter (150 μm). This implies that each of the molten tracks inside the islands overlap with 45 μm to enhance full melting of the powder during the process. There is also a scanning overlap between the islands of 0.15 times the laser diameter, designated as 'a2' in the 'fill vectors exposure' section of Figure 3.6. The outer geometry of each layer has a contour scan along its edge before a new layer of power is coated.

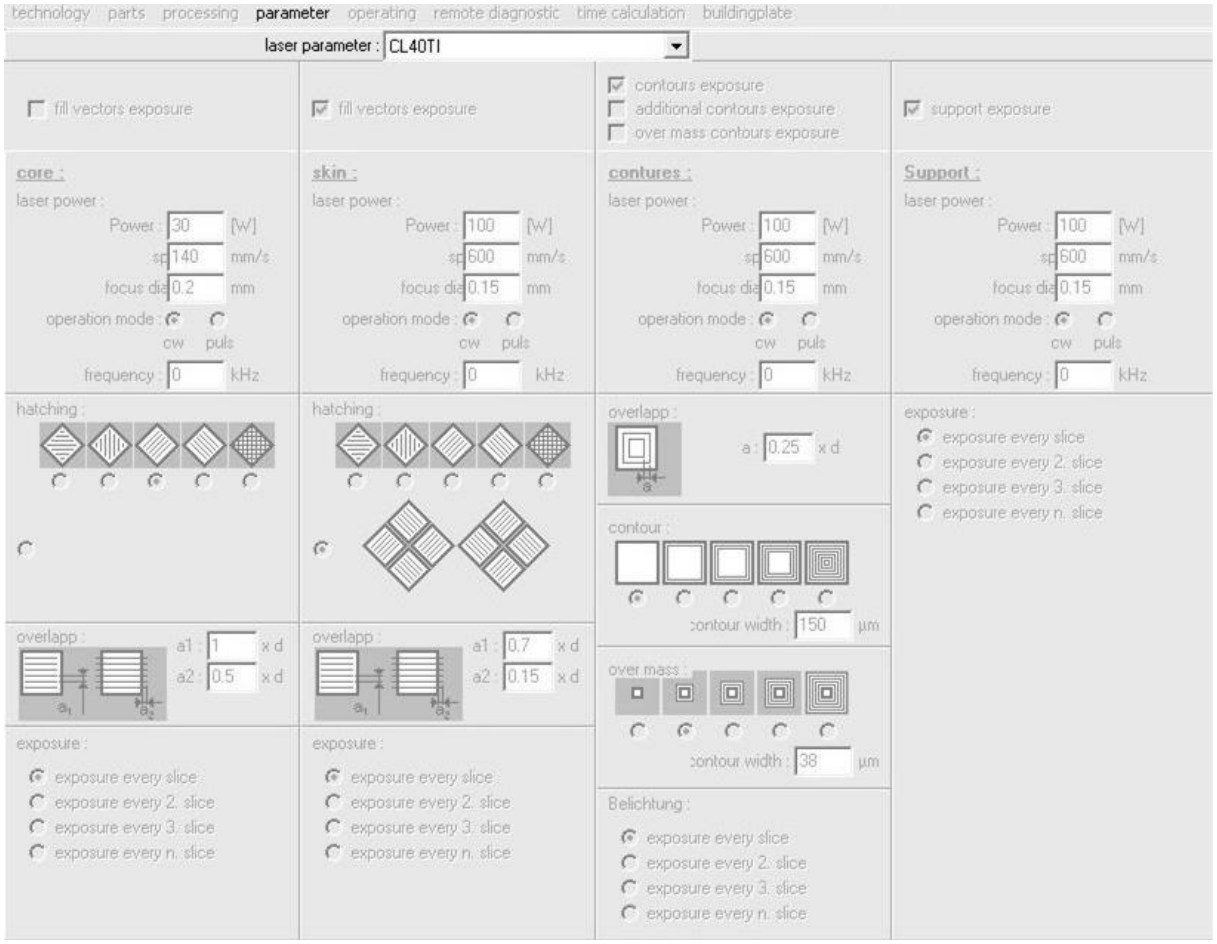

Figure 3.6: Screen capture of process parameters used for LaserCUSING® of samples

3.3 Post-processing of Samples

Samples were removed from the build plate by third party wire-cutting and numbered in a random order upon return from third party removal. Unconsolidated powder particles were manually removed by blasting the samples with a pressurised air gun.

4. Pilot Study for Prophylaxis

The aim of the pilot study was to evaluate the feasibility of the concept for colonisation prevention through antimicrobial elution from a commercial ALBC embedded within the surface of Ti-6Al-4V samples manufactured by LaserCUSING®. Another aspect also investigated was whether Palacos R+G could be used as a type of permeable material when mixed by hand without the application of specialised mixing and preparation techniques.

4.1 Mixing and Introduction of Antibiotic Loaded Bone Cement (ALBC)

The commercial ALBC, Palacos R+G loaded with 12.5mg/g gentamicin, was prepared under atmospheric pressure as per manufacturer's instructions in a monomer-to-polymer ratio of 1 ml to 2 g [170]. With a density for MMA of 0.94 g/cm^3, a 1 ml (or 1 cm^3) to 2 g ratio yields a polymer proportion of $P_{Polymer}$= 2/2.94 =0.68027. The parts were mixed in an Eppendorf tube with a spatula for 30 seconds until cement became doughy and was left for one minute. The mixed cement was then used to manually fill the channels of the samples during the application phase of the cement. The ALBC was left to set inside the samples. Protruding cement was filed down with a sterilised file.

The mass of Palacos R+G loaded into each of the samples, $M_{Palacos\ R+G}$, was determined by averaging the mass of each sample weighed five times on an analytical balance (Sartorius BP110S) before and after Palacos R+G introduction and subtracting the initial mass from the mass after loading. The mass of gentamicin loaded into each sample, $M_{gentamicin}$, was then theoretically approximated by multiplying the mass of Palacos R+G by the constituent polymer proportion, $P_{Polymer}$, and then with the gentamicin proportion, $P_{Gentamicin}$, contained within the polymer powder. It is shown below in Equation 4.1 in which the values for the polymer and gentamicin proportions are 0.68027 and 0.0125 respectively.

$$M_{gentamicin} = M_{Palacos\ R+G} \times P_{Polymer} \times P_{Gentamicin} \tag{4.1}$$

The eventual aim is to create a drug delivery scenario that enables the possibility for utilising the channels as a reservoir from which drugs can be administered. To this extent, an appropriate permeable material is necessary to close off the openings of the channels. PMMA is known to be hydrophobic, but aqueous fluids can penetrate into the cement through imperfections in the

polymer matrix such as cracks and voids [41]. The challenge, however, is to obtain an interconnected porosity that would allow fluids to move through the polymer matrix.

To investigate the effect of monomer-to-polymer mixing ratio on the PMMA porosity, three bone cement cylinders for each of three different monomer-to-polymer volume [ml] to weight [g] ratios (1:2; 1:1.5; 1:1) were made and CT-scanned (General Electric Phoenix VTOMEX L240) at a 10 μm resolution. CT-scans were analysed by the CT-scan group for porosity with *VGStudio Max 2.1* (Volume Graphics). The graphical analyses were reviewed and the solid parts of the material removed with *myVGL 2.2* (Volume Graphics), which is a viewer only version of the *VGStudio* software. The application of ALBC in this study is purely for drug delivery and serves no function in fixation, and therefore, the effects of monomer-to-polymer mixing ratios on the mechanical properties are not relevant.

4.2 t- Test Statistics

To evaluate the significance of different porosity percentages for the varied monomer-to-polymer mixing ratios, two-tailed Student t-tests (assumed equal variances) for independent samples were performed. The sample size for each ratio was three and the significance level was $\alpha = 0.05$ (reject if $p < 0.05$). The null hypothesis was set that the samples are from the same population and that there is no significant difference in the resultant porosities. That is, for each of the three comparison combinations:

$$H_0: \mu_1 = \mu_2$$
$$H_1: \mu_1 \neq \mu_2$$

Therefore, failing to reject the null hypothesis would mean that the mixing ratios selected have no significant influence on the resultant porosity.

4.3 Gentamicin Antibacterial Efficacy

The efficacy of a colonisation prevention strategy for delivering drugs in high enough concentrations to thoroughly maintain the bactericidal effect has to be evaluated in order to be able to prove that the strategy is a feasible concept. The initial testing should therefore be economic and not resource intensive. To this extent, a modified Kirby-Bauer disk diffusion method is a suitable test to be utilised in a semi-quantitative manner [171]. It allows for measuring the area of the zones of bacterial growth inhibition around the biomaterial samples, caused by the elution of gentamicin from the ALBC embedded within the samples [166, 172]. Since this type of test is typically used for determining antibiotic susceptibility of pathogens, it is modified in the sense that it is not used to test whether an organism is susceptible, but rather if an organism with known susceptibility can be prevented from colonising the biomaterial surface [171, 173]. It therefore allows for quantification of bacteria free areas around the biomaterial, as well as for the time period that colonisation can be prevented. By executing this experiment, the feasibility of the concept could be evaluated economically and in a relative short time frame.

4.3.1 Modified Kirby-Bauer Diffusion Test

The preparation and inoculation of *S.aureus* Xen 36 and *S.aureus* Xen 31 for antimicrobial testing was conducted by A.D. van Staden at the Lactic Acid Bacteria and Antimicrobial Peptide Taxonomy Laboratory of the Department of Microbiology at Stellenbosch University. The text in this section is adapted from that of Mr. van Staden as was contributed towards a research paper.

Samples to be loaded with Palacos R+G were sterilized before use by autoclaving at a temperature of 121°C and a pressure of 100 kPa for 15 minutes. The samples were then also subjected to short wavelength (254 nm) UV sterilization for 30 minutes**.** *S.aureus* Xen 36 and *S.aureus* Xen 31 (Caliper Life Sciences) were grown in brain-heart infusion (BHI) broth (Biolab, Merck) which were supplemented with 200 μg/mL kanamycin (Sigma Aldrich), at 37°C for 24 h. Kanamycin is an aminoglycoside antibiotic added to kill possible contaminating bacteria, but does not affect either of the *S.aureus* strains since they are both resistant to kanamycin.

The samples loaded with ALBC were aseptically placed in a Petri dish (150 mm x 25 mm) on top of a thin, sterile BHI agar (Biolab, Merck) base that was pre-introduced into the Petri dish. BHI agar seeded with 0.1% (v/v) *S. aureus* Xen 36 or Xen 31 were used to completely cover the samples (Figure 4.1) and incubated at 37°C for 24 h.

After incubation, 10 megapixel digital images were taken of the ZOIs to monitor the antimicrobial efficacy. The samples were then aseptically removed, lightly washed with 70% ethanol (v/v) and left to dry.

Samples were then transferred to a fresh Petri dish containing a BHI agar base and again completely covered with BHI agar seeded with 0.1% volume/volume (v/v) *S. aureus* Xen 36 or Xen 31 and incubated at 37°C for 24 h. This was continued until no visible zones of inhibition were observed around the samples. The BHI agar base and seeded BHI agar were supplemented with 1% weight/volume (w/v) agar to ensure sufficient bacterial growth, 0.001% (w/v) cycloheximide (Sigma Aldrich) to avoid fungal contamination and 200 µg/mL kanamycin at each time point. *S. aureus* Xen 36 and *S.aureus* Xen 31 were freshly inoculated each day for agar diffusion assays. A control sample without any Palacos R+G was also prepared in the same manner. Samples were done in triplicate and the area of the inhibition zones was measured from the images using *ImageJ*.

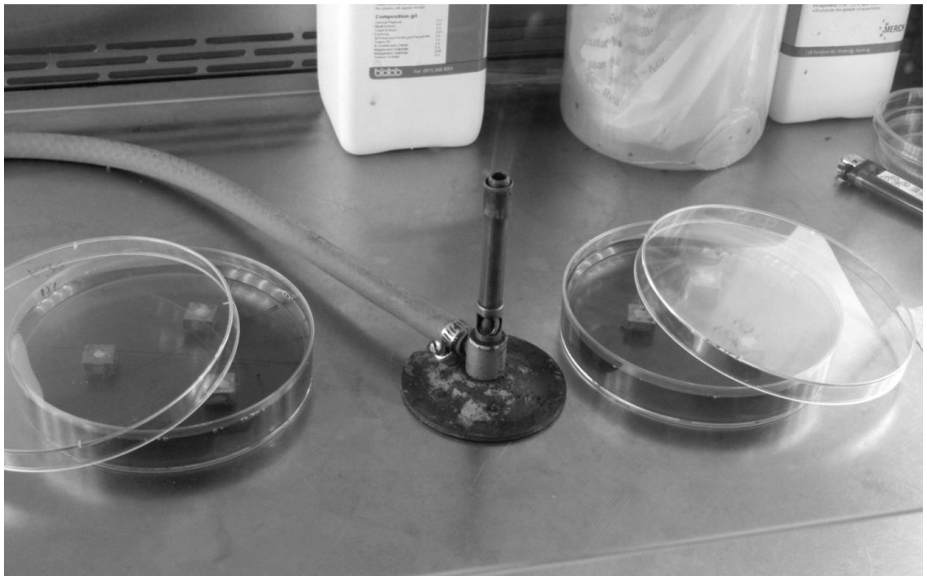

Figure 4.1: Orientation of samples introduced into the agar inoculated with *S.aureus* Xen 36 and *S.aureus* Xen 31 respectively

4.3.2 Zone of Inhibition Measurement

ImageJ is software developed by the NIH in the USA, and is widely used for image processing and analysis. The results of the measurements from *ImageJ* were copied to *MSExcel* where it was organised and further processed. Ten measurements from each of two photographs from the bottom view of the Petri dishes were used for calculating the average ZOI per 24 hours interval. The measuring process is discussed in more detail in the following sections.

4.3.2.1 Calibration of Scale using Pixels

Before any measurements can be made it is necessary to calibrate the software according to known distances in the image. It is therefore important that images be taken as perpendicular as possible to eliminate discrepancies in lengths resulting from photographic perspective. This can easily be evaluated by measuring more than one known distance in the depth of the photograph where the plane of interest is. The plane of interest was selected to be level with the horizontal surface of the sample from the bottom direction of the Petri dish. Since it is known that the sample sides on this surface are each 15 mm, it was used as standard for calibration of the software. The scale was set by using the line selection and drawing a line as accurately as possible across the sample and then using the *set scale* tool to specify the distance for the amount of pixels. Figure 4.2 shows a screen shot of the procedure. The ruler in the picture only serves as a rough guide to give a measure of perspective, but cannot be used for accurate calibration since it does lie within the plane of interest.

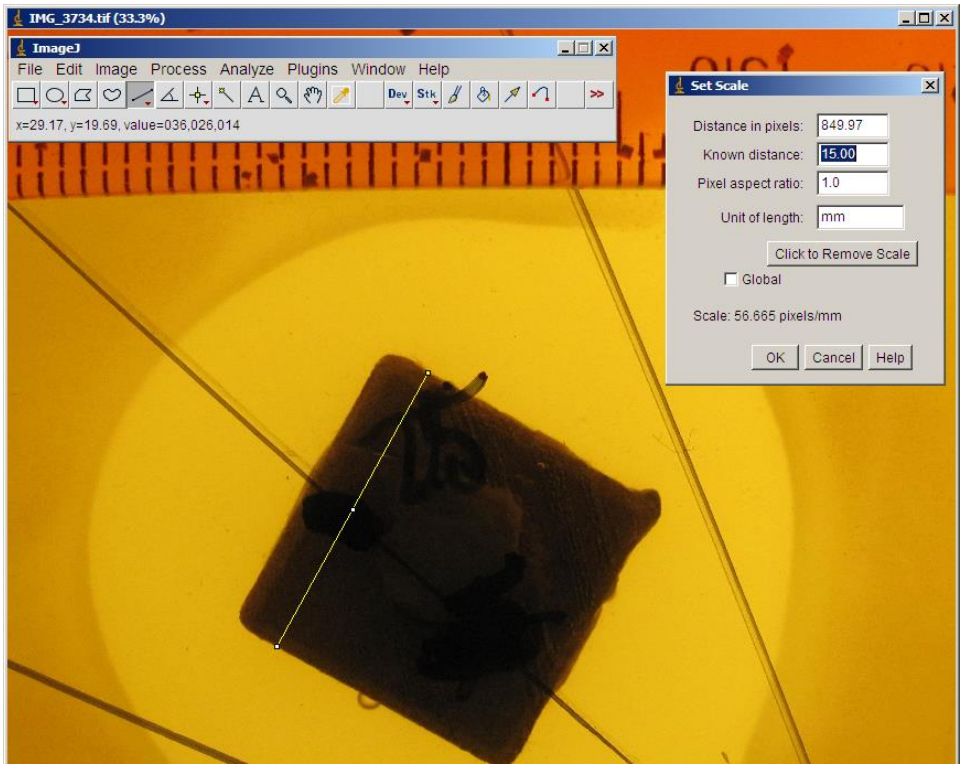

Figure 4.2: Calibration of ImageJ for ZOI measurement

The calibration was first tested by measuring random widths across the surface as well as measuring the surface area of the sample. Only if repeated measurements yielded results very close to the theoretical values (15 mm sides and 225 mm^2 surface area) was the calibration deemed sufficient for ZOI measurement. This is shown in Figure 4.2. The numbers imposed on the lines in Figure 4.3 is for reference to correlate with the measurements in the "Results" window except for "C" which denotes the line used for scale calibration. From the results it can be seen that the test measurements are very close to the known values. Therefore, the average of 20 measurements for each sample was used to reduce these user-induced inaccuracies which cause the measurements to be slightly greater or less than the known theoretical values.

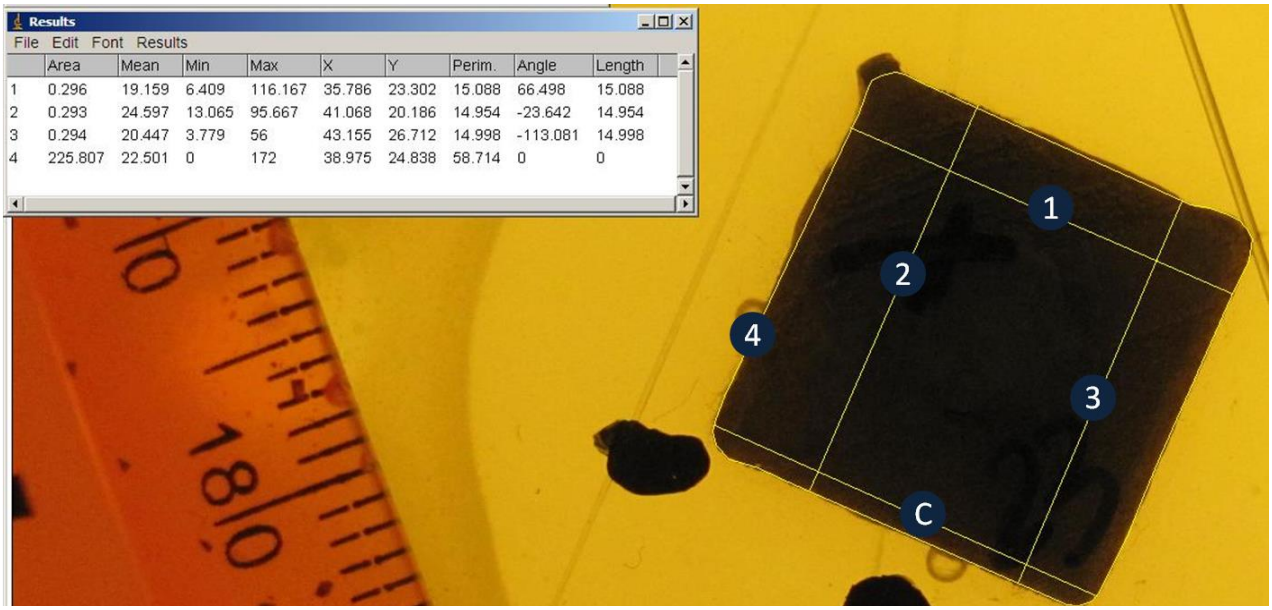

Figure 4.3: Test measurements with known distances to ensure satisfactory calibration

4.3.2.2 Image Adjustment for Definition

The next step was to use the image adjustment tools in order to obtain a visually more clear definition of the ZOI borders. This was especially necessary for the resistant *S.aureus* Xen 31 strain to determine whether the samples were reached within 24 hours and it also became necessary for the susceptible *S.aureus* Xen 36 at later times as the released amount of gentamicin declined and the bacteria neared the samples. A typical example of the image adjustment and subsequent elucidation of the ZOI is presented in Figure 4.4 with (a) the original and (b) the adjusted image. The adjusted image reveals without doubt the ZOI boundary. This was specifically important to establish whether the bacteria reached the samples. The example presented in Figure 4.4 was also selected to convey this importance. Only once the images were adjusted to clearly identify the ZOIs could the measurements be made. In either case, the measurements were made conservatively.

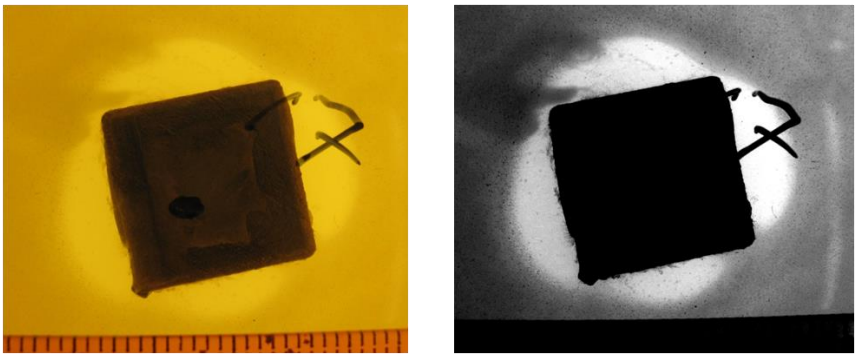

(a) **(b)**

Figure 4.4: Elucidation of ZOI boundary through image adjustment in *ImageJ* with ZOI boundary obscured in a) and clearly visible in b)

4.3.2.3 Measuring the ZOI

The polygon selection tool was used as shown in Figure 4.5 to trace the visible ZOI carefully and the complete area within the zone was measured. Repetitions were made from images cleared of previous traced polygons to avoid biased measurements based on the polygonal selection of the previous measurement. Furthermore, since the interest is on the bacteria free area, and when bacteria reaches any part of the surface it flags a failure, the theoretical surface area of each sample (225 mm^2) was subtracted from its respective measured ZOI.

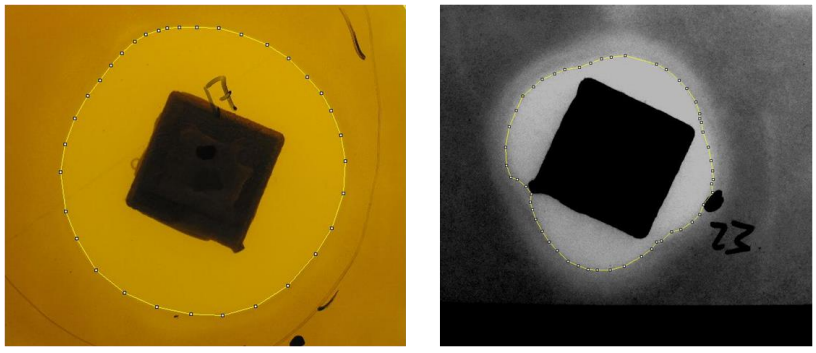

a) **b)**

Figure 4.5: ZOI measurement in *ImageJ* when bacteria free zones were obvious a) and when zones became less obvious b)

5. Prophylactic Proof of Concept – Results Assessment

5.1 Antibiotic Loaded Bone Cement Introduced into Samples

The calculated weight of gentamicin loaded into each sample is shown in Figure 5.1. Samples 1, 9, and 16 were used for testing with *S.aureus* Xen 31 and samples 17, 23, and 25 for *S.aureus* Xen 36.

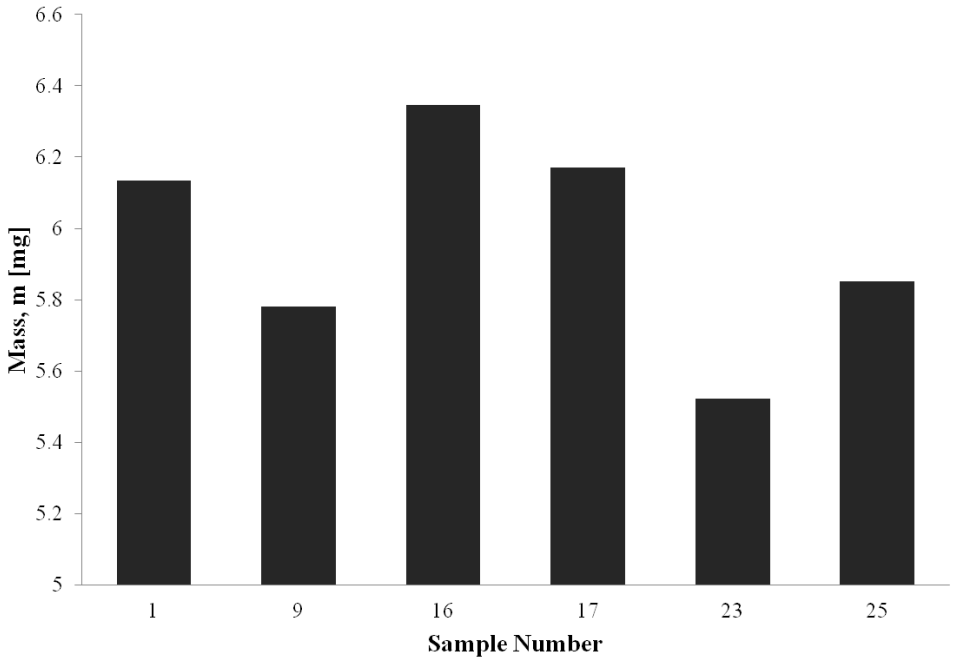

Figure 5.1: Calculated mass of gentamicin loaded into each sample for colonisation prevention testing

The minimum amount loaded was 5.522 mg for sample 23 and the maximum 6.346 mg for sample 16. The range is therefore 0.824 mg with mean and standard deviation of the loaded gentamicin 5.968 ± 0.3 mg. This reveals that even though the manual introduction of the bone cement was rather unrefined, the amount of gentamicin achieved within each sample does not vary much and the samples were reasonably uniformly loaded. The rest of the manufactured titanium alloy drug delivery samples were reserved for reservoir release pilot- and full scale experiments.

5.2 Bone Cement Monomer to Polymer Ratio

A three dimensional rendering of the CT-scan images from the different monomer-to-polymer ratios are presented in Figure 5.2. From top to bottom the rows represent the mixing ratios 1:1, 1:1.5, and 1:2 respectively. From left to right the columns show independent study units within each mixing ratio.

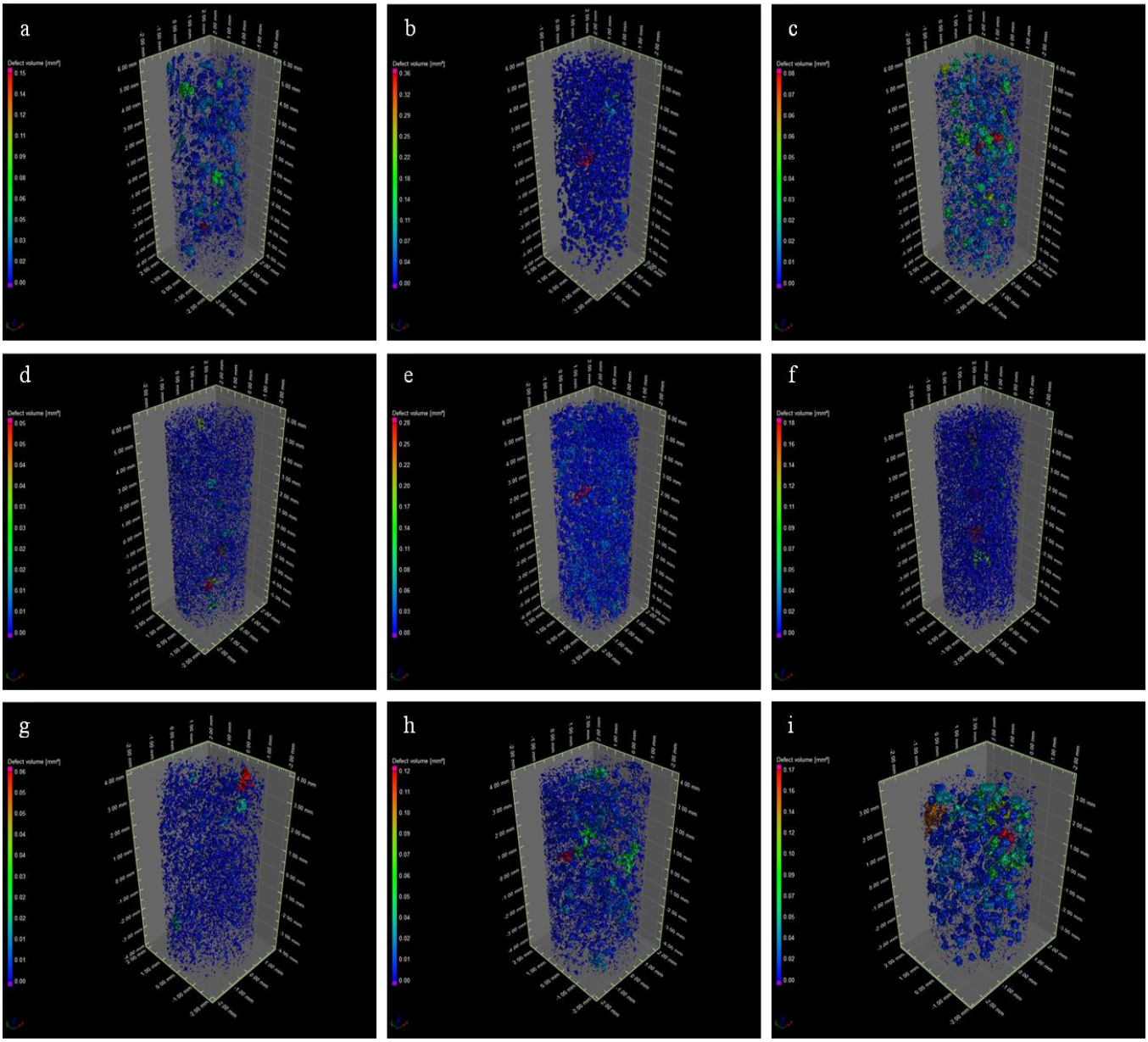

Figure 5.2: CT-scan images of porosity distributions from different monomer-to-polymer mixing ratios, a-c) 1:1, d-f) 1:1.5, g-i) 1:2

The solid material was removed from view in Figure 5.2 with the software and the three dimensional arrangement of the full collection of detected voids within each study unit is presented. A summary with regard to the resulting porosities for each mixing ratio of the independent units is presented in Table 5.1. From Figure 5.2 and Table 5.1 it would appear that the porosity is relatively random distributed throughout the samples and that the mixing ratio does not significantly influences the average porosity of the bone cement cylinders.

Table 5.1: Porosity for different monomer-to-polymer (MM-to-PM) ALBC samples

MM-to-PM Ratio [ml:g]	***Average Sample Volume Scanned [mm3]***	***Average Relative Porosity [%]***
1.0:1.0	159.64	2.82
1.0:1.5	166.20	3.01
1.0:2.0*	103.02	2.61

* *This is the standard mixing ratio specified in the manufacturer's instructions*

The t-test output from *MSExcel* integrated function was compared to a manually calculated t-test for each of the comparing groups. The procedure, as described by Montgomery & Runger [174], and *MSExcel* screenshots are presented in Appendix A. The Student t-tests, shown in Table 5.2, have revealed that there is no evidence to reject the null hypothesis (all study units are from the same population, stated in Section 4.2) with extremely large p-values ($p = 0.8$ for ratios 1:2 and 1:1.5; $p = 0.84$ for ratios 1:2 and 1:1; $p = 0.89$ for ratios 1:1.5 and 1:1).

Table 5.2: t-Test results from comparing porosities

Ratios Compared	***t-critical (two-tailed)***	***t-calculated***	***P-value***
1.0:2.0 and 1.0:1.5	2.776	-0.269	0.8
1.0:2.0 and 1.0:1.0	2.776	-0.217	0.84
1.0:1.5 and 1.0:1.0	2.776	0.142	0.89

Another important aspect that is revealed by the CT-images is that there is very little interconnected porosity, and that the pores are mostly isolated, individual defects within the polymer matrix. Figure 5.3 shows a CT scan of a sample loaded with ALBC. It reveals the lack of interconnectivity between the pores. A detailed investigation into the specifics regarding the chemistry of the polymerisation process and elongation phase of the polymer chains could possibly elucidate these observations, but falls beyond the scope of this study. Either way, it reveals the inability of this commercial ALBC to act as a membrane without any specialised moulds or mixing techniques, such as the addition of chitosan particles which creates voids as it diffuses from the matrix. Therefore nanoporous membranes were investigated for release of reinforcement antibiotics from within the sample reservoir. This is discussed in Chapters 6 and 7.

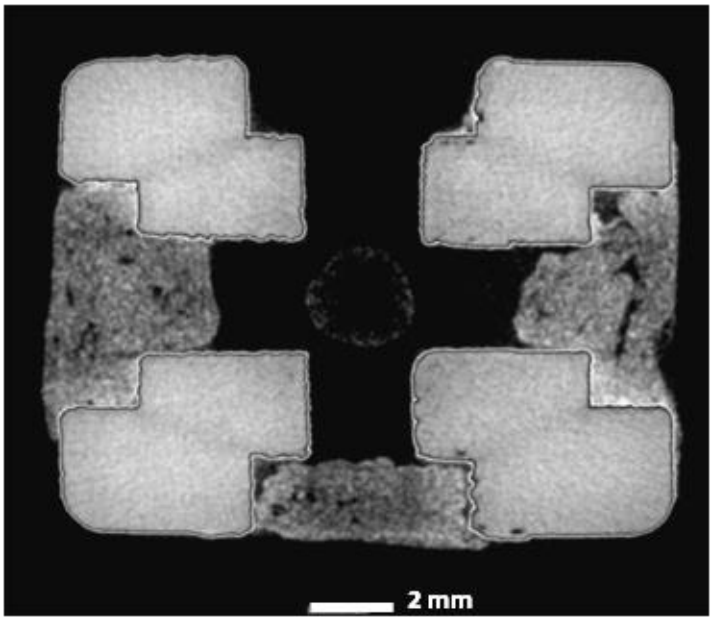

Figure 5.3: CT-scan of a sample loaded with ALBC revealing random and non-interconnected porosity in the PMMA matrix

5.3 Antimicrobial Efficacy

The test was carried out until no inhibition zones were visible anymore, that is 360 hours for *S.aureus* Xen 36 and 48 hours for *S.aureus* Xen 31. Failure to prevent colonisation was however, defined for the moment bacteria reached the titanium-alloy surface. These times were 72-96 hours for *S.aureus* Xen 36 and less than 24 hours for the gentamicin resistant *S.aureus* Xen 31.

Samples were expected to present ZOIs of at least 587.48 mm^2 after 24 hours (Section 3.1) against the gentamicin sensitive *S.aureus* Xen 36 strain. The resultant average zone areas are presented in Table 5.3 with the accompanying measured data in Appendix B, from where it can be seen that this has been achieved.

Table 5.3: ZOI [mm^2] for samples challenged with *S.aureus* Xen 36

	Time [Hours]			
	24	***48***	***72***	***96***
Sample 17	693.15	258.70	239.83	161.30
Sample 23	784.04	254.07	330.48	201.41
Sample 25	695.48	240.00	169.50	122.81
Mean ± SD[a]	724.22 ± 51.82	250.92 ± 9.74	246.60 ± 80.70	161.84 ± 39.30

[a] *SD denotes Standard Deviation*

Images of the collective view of the ZOI after 24, 48, 72, and 96 hours for these three samples are presented in Figure 5.4, in which the zones are clearly visible around the samples. The high reduction in zone areas from 24 to 48 hours is typical for the burst release of these cements. This observation can be made based on the transferral to a new Petri dish, replacement of the entire agar volume and a fresh inoculation of *S.aureus* Xen 36 after each 24 hour interval, thereby removing traces of gentamicin that was released from the embedded Palacos R+G during that interval before the next 24 hour period. Sustained release at lower concentrations can be witnessed for the rest of the periods, with the concentrations declining to below effective inhibitory concentrations towards 96 hours. Bacteria reached sample 25 after 72 hours and all the samples after 96 hours. One specific reason for this was not identified, but rather a multitude of factors can play a role such as the positioning of the antibiotic crystals within the bone cement matrix, the formation or lack of cracks and voids through which the dissolution medium could penetrate the cement, the growth rate of bacteria in the specific vicinity of the sample and even

possible convective elements transporting bacteria towards the sample. When zones became visually obscure, as with Figures 5.4 c) and d), images were further adjusted to unveil whether the surfaces have been reached

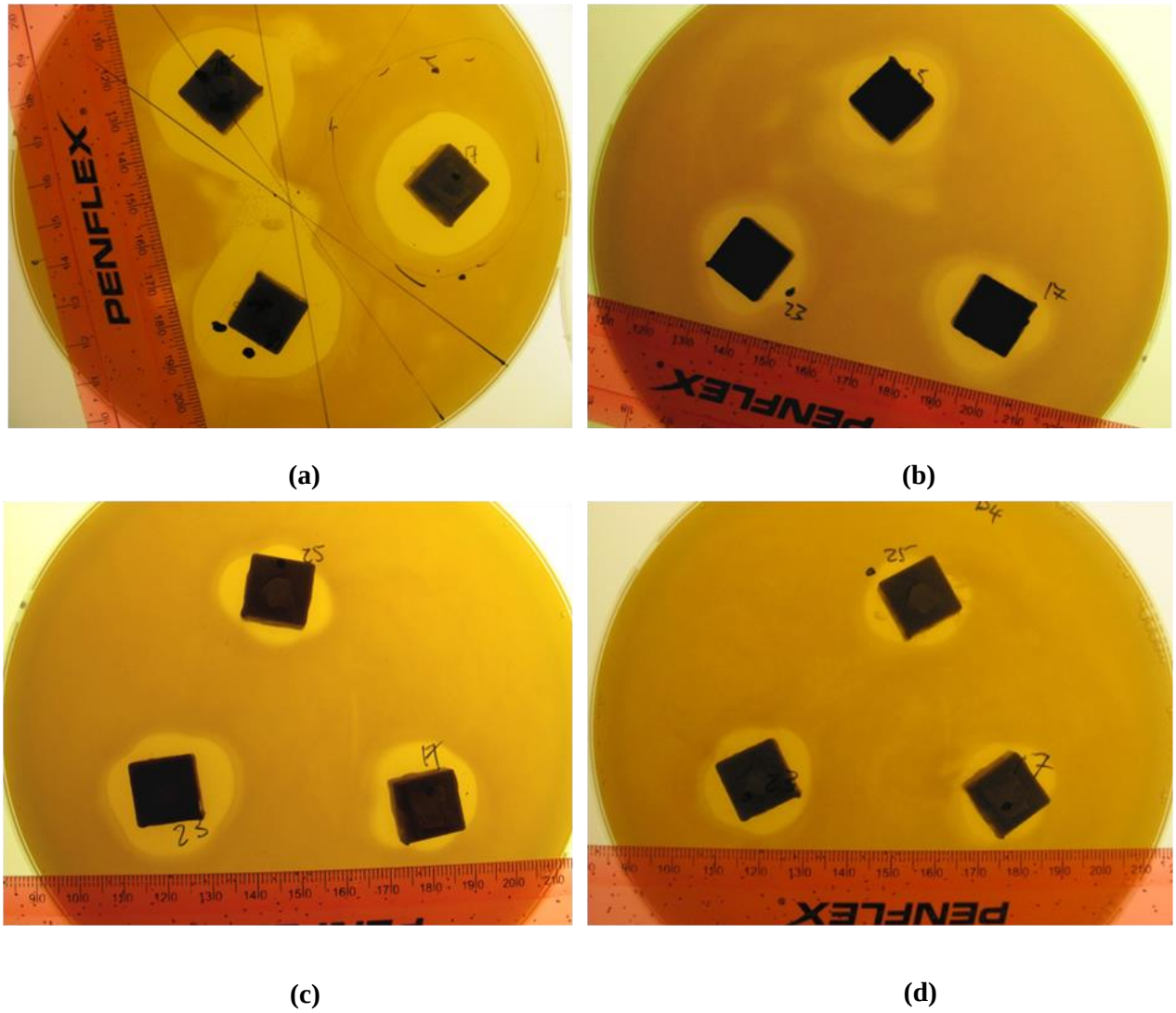

Figure 5.4: Collective view of ZOI against *S.aureus* Xen 36 after a) 24 hours b) 48 hours c) 72 hours and d) 96 hours

The effect of adjusting the images with *ImageJ* can be seen in Figure 5.5. For example, in Figure 5.4 (d) it is difficult to distinguish whether sample 23 (bottom left sample in the image) is reached or not. When the perpendicular images, however, are adjusted and used for analysis it becomes evident that sample 23 (Figure 5.5(b)) was indeed reached, as indicated with the circles, hence signalling a failure.

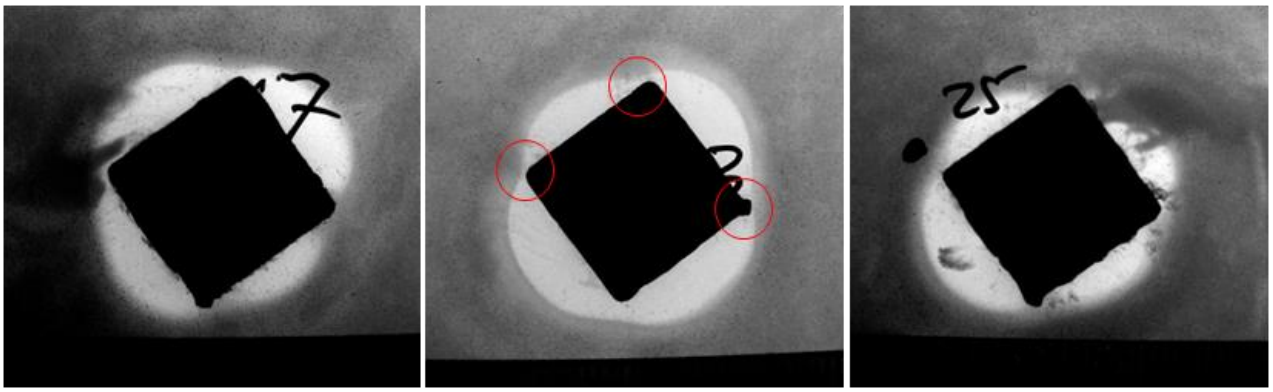

(a) **(b)** **(c)**

Figure 5.5: Images after 96 hours adjusted to reveal partial inhibition with bacteria reaching all samples a) 17, b) 23, and c) 25

The resultant ZOI areas are graphically presented in Figure 5.6 (X's indicate the time period at which bacteria reached the surface) and Figure 5.7. The control sample was completely overgrown after 24 hours, eliminating the need to investigate for any possible bactericidal effects of potentially releasing Titanium-oxide ions.

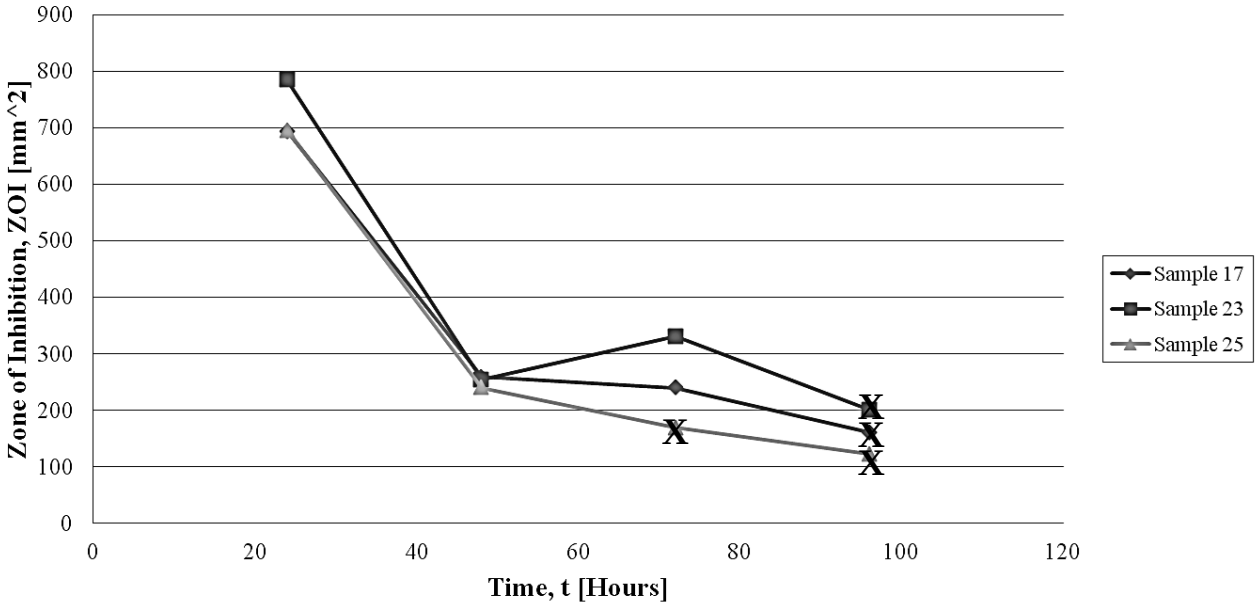

Figure 5.6: ZOI areas against *S.aureus* Xen 36 over a period of 96 hours

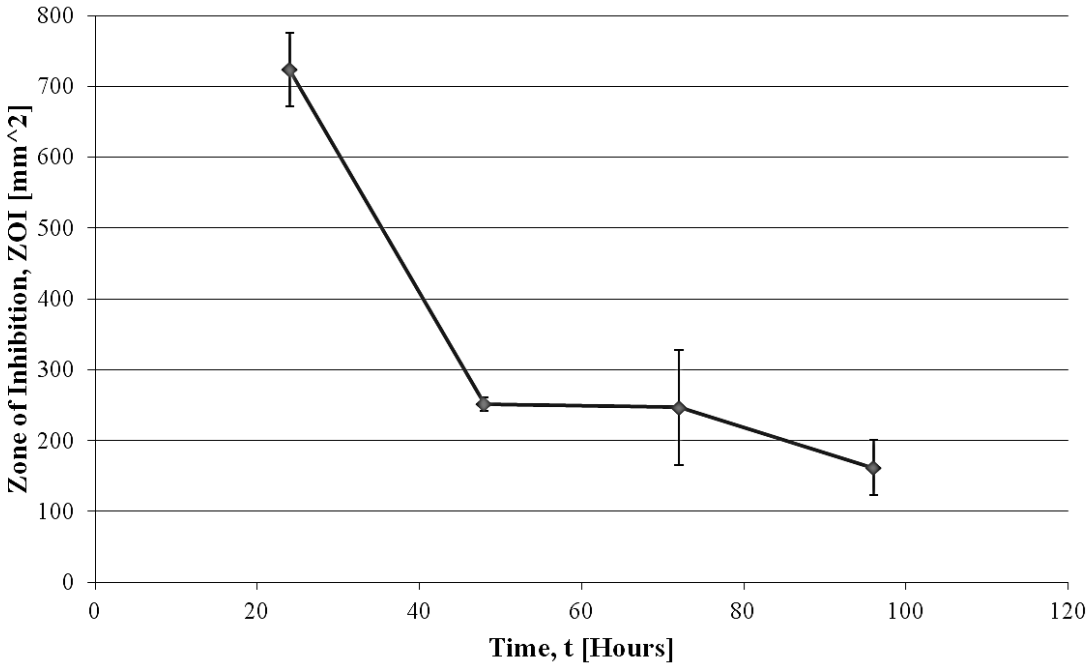

Figure 5.7: Mean and standard deviation of ZOI areas against *S.aureus* Xen 36 over a period of 96 hours

In contrast to the results obtained above, but as expected, the Xen 31 strain was not inhibited by gentamicin concentrations released from the commercial Palacos R+G. The samples were all reached within 24 hours. This is presented in Figure 5.8, where although some inhibition is visible, the samples were reached and therefore signals failure. Consequently there was no sense in measuring any ZOI. This observation also advocates the importance of appropriate selection and use of drugs according to the offending pathogen for both treatment and prophylaxis in medical device associated infections.

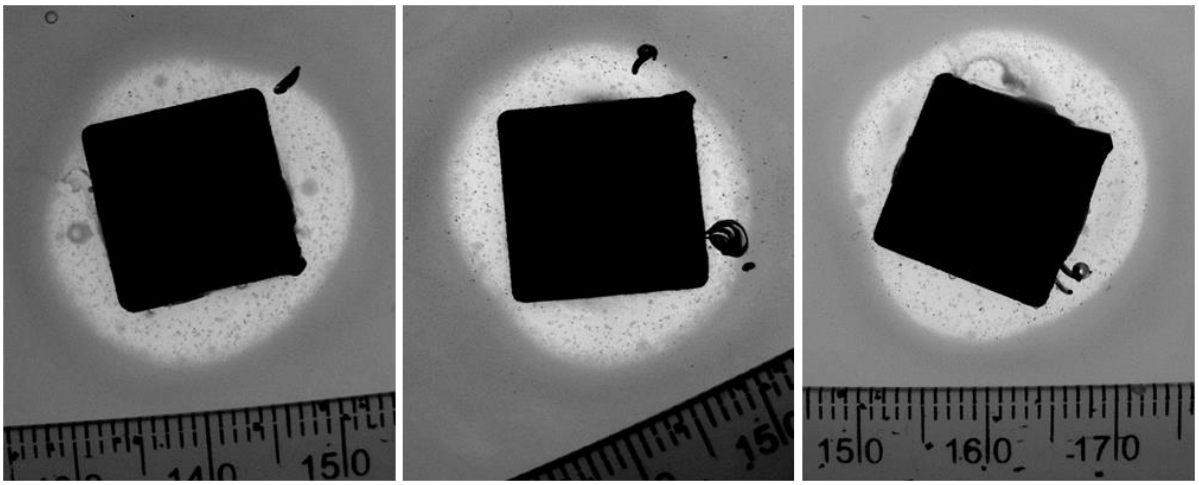

(a) **(b)** **(c)**

Figure 5.8: Resistant *S.aureus* Xen 31 reaching each of samples (a) 1, (b) 9, and (c) 16, within 24 hours

In summary, the time duration of colonisation prevention for each sample are shown in Table 5.4. The susceptible Xen 36, the pathogen of interest, was prevented from colonising for a minimum of 72 hours (sample 25), which is well above the reported 6 – 8 hour critical post implantation period [175].

Table 5.4: Colonisation prevention duration for samples

Sample	*S.aureus Strain*	*Duration [Hours]*
17	Xen 36	96
23	Xen 36	96
25	Xen 36	72
1	Xen 31	<24
9	Xen 31	<24
16	Xen 31	<24

5.4 Concluding Remarks

This pilot study investigated the concept of utilising LaserCUSING® as enabler technology to incorporate features in cementless femoral stems from which antimicrobial drugs can be eluted to prevent bacterial colonisation. Gentamicin susceptible *S.aureus* Xen 36 was successfully prevented from reaching the biomaterial, whereas the MRSA strain (*S.aureus* Xen 31) reached all the samples within the first 24 hours. This also correlates with results published in literature when cement discs alone were tested [108].

Various works have reported on the modification and treatment of implant surfaces for drug delivery [42]. The novelty of the current concept lies in the objective that it is not only meant to be a once-off drug delivery strategy, but that such implants can be reinforced with a liquid drug solution via minimally invasive techniques. Therefore, this study also investigated the porosity of a commercial PMMA ALBC, when mixed at different monomer-to-polymer ratios, and the possibility of utilising it for controlled drug release. The main reasons for this were the FDA approval status of the cement, the amount of published release studies that could be consulted for expected results, and the commercial availability of the product for research purposes. The mixing ratio did not have any significant effect on the porosity ($p \geq 0.8$ in all cases) and the porosity remained apparent random, individual defects without proper interconnections between the pores. It can be concluded that PMMA ALBC, hand mixed without extra, specialised steps such as moulds or inclusion of extra elements, for example chitosan, in the polymer mixture, does not readily offer this possibility. It therefore necessitates the investigation of alternative means to enable the administration of multiple drug doses from within the reservoir.

Another issue regarding PMMA ALBCs is the reported concerns on the long lasting release of sub inhibitory antibiotic concentration, provoking bacterial resistance [40, 176]. It has been reported that as much as more than 90 % of the original loaded amount of antibiotic does not release, and reside in the polymer matrix, releasing low concentrations of antimicrobials sporadically at unpredictable time periods due to penetration of the dissolution medium through cracks and voids into the PMMA matrix [41]. This was also witnessed in the current study, where the samples revealed some antimicrobial activity for up to 336 hours against *S.aureus* Xen 36, but adequate concentrations for colonisation prevention were only released for a minimum of 72 hours and a maximum of 96 hours.

6. Experimental Method for Reservoir Drug Delivery

This chapter describes the experimental method for the evaluation of reservoir drug delivery from within the samples. The objective of the experiment is to achieve adequate drug release through passive diffusion across nanoporous membranes for multiple injections. An important aspect is the reinforcement possibility, rendering the concept not only a once-off strategy, but one in which multiple doses can be administered. Firstly the experimental setup is described after which the quantification method of released vancomycin by RP-HPLC is described.

6.1 In Vitro Release Study

This part evaluates a commercial nanoporous membrane for localised controlled drug release as depicted in Figure 6.1. The objective is to reach a lower bound of a vancomycin concentration of 4 x MIC for MRSA (MIC = ±2 μg/ml) quickly. No restrictions were placed upon an upper boundary for local concentrations reached for the reasons discussed in Section 2.2.4.4.

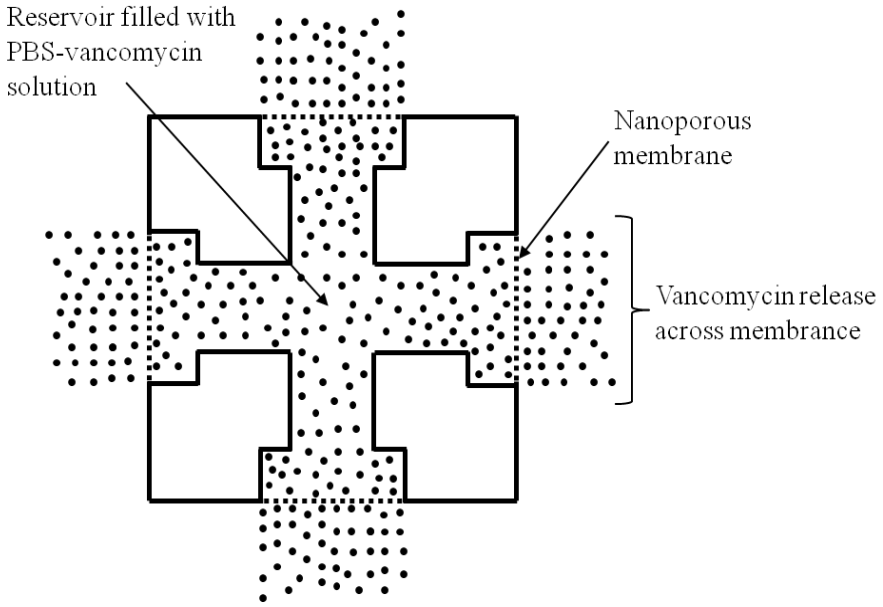

Figure 6.1: Schematic of vancomycin release across nanoporous membranes from within the internal reservoir samples

6.1.1 Reservoir Sample Assembly

To investigate drug delivery by passive diffusion from within the Ti6Al4V reservoir samples, PES ultrafiltration flat sheet membranes with a MWCO of 5,000 Da (*YMMT 3001,* Synder Filtration) were identified for incorporation. Details regarding the selection are documented in a different in-house study.

The membranes were cut from the stock into small discs ±8 mm in diameter (Figure 6.2a). A layer of Araldite *Rapid* epoxy adhesive was carefully spread on the steel ring of stainless steel washers having an internal diameter of 6 mm to fit over the channel openings. Membrane discs were then placed onto the stainless steel washers, completely covering the 6 mm internal diameter of the washers (Figure 6.2a). This part is referred to as the sub-assembly (Figure 6.2b). Another layer of adhesive was also carefully applied onto the sample around each channel opening. A sub-assembly was then fixed over a channel opening of the reservoir sample and clamped for a minimum 15 minutes. This was repeated for each channel opening, yielding four membranes in a vertical position for passive diffusion (Figure 6.2c). The bottom channel opening was sealed off completely with a commercial antifungal clear silicone (Bostik *Mirror*), suitable for application in damp and warm conditions. This was to eliminate any possible effects of gravity on the simultaneous passive diffusion across membranes placed both vertically and horizontally.

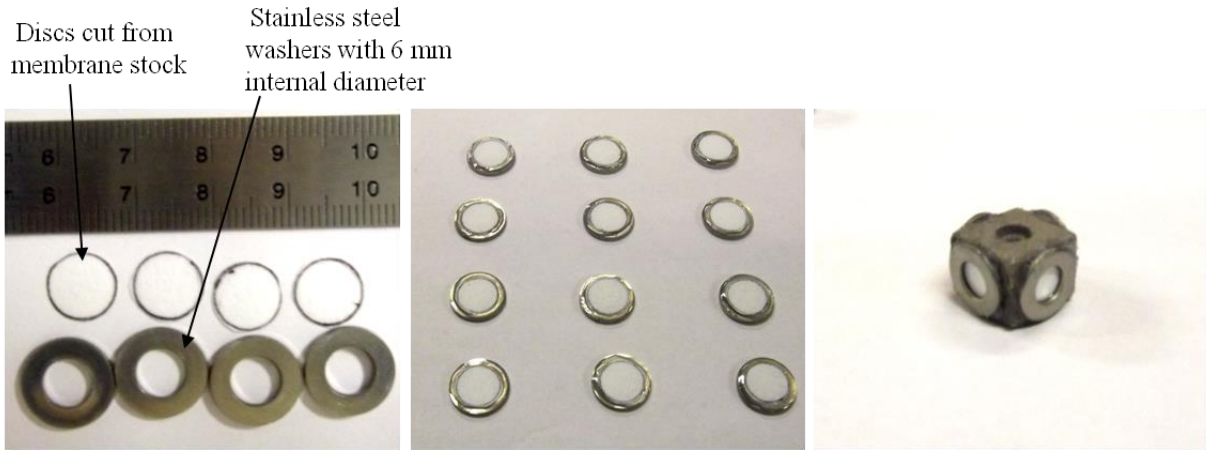

(a) **(b)** **(c)**

Figure 6.2: a) Membrane discs and stainless steel washers separately and b) the sub-assembly for fixation to the channel openings and c) final reservoir sample assembly

6.1.2 Preconditioning of Membranes

Preconditioning is an important step in the application of ultrafiltration membranes to avoid encountering variable fluxes and diffusion behaviours. A mixture of 60% 1X PBS pH 7.4 and 40% ethanol (95%) was used for the pre-wetting of the membranes. The composition of the 1X PBS pH 7.4 used is presented in Table 6.1.

Table 6.1: Composition of 1X PBS pH 7.4

Salt Compound	***Concentration [g/L]***	***Concentration [mmol/L]***
NaCl	8.0	137
KCl	0.2	2.7
Na_2HPO_4	1.44	10
KH_2PO_4	0.24	1.8

When PBS alone was used for preconditioning, it was found that air trapped inside the channels created a barrier between the introduced liquid and the membrane surface, prohibiting the liquid from reaching the inlet side of the membrane for pre-wetting. The addition of ethanol lowered the surface tension of the PBS significantly and allowed the trapped air bubbles to rise through the injected liquid and out of the reservoir through the top channel opening. The PBS-ethanol mixture was only utilised for the preconditioning of the membranes. A syringe needle was used to access each channel of the sample individually during the injection of the pre-wetting mixture, shown in Figure 6.3. It was clearly visible when the PBS-ethanol mixture reached and wetted the membranes and therefore the membranes were easily monitored for wetting by visual inspection.

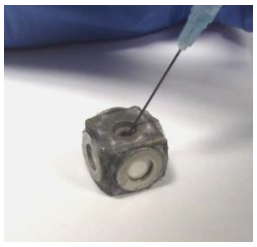

Figure 6.3: Injection of PBS-ethanol mixture into sample for preconditioning of the membranes

Since the wetting procedure consumes amounts of the mixture as it is absorbed into the membrane, the samples were continuously monitored and filled up during the process to ensure complete wetting for preconditioning from the inlet side of each membrane for a minimum of six hours, after which the samples were stored fully submerged in a PBS solution. Each sample was also carefully monitored for any signs of leakage during the preconditioning stage before being submerged for storage.

6.1.3 Vancomycin Solution Injection

The vancomycin hydrochloride (Sigma-Aldrich) used in the study was first sent for Liquid Chromatography-Mass Spectrometry (LC-MS) with electrospray ionisation (ESI) to the Central Analytical Facilities (CAF) at Stellenbosch University to evaluate whether the antibiotic has degraded. The setup and resulting mass spectra are presented in Appendix D. The molecular ion $[M+H]^+$ can be seen in Figure D.2 at mass-to-charge (m/z) 1450.4473 which when reduced by the one surplus mass unit becomes 1449.4473 Da, is very much in accordance with the theoretical value of 1449.25 Da. The isotopic cluster at 2 charges is presented in Figure D.3 in Appendix D. Clear resolution can be witnessed between the isotopes from which the monoisotopic mass is calculated as 1447.439 Da, which closely resembles the theoretical value of 1447.4304 Da. It was concluded that the vancomycin was still intact and suitable for use in the reservoir drug delivery experiments.

Vancomycin hydrochloride was dissolved in PBS to a stock concentration of 2.5 mg/ml in reference to the bolus injections investigated by Young *et al.* [126]. The Samples were injected with the vancomycin solution according to the same procedure followed for membrane preconditioning, after which the top channel opening were blocked off with a sheet of parafilm. Three injections were made during the duration of the release experiment to test the reinforcement possibility. Each injection volume was set to 400 μl, yielding an injection mass of 1 mg vancomycin per dose for the release testing.

6.1.4 Experimental Setup for Reservoir Drug Release

Standard 50 ml laboratory glass beakers were used as vessels for the elution tests. The reservoir samples were placed in the centre at the bottom of the beaker. Each beaker was then filled with PBS, which was stored at 37 °C, until the membranes were completely submerged in the buffer as presented in Figure 6.4. Beakers were selected based on the diameter of its base to allow the volume of PBS buffer to be large enough for maintaining sink conditions when filled until the membranes were submerged. The selected beakers yielded a buffer volume of 16 ml, which adheres to the criteria utilised by Miola *et al.* [167] where the volume of buffer, V_{buffer} [ml], is greater than or equal to the surface area [mm^2] of release divided by 10. That is,

$$V_{buffer} \geq \frac{A_{surface}}{10} \tag{6.1}$$

and equation 6.1 applied specifically in this study, where the surface area for release is the combined area of the four membranes, yields the condition for buffer volume,

$$\begin{aligned} V_{buffer} &\geq \frac{4\pi r^2}{10} \\ &\geq \frac{4\pi(3^2)}{10} \\ &\geq 11.31 \text{ m}l \end{aligned}$$

which is satisfied by a buffer volume of 16 m*l*. Sink conditions are used so the released drug concentrations in the dissolution medium does not affect the diffusion rate of the drug through the respective membrane effectively resulting in one directional movement of the vancomycin molecules from inside the reservoir into the buffer.

The beakers were then sealed with plastic wrap to avoid evaporation and placed on a *Classic C1* orbital shaker (New Brunswick Scientific) for continuous agitation at 7 revolutions per minute to reduce any boundary layer effects that could affect the release during the experiment (Figure 6.4). Samples were kept in the incubator at 37°C for the duration of the elution test intervals and briefly removed for aliquot sampling and buffer replacement.

Figure 6.4: Experimental setup for reservoir drug release testing

6.1.5 Sampling Procedure

The sampling schedule is presented in Table 6.2. Release intervals were determined based on a preliminary test during which aliquots were taken and the buffer replaced after intervals of 1, 4, and 18 hours, with a cumulative release time of 23 hours. After 23 hours, a total mass of 635μg from the loaded 1 mg vancomycin was released. Therefore, with the expected release to be constrained or near zero order, the injection times were selected accordingly, with the exception of the final interval, in an attempt to avoid release of the entire vancomycin reservoir before reinforcing the samples with a new vancomycin injection.

Table 6.2: Sampling times for vancomycin release

Aliquot Number	***Release Interval [Hours]***	***Cumulative [Hours]***
N/A	0	0*
1	1	1
2	3	4
3	5	9
4	8	17
5	16	33*
6	24	57*
7	43	100

** indicates times at which samples were injected with reinforcing vancomycin solution*

At each sampling interval the reservoir samples were briefly removed from the beaker, the buffer medium inside the beaker stirred by hand for 30s, and a 1 ml aliquot withdrawn. The aliquots were placed in 1.5 ml Eppendorf tubes and stored at -20°C. The rest of the buffer was discarded and the beaker rinsed with PBS. The samples were placed in the middle of the beakers and again 16 ml of PBS buffer was added. At the indicated injection times, the remaining content in the reservoir was first withdrawn before injected with fresh vancomycin solution. The top channels were covered with parafilm and the beaker with clear plastic wrap. The samples were then returned to the incubator and placed upon the orbital shaker for the next release interval.

6.2 Vancomycin Quantification with RP-HPLC

The aliquots taken during the release phase were thawed, filtered and transferred to *Chromacol* autosampler vials (Thermo Scientific) using 17 mm diameter polyvinylidene fluoride (PVDF) 0.2 μm pore size disposable syringe filters (Thermo Scientific). The RP-HPLC instrumentation utilised was a commercial Finnigan *Surveyor Plus* unit equipped with its stock *Surveyor Plus* pump and autosampler systems using a sample injection volume of 20 μl. Detection was done by a *Surveyor UV/Vis Plus* detector set for dual wave length scanning at 254 nm and 280 nm (280 nm detection specified in the British Pharmacopoeia [132]).

6.2.1 Mobile and Stationary Phases

For the mobile phase, HPLC grade acetonitrile (AcN) (Merck) with 0.1% trifluoroacetic acid (TFA) and, Milli-Q water (EMD Millipore) also with 0.1 % TFA were used. The stationary phase consisted of a Thermo Scientific *Hypersil GOLD* reversed phase chromatographic column, 100 mm x 4.6 mm (internal diameter) with C_{18} chemistry and 5 μm silica particle size.

6.2.2 Gradient Elution Program

In RP-HPLC, the character of the mobile phase influences the retention time of the solute. Milli-Q is a weaker solvent than AcN in RP-HPLC due to the Milli-Q not interacting with the hydrophobic surfaces of the stationary phase the solute adsorbs to (Section 2.2.5.2). The addition of AcN enables this interaction which breaks the bonds between solute and stationary phase and elutes the solute.

By adjusting the composition of the mobile phase over time, the retention time of the solute of interest can therefore be tailored. For vancomycin, the retention time was much too low under isocratic conditions with a sufficient amount of AcN in the mobile phase, necessitating a gradient elution program, presented in Table 6.3. Preliminary runs revealed an average retention time of 4.672 ± 0.016 minutes for 14 vancomycin sample injections.

Table 6.3: Mobile phase elution program

Time [min]	*Milli-Q (0.1% TFA) [%]*	*AcN (0.1% TFA) [%]*	*Elution Type*
0-1	95	5	isocratic
1-5	95 - 0	5 – 100	linear gradient
5-6	0	100	isocratic
6-11	0-95	100-5	linear gradient
11-12	95	5	isocratic

6.2.3 Calibration Curve

The known concentration series used for calibration consisted of vancomycin hydrochloride in PBS solutions of 0, 5, 12.5, 25, 50, 125, and 250 μg/ml concentrations, injected twice for evaluation of linearity. Integration of the detection peaks as well as the simple linear regression was performed automatically by the accompanying control software (*ChromQuest 4.2.34 version 3.1.6*). Linearity of absorbance over this range was also manually evaluated in *MSExcel* by simple linear regression according to the method described by Montgomery and Runger [174]; the procedure is presented in Appendix E. Once the calibration curve was established, the unknown vancomycin concentrations in the aliquots could be determined by simply finding the x-coordinate (of the unknown concentration) for the measured y-coordinate (absorbance). For this once-off proof of concept application, a full validation of the method according to USP specifications is outside the scope of the study and not economically feasible. This will however become necessary in the future when the research moves beyond conceptual features and towards functional prototypes. An achievement of a coefficient of determination (R^2) greater than 0.998 for all calibration curves was considered sufficient.

7. Reservoir Drug Delivery – Results Assessment

7.1 Reversed Phase High Performance Liquid Chromatography

A total of 60 injections were made during the sequence in the RP-HPLC analysis. It consisted of 7 reference standards for calibration, each injected twice, the 42 samples taken during the release period, and 4 internal standards of known concentrations 0, 25, 125, and 250 μg/ml placed at arbitrary positions amongst the samples.

7.1.1 Identification of Vancomycin

The retention time for vancomycin averaged 4.68 ± 0.017 min. A selection of chromatograms for UV detection at 280 nm is presented in Figure 7.1. The chromatograms result from reference standard injections of 5, 50, and 250 μg/ml. Identified vancomycin peaks, the retention time and peak area are indicated for each of the chromatograms. At the indicated retention time for each, the increase in absorbance is clearly visible as the vancomycin concentration increases.

The peaks other than that of vancomycin can be any of a number of compounds either resulting from compounds maintained inside the column even after wash, compounds in the mobile phase and PBS buffer, compounds or ions released from the materials used for the reservoir samples, or degradation products from the vancomycin. These peaks are not of interest towards the investigation of vancomycin release from the reservoir concept. It is clear from Figure 7.1 that the noise imposed by these peaks becomes negligent at very high concentrations of vancomycin confirming that the specific compound at the retention time is in fact the vancomycin.

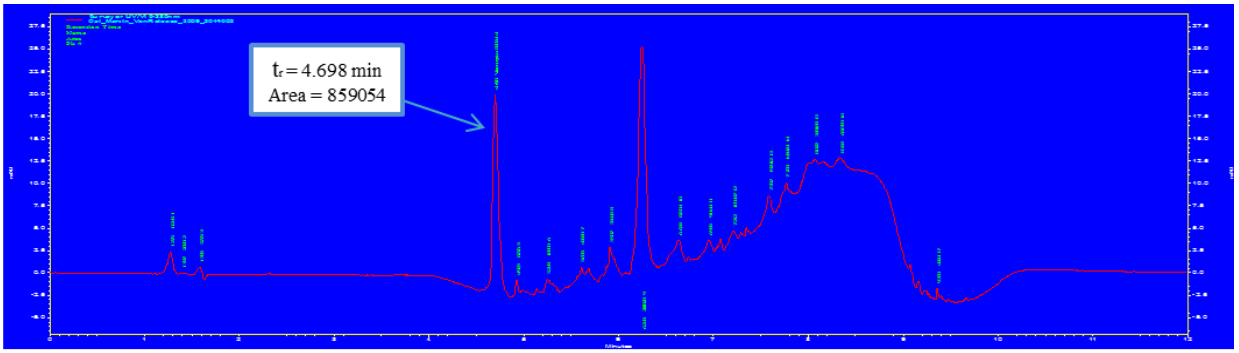

a)

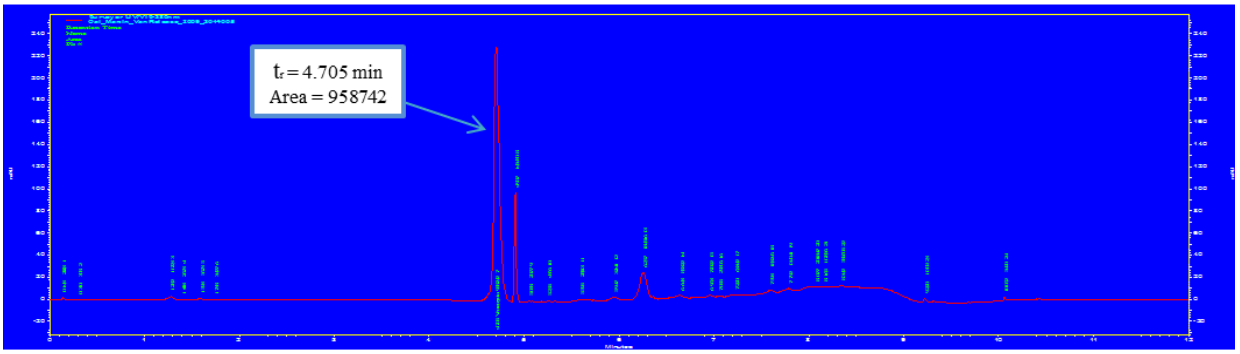

b)

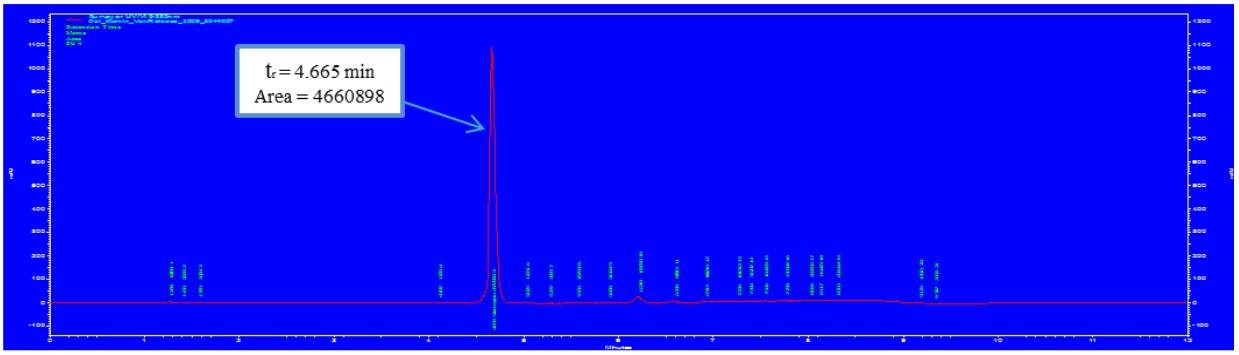

c)

Figure 7.1: Chromatograms for reference values of a) 5 b) 50 and c) 250 μg/ml with UV detection at 280 nm wavelength

7.1.2 Calibration Curves for 254 nm and 280 nm Detection

Two injections for reference standards of 0, 5, 12.5, 25, 50, 125, and 250 μg/ml concentrations were made for evaluating the calibration curve. Utilising simple linear regression, all four calibration curves (two injection series scanned at two wavelengths) revealed linearity with R^2 values greater than 0.998. The curves from the first injection did however reveal slightly greater R^2 values and are presented in this section with the other curves in Appendix E.

The two replicates of calibration series injections revealed very little, but typical variation in detection with the relative ratio of second injection to first injection fluctuating very closely around one. Response peak areas of absorbance for the two replicates are presented for 254 nm in Table 7.1 and 280 nm in Table 7.2. It is important to note that the second injection of the first aliquot, a blank consisting only of PBS, did not withdraw enough from the vile, and therefore did not inject any sample, consequently yielding no detection.

Table 7.1: Reference standards and peak response areas for calibration dilution series at 254 nm UV detection

Standard Number	*Concentration [µg/ml]*	*Response Peak Area @ 254 nm*		*Ratio I2/I1*
		Injection1 (I1)	*Injection2 (I2)*	
1	0	178681	---[a]	---
2	5	244618	243882	0.9970
3	12.5	395502	391505	0.9899
4	25	652763	652588	0.9997
5	50	1119492	1120264	1.0007
6	125	2497347	2509887	1.0050
7	250	4611234	4586338	0.9946

[a]*No response peak detected for the second injection due to a lack of sample quantity in the vial*

Table 7.2: Reference standards and peak response areas for calibration dilution series at 280 nm UV detection

Standard Number	*Concentration [µg/ml]*	*Response Peak Area @ 280 nm*		*Ratio I2/I1*
		Injection1 (I1)	*Injection2 (I2)*	
1	0	36356	---[a]	---
2	5	93726	89054	0.9502
3	12.5	235294	259945	1.1048
4	25	484550	487392	1.0059
5	50	948790	958742	1.0105
6	125	2360237	2379099	1.0080
7	250	4692199	4660898	0.9933

[a]*No response peak detected for the second injection due to a lack of sample quantity in the vial*

In accordance with the RP-HPLC software, the response area of the first injection for standard 1 was also used for injection 2 to determine the calibration curves for the second injections (Appendix E). The resulting calibration curves for the first injections are presented in Figures 7.2 and 7.3 with the estimated parameters of the linear regression models in Table 7.3 for UV detection at wavelengths 254 and 280 nm respectively.

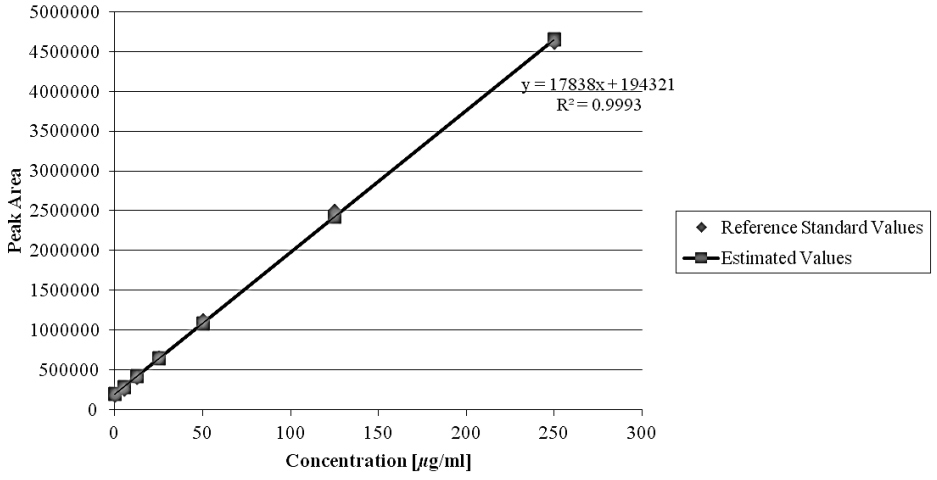

Figure 7.2: Calibration curve for UV detection at 254 nm

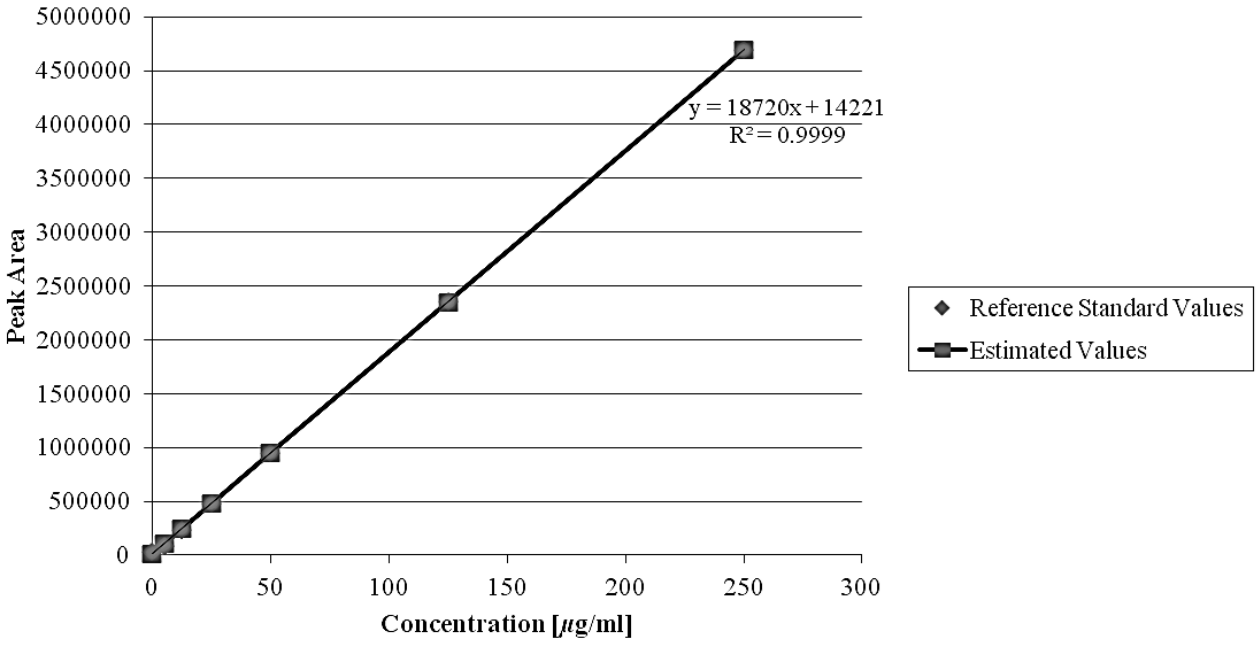

Figure 7.3: Calibration curve for UV detection at 280 nm

Table 7.3: Regression parameters for calibration curves

Regression Parameters	***Detection Wavelength [nm]***	
	254	***280***
Slope Estimator	17838.27	14220.68
Intercept Estimator	194321.08	18720.02
Coefficient of Determination [R^2]	0.99933	0.99995

The released mass of vancomycin is obtained by multiplying the detected concentration by the buffer volume. A two-tailed Student t-test (assumed equal variances) for independent samples was executed in *MSExcel* to evaluate for any statistical significant difference between average concentrations and released masses obtained from the two wavelengths both for intervallic and cumulative arrangements. The sample size was seven and the significance level, $\alpha = 0.05$. The null hypothesis states that all concentrations are from the same population irrespective of the wavelength.

$$H_0: \mu_1 = \mu_2$$
$$H_1: \mu_1 \neq \mu_2$$

The results are presented in Table 7.4. Since the *MSExcel* procedure was already manually verified, it was not repeated here. There is absolutely no statistical significance in whether concentrations calculated from either of the wavelengths are utilised. However, the R^2 value for the calibration curve at 280 nm wavelength detection is more accurate. It is also the wavelength specified in the prior mentioned pharmacopoeias. Hence the results from 280 nm wavelength are used.

Utilising this calibration curve (Figure 7.3) the concentrations detected for the known internal standards containing vancomycin were 24.29, 127.86, and 254.91 μg/ml respectively, yielding accuracies of 97.18%, 102.29%, and 101.97% which are all within a 5% deviation. An anomalous detection of 8.08 μg/ml was found for the 0 μg/ml standard. The exact causes of which are unknown but possible influences could be vancomycin transfer within the column or other areas such as the syringe in the autosampler, or vancomycin contamination during preparation of the standard. Based on the high accuracy of detection regarding the other three standards, and that the preparation of the standards occurred at a physically different location than preparation of the vials containing aliquots taken during the release period, the method is still considered applicable.

Table 7.4: t-Test results revealing no significant difference in concentrations obtained from detection at 254 nm or 280 nm

Mode	***Time [Hours]***	***Average Concentration [µg/ml] @***		***P – Value***	***Average Mass Released [µg] @***		***P-Value***
		254 nm Detection	***280 nm Detection***		***254 nm Detection***	***280 nm Detection***	
Intervallic	1	3.03	3.96		48.46	63.42	
	3	6.55	7.45		104.73	119.19	
	5	8.21	9.19		131.31	146.97	
	8	9.80	10.59	0.9768	156.74	169.45	0.9766
	16	10.90	11.71		174.32	187.35	
	24	42.04	41.52		672.56	664.30	
	43	69.82	68.66		1117.07	1098.63	
Cumulative	1	3.03	3.96		48.46	63.42	
	4	9.57	11.41		153.19	182.61	
	9	17.78	20.60		284.50	329.58	
	17	27.58	31.19	0.9195	441.24	499.04	0.9195
	33	38.47	42.90		615.56	686.38	
	57	80.51	84.42		1288.13	1350.69	
	100	150.32	153.08		2405.19	2449.31	

It is also evident from Table 7.4 that the release is closely related to that of the preliminary experiments on which the sampling times for the actual experiment were based. As expected, the total amount of injected vancomycin did release in the 43 hour interval. This indicates both that effective sink conditions were maintained and that drug molecules did not re-enter the reservoir once they were released. The average mass released is greater than 1000 μg, which can be ascribed to slight variations in injection volumes as a result of imprecise measurements taken visually from the syringe volume scale, imprecise calibration of the syringe volume scales, or injection technique introduced variations. It is nevertheless very close to the intended 1000 μg.

7.2 Release Profile and Mechanism

7.2.1 Identification of Release Profile

The release for the entire 100 hour period is indicated in Figure 7.4 as cumulative concentration that would have been present in the buffer and in Figure 7.5 as the cumulative of the vancomycin mass released, based on the intended 400 μl (containing 1000 μg vancomycin) injection volumes. The instances of injection times are indicated in both of these figures.

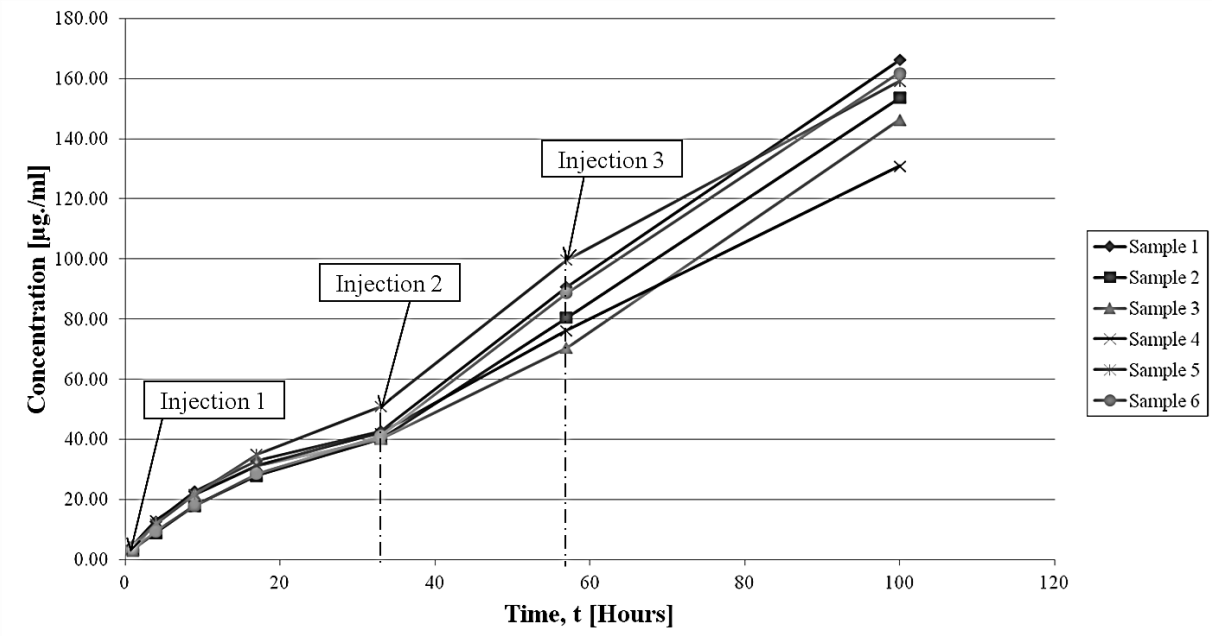

Figure 7.4: Cumulative concentration in PBS buffer of vancomycin released over 100 Hours

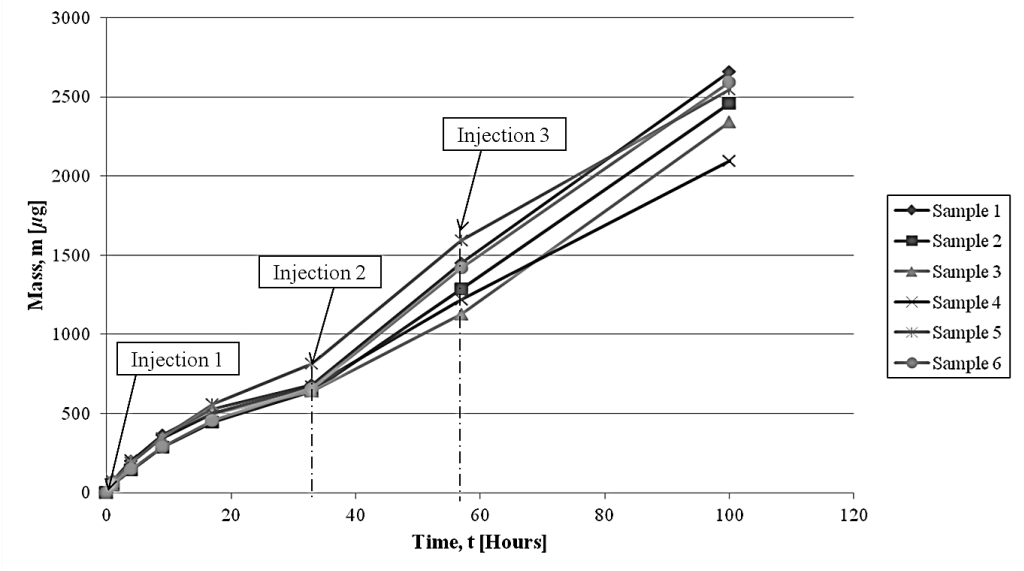

Figure 7.5: Cumulative mass of vancomycin released from reservoir

The release profile can be deduced from the samples takes within the first injection period. Since the reservoirs were emptied before new injections, and sink conditions were maintained, it is argued that the release profile obtained within the first would also be present in each of the release periods following a fresh injection. The profile, based on the first injection, is shown in Figure 7.6.

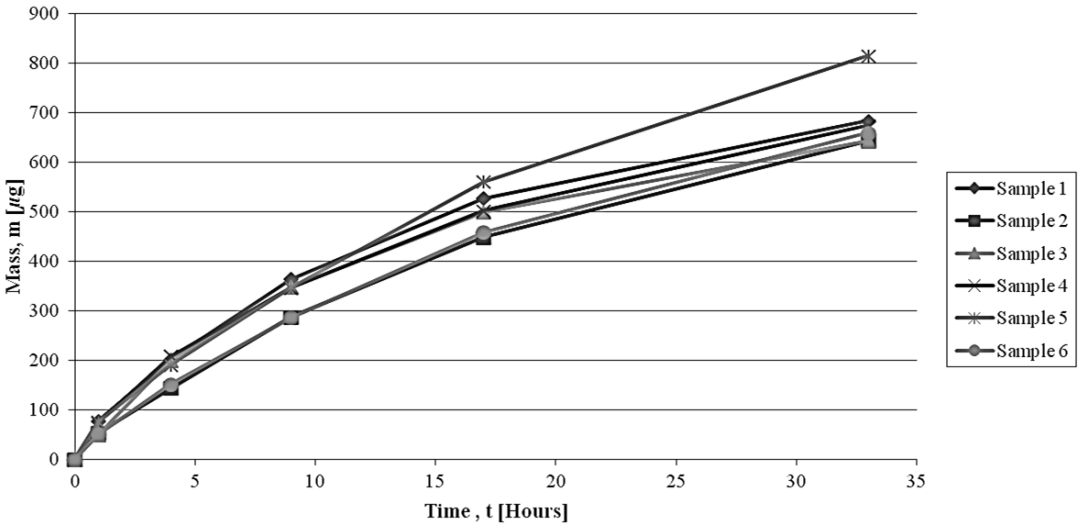

Figure 7.6: Cumulative release profile for vancomycin mass released during first injection

7.2.2 Establishment of Release Mechanism

Visually from Figure 7.6, the release mechanism appears to be neither Fickian nor zero-order release, but a type of constraint release as effected by the nanoporous nature of the PES membrane. The Korsmeyer-and-Peppas model (Equation 2.1) discussed in Section 2.2.4.5 is applied to determine the release mechanism. Since the Korsmeyer and Peppas model requires for the release fraction to not exceed 60%, only the data for the average release that falls below 60% of the total injected amount is considered. It is presented in Figure 7.7 as the average and standard deviation for the six samples' cumulative release percentage below 60%.

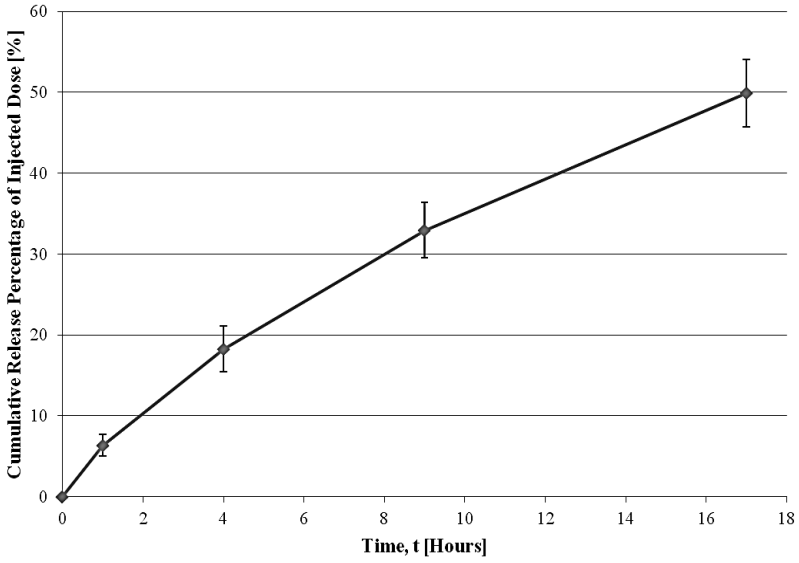

Figure 7.7: Average and standard deviation of cumulative release percentage for all samples below 60% of total introduced amount

In order to determine the values of *K* and *n* for the Korsmeyer-and-Peppas model, the model is first linearised from Equation 7.1 by employing natural logarithms as follows,

$$\frac{M_t}{M_\infty} = Kt^n \tag{7.1}$$

$$ln\left(\frac{M_t}{M_\infty}\right) = ln(Kt^n)$$

$$ln\left(\frac{M_t}{M_\infty}\right) = lnK + ln(t^n) \tag{7.2}$$

The cumulative released percentage can be plotted in the linearised form and evaluated with simple linear regression. This linearised form of data is represented as a plot of the natural logarithms of the cumulative release percentage to the natural logarithm of time. The resulting graph of the linearised data, along with its linear regression line is presented in Figure 7.8.

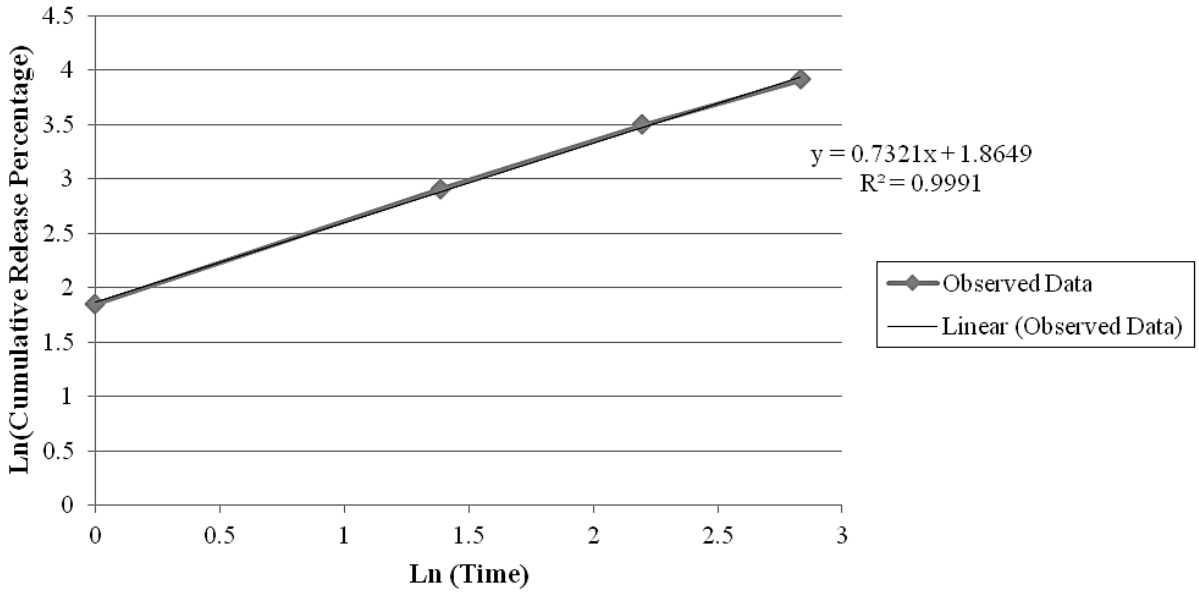

Figure 7.8: Observed cumulative release percentage linearised according to Korsmeyer-and-Peppas release model

It is evident that observed data exhibits a very high degree of linearity, indicating that the Korsmeyer-and-Peppas model would indeed be a good fit. The value of K can be determined by utilising Equation 7.2, that is,

$$\ln K = 1.8649$$
$$K = e^{1.8649}$$
$$= 6.4551$$

The value of n is then determined by utilising Equation 7.1, together with the observed data and employing a minimise function with *MSExcel Solver*, based on the sum of square errors method.

Another two-tailed Student t-test (assumed equal variances) for independent samples was executed in *MSExcel* to evaluate for any statistical significant difference between observed and modelled cumulative release percentage values below 60%. The sample size was four and the significance level, α = 0.05. The null hypothesis states that all cumulative release percentages are from the same population.

Therefore,

$$H_0: \mu_1 = \mu_2$$
$$H_1: \mu_1 \neq \mu_2$$

The resulting approximations, minimised sum of square errors and P-value for the t-Test on the means are presented in Table 7.5. The value obtained for *n* is **0.7264**, identifying the release mechanism as non-Fickian anomalous (constraint) release. This indicates that the drug is not released through diffusion alone, but interactions between the drug and the polymer structure also affects and controls the rate of release, a desired release profile for quickly reaching and then sustaining high concentrations of the drug in the local vicinity of the implant.

Table 7.5: Fitting of Korsmeyer-and-Peppas model to first 60% of cumulative drug release

Time [Hours]	***Observed Cumulative Release [%]***	***Estimated Cumulative Release [%]***	***Square Error***	***Sum of Square Errors***	***P-Value***
1	6.342	6.455	0.013	2.012	0.9686
4	18.261	17.670	0.350		
9	32.958	31.847	1.235		
17	49.904	50.548	0.415		

The release can therefore be considered as a non-specific constraint release. Calculated values for the parameters of the Korsmeyer-and-Peppas model are substituted into Equation 7.1 and plotted against the observed data in Figure 7.9 for the cumulative release percentage below 60% of the injected amount over time. The high P-value in Table 7.5 indicates that there is absolutely no reason to reject the hypothesis that the two curves represents the same population.

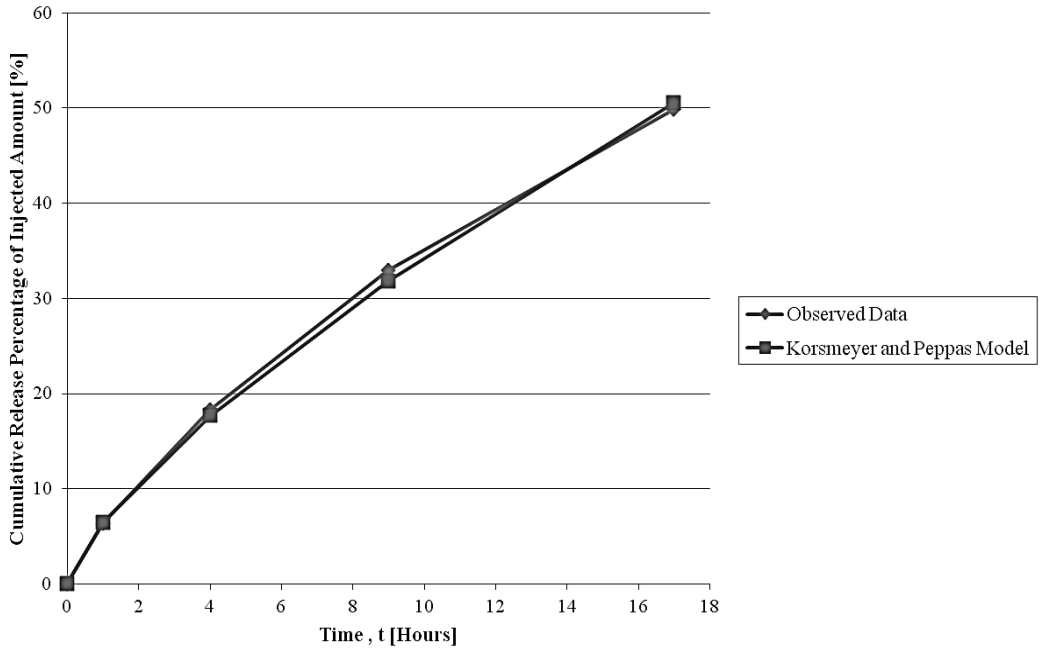

Figure 7.9: Observed data and Korsmeyer-and-Peppas Model data for cumulative release percentage below 60% of injected amount

Since the concentration of vancomycin in the buffer is dependent on buffer volume when released mass is kept constant, determining the exact time it took to reach 8 μg/ml bares not that much information. Instead the fitted Korsmeyer-and-Peppas model can be modified in terms of the method utilised in this study to represent the time to 4 times MIC as an equation dependent on concentration and buffer volume. Consider the fitted model,

$$\frac{M_t}{M_\infty} = 6.4551t^{0.7264} \qquad (7.3)$$

in which the mass released at time t, is determined by measuring the concentration in the buffer at time t, C_t, and multiplying it with the buffer volume, V_{buffer}, that is,

$$M_t = C_t \times V_{buffer} \qquad (7.4)$$

Substituting Equation 7.4 into Equation 7.3,

$$\frac{\left(C_t \times V_{buffer}\right)}{M_\infty} = 6.4551 t^{0.7264}$$

and rearranging to let time, *t*, be the subject the equation becomes,

$$t = \left[\frac{1}{0.64551}\left(\frac{C_t \times V_{buffer}}{M_\infty}\right)\right]^{\frac{1}{0.7264}} \qquad (7.5)$$

which can be utilised to find times to reach desired concentrations in different buffer sizes given that the cumulative released mass percentage is below 60% and the buffer is maintained at sink conditions. Applied to this study, Equation 7.5 yields a time of **2.57 hours** for reaching a concentration of 8 μg/ml.

7.3 Concluding Remarks

The reservoir release for multiple injections of a vancomycin hydrochloride – PBS solution by means of passive diffusion across a nanoporous membrane into a PBS buffer under sink conditions has been investigated. Three injections were made at specific time intervals during a total experimental release period of 100 hours. For a single injection, and with reference to the buffer volume in this study, concentration levels above the MIC for MRSA were reached after 1 hour, with a 4 times MIC (8 μg/ml) concentration reached within 3 hours of release.

Three injections were made to evaluate the use of the concept as a non once-off strategy, but as one during which multiple doses could be administered. Similar release rates were observed throughout these injections, with the last injection interval of 43 hours releasing the entire reservoir as was expected from preliminary tests. The release mechanism was determined to be non-Fickian, possibly being controlled by both diffusion and factors relating to changes in the structure of the polymer matrix such as relaxation, ultimately resulting in a constraint release. An appealing aspect of this profile is that the desired concentration can be achieved quicker than with single file diffusion whilst avoiding a burst release, and the release rate then maintained at a near zero-order level. Furthermore, since the idea behind single file diffusion is that molecules are released singularly from pores or vacancies inside the polymer matrix, it stands to reason that one of very

few ways to increase the release amount from such a system would be to increase the surface area of the polymer used as release membrane. This is not necessarily feasible for application in implants where space is limited and the detrimental effects on mechanical properties due to material removal should be minimised.

In conclusion, the concept has proven to allow for adequate vancomycin release from the reservoir for three injections, therefore moving the concept beyond the barrier of once-off release strategies. A new approach regarding LaserCUSING® as the enabler technology opens possibilities for drug delivery from within medical implants as part of an infection treatment regimen.

The Korsmeyer-and-Peppas model was used to evaluate the release mechanism and also resulted in a very close approximation for the first 60% of cumulative mass released from the reservoir. Once the model has been fitted to a given situation empirically, it could be modified to indicate the time needed for achieving a desired concentration, providing that the buffer volume is known and is maintained at sink conditions.

8. Conclusion and Future Research

8.1 Conclusion

Bacterial colonisation onto hip replacement stems remains a devastating complication with escalating expenses and serious morbidity for the patient. The current two-stage treatment procedure for biofilm infection leaves the patient with an interim period of a minimal load bearing antibiotic loaded spacer, an aggressive regimen of antibiotic treatment, and very little mobility. Furthermore, eradication of infection cannot be guaranteed and the interim cycle may need to be repeated. Therefore the overall objective of the study was to contribute to the field of infection prevention and treatment strategies for cementless femoral stems. This objective has been achieved by working on each of the supporting objectives as set out in Section 1.3.

- Reports on the performance of commercial ALBC was translated from literature to develop conceptual drug delivery features which were successfully used to both convey the idea behind and evaluate the concept
- AM in the proprietary form of LaserCUSING® was applied appropriately for the fabrication of samples containing these drug delivery features
- It has been shown that when an antibiotic is applied appropriately according to the main pathogen of concern that colonisation of the titanium alloy can be prevented *in vitro* using an FDA approved commercial ALBC within these samples, thereby creating a way to incorporate these materials for prophylaxis in cementless stems too
- The drug delivery concept allowed the *in vitro* sustained release of multiple dosages of a high level antibiotic typically used in the treatment of MRSA infections.

The main research question can thus be answered that it is possible to prevent colonisation onto, and enable controlled drug release through samples containing drug delivery features manufactured by SLM. This however has been an initial investigation into this field for application of SLM towards infection prevention and treatment strategies but provides a basis for more detailed and specialised studies towards developing a fully functional prototype. Such a functional cementless femoral stem is envisioned to reduce the current two-stage procedure used for treating serious implant infections to a single stage procedure, removing the need for interim cement spacers. This will lead to a significant reduction in operating theatre occupation times and a reduction in costs for both the patients and medical aid companies

8.2 Future Research

An important aspect of the concept is that it is not restricted to hip replacement stems, but can be incorporated in any bulk metallic implants for example shoulder, knee or pelvic implants. It is also not restricted to the administration of antimicrobial drugs, and can also be utilised to release for example, anti-inflammatories or osteoconductive compounds.

The evaluation of drug formulations can ensue to find those which would exhibit adequate stability over a long term period. Each drug molecule has unique properties with regard to degradation, and these need to be considered in future research when developing a formulation for a specific application.

As technology advances and the tempo at which novel research is published, it would be necessary to maintain an outlook at alternatives for release membranes should this option be considered in additional studies. A very suitable system could be one consisting of the same material than the implant itself, such as titanium alloy, which would not be biodegradable to the extent that would cause rupturing and bulk release of the reservoir drug.

Medical devices are monitored and need to adhere to stringent regulatory issues. Therefore future research should also evaluate the effects on the mechanical properties by removing material from the bulk structure for the internal channels. Load bearing medical implants such as hip stems have to be proven to conform to international standards for cementless femoral stems, especially with regards to fatigue strength.

In terms of osseointegration, an additional research avenue is the investigation of possible porous surfaces for bone ingrowth onto as-built LaserCUSING® parts. The compliance of these surfaces, however, has not yet been tested according to international specifications for medical implants. Consequently, part of the outlook is the characterisation of the as-build surfaces according to ASTM standards (ASTM F2068, F1044, F1147, F1978) for porous coatings of medical implant devices.

9. References

[1] Gosling, J.A., Harris, P.F., Humpherson, J.R., Whitmore, I, and Willan, P.L.T., 2008, *Human Anatomy: Color Atlas and Textbook*, Fifth Edition ed., Hyde, M., Ed.: Elsevier.

[2] Anderson, A.E., 2007, "Computational Modeling of Hip Joint Mechanics." *PhD Dissertation*, The University of Utah.

[3] Bergmann, G., Graichen, F., Rohlmann, A., Bender, A., Heinlein, B., Duda, G.N., Heller, M.O., and Morlock, M.M., 2010, "Realistic loads for testing hip implants," *Bio-Medical Materials and Engineering*, vol. 20, pp. 65-75.

[4] Malchau, H., Herberts, P., Eisler, T., Garellick, G., and Söderman, P., 2002, "The Swedish Total Hip Replacement Register," *The Journal of Bone and Joint Surgery, Inc*, vol. 84-A Supplement 2, pp. 2-20.

[5] Espehaug, B., Furnes, O., Engesæter, L.B., and Havelin, L.I., 2009, "18 years of results with cemented primary hip prostheses in the Norwegian Arthroplasty Register - Concerns abour some newer implants," *Acta Orthopaedica* , vol. 80, no. 4, pp. 402-412.

[6] Parvizi, J., Keisu, K.S., Hozack, W.J., Sharkey, P.F., and Rothman, R.H., 2004, "Primary Total Hip Arthroplasty With an Uncemented Femoral Component," *The Journal of Arthroplasty*, vol. 19, no. 2, pp. 151-156.

[7] Stockley, I., Mockford, B.J., Hoad-Reddick, A., and Norman, P., 2008, "The use of two-stage exchange arthroplasty with depot antibiotics in the absence of long term antibiotic therapy in infected total hip replacement," *The Journal of Bone & Joint Surgery (Br)*, vol. 90-B, no. 2, pp. 145-148.

[8] Ganz, R., Leunig, M., Leunig-Ganz, K., and Harris, W., 2008, "The Etiology of Osteoarthritis of the Hip," *Clinical Orthopaedic Related Research*, vol. 466, pp. 264-272.

[9] Siopack, J.S., and Jergesen, H.E., 1995, "Total hip arthroplasty," *Western Journal of Medicine*, vol. 162, no. 3, pp. 243-249.

[10] OECD, 2011, "Health at a Glance 2011: OECD Indicators". [Online]. http://dx.doi.org/10.1787/health_glance-2011-en

[11] Zimmerli, W., and Ochsner, P.E., 2003, "Management of Infection Associated with Prosthetic Joints," *Infection*, vol. 30, pp. 99-108.

[12] Kurtz, S., Ong, K., Lau, E., Mowat, F., and Halpern, M., 2007, "Projections of Primary and Revision Hip and Knee Arthroplasty in the United States from 2005 to 2030," *The Journal of Bone and Joint Surgery, Incorporated*, vol. 89, pp. 780-785.

[13] Harryson, O. L., Cansizoglu, O., Marcellin-Little, D.J., Cormier, D.R., and West II, H.A., 2008, "Direct metal fabrication of titanium implants with tailored materials and mechanical properties using electron beam melting technology," *Materials Science & Engineering*, vol. C, no. 28, pp. 366-373.

[14] Viceconti, M., Monti, L., Muccini, R., Bernakiewicz, M., and Toni, A., 2001, "Even a thin layer of soft tissue may compromise the primary stability of cementless hip stems," *Clinical Biomechanics*, vol. 16, pp. 765-775.

[15] Viceconti, M., Brusi, G., Pancanti, A., and Cristofolini, L., 2006, "Primary stability of an anatomical cementless hip stem: A statistical analysis," *Journal of Biomechanics*, vol. 39, pp. 1169-1179.

[16] Søballe, K., Hansen, E., Rasmussen, H.B., Jørgensen, P.H., and Bünger, C., 1992, "Tissue Ingrowth into Titanium and Hydroxyapatite-Coated Implants During Stable ans Unstable Mechanical Conditions," *Journal of Orthopaedic Research*, vol. 10, pp. 285-299.

[17] Huiskies, R., Weinans, H., and Van Rietbergen, B., 1992, "The Relationship Between Stress Shielding and Bone Resorption Around Total Hip Stems and the Effects of Flexible Materials," *Clinical Orthopaedics and Related Research*, vol. 274, pp. 124-134. [Online]. http://repub.eur.nl/res/pub/15376

[18] Kurtz, S.M., Lau, E., Schmier, J., Ong, K.L., Zhao, K., and Parvizi, J., 2008., "Infection Burden for Hip and Knee Arthroplasty in the United Stated," *The Journal of Arthtoplasty*, vol. 23, no. 7, pp. 984-991.

[19] Lange, J., Troelsen, A., Thomsen, R.W., and Soballe, K., 2012, "Chronic infections in hip arthroplasties: comparing risk of infection following one-stage and two-stage revision: a systematic review and meta-analysis," *Clinical Epidemiology*, vol. 2012, no. 4, pp. 57-73.

[20] Hsieh, P-H., Shih, C.-H., Chang, Y.-H., Lee, M.S., Shih, H.-N., and Yang, W.-E., 2004, "Two-Stage Revision Hip Arthroplasty for Infection: Comparison Between the Interim Use of Antibiotic-Loaded Cement Beads and a Spacer Prosthesis," *The Journal of Bone and Joint Surgery, Incorporated*, vol. 86-A, no. 9, pp. 1989-1997.

[21] Albrektsson, T., Brånemerk, P.I., Hansson, H.A., and Lindström, J., 1981, "Osseointegrated Titanium Implants. Requirements for ensuring a long-lasting, direct bone-to-implant anchorage in man," *Acta orthop. scand.*, vol. 52, pp. 155-170.

[22] Maloney, W.J., and Hartford, J.M., 1998, "The Cemented Femoral Component," in *The Adult Hip Volume II*, Callaghan, J.J, Rosenberg, A.G., and Rubash, H.E., Eds. Philadelphia, United States of America: Lippincott-Raven, ch. 60, pp. 959-979.

[23] Engelsman., A.F., Saldarriaga-Fernandez, I.C., Nejadink, M.R., Van Dam, G.M., Francis, K.P., Ploeg, R.J., Busscher, H.J., and Van der Mei, H.C., 2010, "The risk of biomaterial-associated infection after revision surgery due to an experimental primary implant infection," *Biofouling*, vol. 26, no. 7, pp. 761-767.

[24] Kurtz, S.M., Lau, E., Watson, H., Schmier, J.K., and Parvizi, J., 2012, "Economic Burden of Periprosthetic Joint Infection in the United States," *The Journal of Arthroplasty*, vol. 27, no. 8 Supplement 1, pp. 61-65.e1.

[25] Subbiahdoss, G., Kuijer, R., Grijpma, D.W., Van der Mei, H.C., and Busscher H.J., 2009, "Microbial biofilm growth vs. tissue integration: "The race for the surface" experimentally studied," *Acta Biomaterialia*, vol. 5, pp. 1399-1404.

[26] I Francolini, I., and Donelli, G., 2010, "Prevention and control of biofilm-based medical-device-related infections," *FEMS Immonol Med Microbiol*, vol. 59, pp. 227-238.

[27] Arciola, C.R., Campoccia, D., Gamberini, S., Donati, M.E., Pirini, V., Visai, L., Speziale, P., and Montanaro, L., 2005, "Antibiotic resistance in exopolysaccharide-forming Staphylococcus epidermidis clinical isolates from orthopaedic implant infections," *Biomaterials*, vol. 26, pp. 6530-6535.

[28] Hoiby, N., Bjarnsholt, T., Givskov, M., Molin, S., and Ciofu, O., 2010, "Antibiotic resistance of bacterial biofilms," *International Journal of Antimicrobial Agents*, vol. 35, pp. 322-332.

[29] Gallo, J., Kolár, M., Novotny, R., Riháková, P., and Tichá, V., 2003, "Pathogenesis of Prosthesis-Related Infection," *Biomed. Papers*, vol. 147, no. 1, pp. 27-35.

[30] Haddad, F.S., Muirhead-Allwood, S.K., Manktelow, A.R.J., and Bacarese-Hamilton, I., 2000, "Two-stage uncemented revision hip arthroplasty for infection," *The Journal of Bone and Joint Surgery (Br)*, vol. 82-B, no. 5, pp. 689-694.

[31] Hsieh, P.-H., Shih, C.-H., Chang, Y.-H., Lee, M.S., Yang, W.-E., and Shih, H.-N., 2004, "Treatment of deep infection of the hip associated with massive bone loss: Two-stage revision with an antibiotic-loaded interim cement prosthesis followed by reconstruction with allograft," *The Journal of Bone & Joint Surgery (Br)*, vol. 87-B, pp. 770-775.

[32] Sudo, A., Hasegawa, M., Fukuda, A., and Uchida, A., 2008, "Treatment of Infected Hip Arthroplasty with Antibiotic-Impregnated Calcium Hydroxiapatite," *The Journal of Arthroplasty*, vol. 23, no. 1, pp. 145-150.

[33] McKenna, P.B., O'Shea, K., and Masterson, E.L., 2009, "Two-stage revision of infected hip arthroplasty using a shortened post-operative course of antibiotics," *Archives of Orthopaedic and Trauma Surgery*, vol. 129, pp. 489-494.

[34] Marculescu, C.E., Berbari, E.F., Hanssen, A.D., Steckelberg, J.M., Harmsen, S.W., Mandrekar, J.N., and Osmon, D.R., 2006, "Outcome of Prosthetic Joint Infections Treated with Debridement and Retention of Components," *Clinical Infectious Diseases*, vol. 42, pp. 471-478.

[35] Disch, A.C., Matziolis, G., and Perka, C., 2007, "Two-stage operative strategy without local antibiotic treatment for infected hip arthroplasty: clinical and radiological outcome," *Archives of Orthopaedic and Trauma Surgery*, vol. 127, pp. 691-697.

[36] Giulieri, S.G., Graber, P., Ochsner, P.E., and Zimmerli, W., 2004, "Management of Infection Associated with Total Hip Arthroplasty according to a Treatment Algorithm," *Clinical and Epidemiological Study*, vol. 32, pp. 222-228.

[37] Fenelon, G.C.C., Von Foerster, G., and Engelbrecht, E., 1980, "Disarticulation of the Hip as a Result of Failed Arthroplasty - A Series of 11 Cases," *The Journal of Bone and Joint Surgery (Br)*, vol. 62-B, no. 4, pp. 441-446.

[38] Berend, K.R., Lombardi, A.V., Morris, M.J., Bergeson, A.G., Adams, J.B., and Sneller, M.A., 2013, "Two-stage Treatment of Hip Periprosthetic Joint Infection Is Associated With a High Rate of Infection Control but High Mortality," *Clinical Orthopaedics and Related Research*, vol. 471, pp. 510-518.

[39] Gallo, J., Kolár, M., Florschütz, A.V., Novotny, R., Pantucek, R., and Kesselová, M., 2005, "In Vitro Testing of Gentamicin-Vancomycin Loaded Bone Cement to Prevent Prosthetic Joint Infection," *Biomedical Papers*, vol. 149, no. 1, pp. 153-158.

[40] Hendriks, J.G.E., Van Horn, J.R., Van der Mei, H.C., and Busscher, H.J., 2004, "Backgrounds of antibiotic-loaded bone cement and prosthesis-related infection," *Biomaterials*, vol. 25, pp. 545-556

[41] Van de Belt., H., Neut, D., Uges, D.R.A., Schenk, W., Van Horn, J.R., Van der Mei, H.C., and Busscher, H.J., 2000, "Surface roughness, porosity and wettability of gentamicin-loaded bone cements and their antibiotic release," *Biomaterials*, vol. 21, pp. 1981-1987.

[42] Campoccia, D., Montanaro, L., and Arciola, C.R., 2013, "A review of the biomaterials technologies for infection-resistant surfaces," *Biomaterials*, vol. 34, pp. 8533-8554.

[43] Nag, S., and Banarjee, R., 2012, "Fundamentals of Medical Implant Materials," *ASM Handbook*, vol. 23, no. Materials for Medical Devices, pp. 6-17.

[44] Mueller, B., Toeppel, T., Gebauer, M., and Neugebauer, R., 2012, "Innovative features in implants through Beam Melting - a new approach for Additive Manufacturing of endoprostheses," in *Innovative Developments in Virtual and Physical Prototyping*, Leira, pp. 519-523.

[45] Wohlers, T., 2012, *Wohlers Report 2012: Additive Manufacturing and 3d Printing State of the Industry Annual Worldwide Progress Report*, Wohlers, T., Ed. Fort Collins, Colorado, United States of America: Wohlers Associates, Inc..

[46] FDA., 2013, 510(k) Premarket Notification for Medical Devices. [Online]. www.accessdata.fda.gov

[47] ISO 7206-4, 2002, Implants for surgery - Partial and total hip joint prostheses - Part4: Determination of endurance properties of stemmed femoral components.

[48] ISO 7206-8, 1995, Implants for surgery - Partial and total hip joint prosthesis - Part 8: Endurance performance of stemmed femoral components with application of torsion.

[49] Bhende, S., and Spangler, D., 2004, "In Vitro Assessment of Chlorohexidine Gluconate-Impregnated Polyurethane Foam Antimicrobial Dressing Using Zone of Inhibition Assays," *Infection Contral and Hospital Epidemiology*, vol. 25, no. 8, pp. 664-667.

[50] Okazaki, Y., and Gotoh, E., 2005, "Comparison of metal release from various metallic biomaterials," *Biomaterials*, vol. 26, pp. 11-21.

[51] Browne, M., and Gregson, P.J., 1994, "Surface modifications of titanium alloy implants," *Biomaterials*, vol. 15, no. 11, pp. 894-898.

[52] Hinüber, C., Kleemann, C., Friederichs, R.J., Haubold, L., Scheibe, H.J., Schuelke, T., Boehlert, C., and Baumann, M.J., 2010, "Biocompatibility and mechanical properties of diamond-like coatings on cobalt-chromium-molybdenum steel and titanium-aluminium-vanadium biomedical alloys," *Journal of Biomedical Materials Research A*, vol. 95A, no. 2, pp. 388-400.

[53] Van de Belt, H., Neut, D., Schenk, W., Van Horn, J.R., Van der Mei, H.C., and Busscher, H.J., 2001, "Staphylococcus aureus biofilm formation on different gentamicin-loaded polymethylmethacrylate loaded bone cements," *Biomaterials*, vol. 22, pp. 1607-1611.

[54] Feng, Y., Chen, C-J., Su, L.-H., Yu, J., and Chiu, C.-H., 2008, "Evolution and pathogenesis of Staphylococcus aureus: Lessons learned from genotyping and comparative genomics," *Federation of European Microbiological Societies*, vol. 32, pp. 23-37.

[55] National_Institutes_of_Health, 1994, "Total Hip Replacement," *NIH Consensus Statement*, vol. 12, no. 5, pp. 1-31.

[56] OECD, 2013, www.oecd.org. [Online]. http://www.oecd.org/statistics/

[57] Pabinger, C., and Geissler, A., 2014, "Utilization rates of hip arthroplasty in OECD countries," *Osteoarthritis and Cartilege*, vol. 22, pp. 734-741.

[58] Holzwarth, U., and Cotogno, G., 2012, "Total Hip Arthroplasty," European Commission, Ispra, Scientific and Policy Report 978-92-79-25279-2 (pdf).

[59] Learmonth, I.D., Young, C., and Rorabeck, C., 2007, "The operation of the century: total hip replacement," *The Lancet*, vol. 370, no. 9597, pp. 1508-1519.

[60] Geetha, M., Singh, A.K., Asokamani, R., and Gogia, A.K., 2009, "Ti based biomaterials, the ultimate choice for orthopaedic implants - A review," *Progress in Materials Science*, vol. 54, pp. 397-425.

[61] Black, J., 1998, "Biomaterials Overview," in *The Adult Hip Volume I*, Callaghan, J.J, Rosenberg, A.G., and Rubash, H.E., Eds. Philadelphia, United States of America: Lippincott-Raven, ch. 5, pp. 87-96.

[62] Bartolo, P., Kruth, J.-P., Silva, J., Levy, G., Malshe, A., Rajurkar, K., Mitsuishi, M., Ciurana, J., and Leu, M., 2012, "Biomedical production of implants by additive elctro-chemical and physical processes," *CIRP Annals - Manufacturing Technology*, vol. 61, pp. 635-655.

[63] Niinomi, 2008, "Mechanical biocompatibilities of titanium alloys for biomedical applications," *Journal of the Mechanical Behavior of Biomedical Materials* , vol. I, pp. 30-42.

[64] Niinimäki, T., Junila, J., and Jalovaara, P., 2001, "A proximal fixed anatomic femoral stem reduces stress shielding," *International Orthopaedics (SICOT)*, vol. 25, pp. 85-88.

[65] Sumner, D.R., Turner, T.M., Igloria, R., Urban, R.M., and Galante, J.O., 1998, "Functional adaptation and ingrowth of bone vary as a function of hip implant stiffness," *Journal of Biomechanics*, vol. 31, pp. 909-917.

[66] Shapiro, I.M., Hickok, N.J., Parvizi, J., Stewart, S., and Schaer, T.P., 2012, "Molecular Engineering of an Orthopaedic Implant: From Bench to Bedside," *European Cells and Materials*, vol. 23, pp. 362-370.

[67] Biomet_Orthopedics, 2012, Taperloc Complete Hip System. [Online]. http://www.biomet.co.uk/userfiles/files/Hips/Taperloc/FLH235_Taperloc_Broch_EMEA_final.pdf

[68] Zimmer, 2009, Zimmer M/L Taper Hip Prosthesis. [Online]. http://www.zimmer.com/en-US/hcp/hip/product/ml-taper.jspx

[69] Zimmer_Inc., 2009, Fitmore Hip Stem. [Online]. http://www.zimmer.com/content/pdf/en-US/Fitmore_Hip_Stem_Brochure_%2897-0551-001-00%29_%2804_2010%29_US_MARKETS_ONLY.pdf

[70] Zimmer_Inc., 2005, Trabecular Metal Primary Hip Prosthesis. [Online]. http://www.zimmer.com/content/pdf/en-US/Trabecular_Metal_Primary_Hip_Prosthesis_Brochure_%2897-7864-001-00%29_%2805_2006%29.pdf

[71] Zimmer_GmbH, 2005, Alloclassic Zweymüller Stem. [Online]. http://www.zimmer.com/content/pdf/en-GB/Alloclassic_Zweymuller_Stem_Brochure_06.01100.012X.pdf

[72] Zimmer_Inc., 2009, VerSys Epoch FullCoat Hip System. [Online]. http://www.zimmer.com/content/pdf/en-US/VerSys_Epoch_Fullcoat_Hip_System_Brochure_%2897-4088-101-00%29_%2804_2010%29_.pdf

[73] DePuy_Orthopaedics_Inc., 2001, Summit Tapered Hip System Design Rationale. [Online]. http://www.depuy.com/sites/default/files/products/files/DO_Summit_Tapered_Hip_DR_0611-81-050r1.pdf

[74] DePuy_International_Ltd_and_DePuy_Orthopaedics_Inc., 2011, S-ROM Total Hip System Surgical Technique. [Online]. http://www.depuy.com/sites/default/files/products/files/9068-91-000%20v4%20S-ROM%20ST_EN.pdf

[75] Plaster, R.L., 2011, TRI-LOCK Bone Presevation Stem: Performing an Effective, Efficient THA Utilising a Contemporary Broach-Only Femoral Stem. [Online]. http://www.depuy.com/sites/default/files/products/files/0612-89-101%20Plaster%20White%20Paper.pdf

[76] DePuy_International_Ltd., 2010, Corail Hip System Product Portfolio. [Online]. http://www.depuy.com/sites/default/files/products/files/9066-35-025-v2-Corail-Product-Portfolio_EN_1.pdf

[77] Coringroup, 2012, MetaFix Total Cementless Hip Replacement Design Rationale. [Online]. http://www.coringroup.com/medical_professionals/products/hips/metafix/introduction/

[78] Coringroup, 2013, TriFit Cementless Tapered Femoral Stem Technical Summary. [Online]. http://www.coringroup.com/medical_professionals/products/hips/trifit_ts/stability/

[79] Morshed, S., Bozic, K.J., Ries, M.D., Malchau, H., and Colford, J.M., 2007, "Comparison of cemented and uncemented fixation in total hip replacement," *Acta Orthopaedica*, vol. 78, no. 3, pp. 315-326.

[80] Brånemerk, P.-I., 1983, "Osseointegration and its experimental background," *The Journal of Prosthetic Denstistry*, vol. 50, no. 3, pp. 399-410.

[81] Kienapfel, H., and Griss, P., 1998, "Fixation by Ingrowth," in *The Adult Hip Volume I*, Callaghan, J.J, Rosenberg, A.G., and Rubash, H.E., Eds. Philadelphia, United States of America: Lippincott-Raven, ch. 13, pp. 201-209.

[82] Khanuja, H.S., Vakil, J.J., Goddard, M.S., and Mont, M.A., 2011, "Cementless Femoral Fixation in Total Hip Arthroplasty," *The Journal of Bone and Joint Surgery, Incorporated*, vol. 93, pp. 500-509.

[83] Tamaki, Y., Takakubo, Y., Goto, K., Hirayama, T., Sasaki, K., Konttinen, Y.T., Goodman, S.B., and Takagi, M., 2009, "Increased Expression of Toll-like Receptors in Aseptic Loose Periprosthetic Tissues Septic Synovial Membranes Around Total Hip Implants," *The Journal of Rheumatology*, vol. 36, no. 3, pp. 598-608.

[84] Nercessian, O.A., and Joshi, R.P., 1998, "General Principles of Surgical Technique," in *The Adult Hip Volume II*, Callaghan, J.J, Rosenberg, A.G., and Rubash, H.E., Eds. Philadelphia, United States of America: Lippincott-Raven, ch. 59, pp. 951-958.

[85] Zilberman, M., and Elsner, J.J., 2008, "Antibiotic-eluting medical devices for various applications," *Journal of Controlled Release*, vol. 130, pp. 202-215.

[86] McAuley, J.P., and Moreau, G., 1998, "Sepsis: Etiology, Prohylaxis, and Diagnosis," in *The Adult Hip: Volume II*, Callaghan, J.J, Rosenberg, A.G., and Rubash, H.E., Eds. Philadelphia, United States of America: Lippincott-Raven, ch. 79, pp. 1295-1306.

[87] Hetrick, E.M., and Schoenfisch, M.H., 2006, "Reducing implant-related infections: active release strategies," *Chemical Society Reviews*, vol. 35, pp. 780-789.

[88] Peltier, L.F., 1998, "A History of Hip Surgery," in *The Adult Hip Volume I*, Callaghan, J.J, Rosenberg, A.G., and Rubash, H.E., Eds. Philadelphia, United States of America: Lippincott-Raven, ch. 1, pp. 3-36.

[89] Charnley, J., 1964, "A Clean-Air Operating Enclosure," *British Journal of Surgery*, vol. 51, no. 3, pp. 202-205.

[90] Ofek, I., Hasty, D.L., and Doyle, R.J., 2003, *Bacterial Adhesion to Animal Cells and Tissues*, 1st ed., ASM Press, Ed. Washington, District of Columbia: ASM Press.

[91] Geisinger, E., and Novick, R.P., 2008, "Signal Integration and Virulence Gene Regulation in Staphylococcus Aureus," in *Chemical Communication among Bacteria*, S.C. Winans and B.L. Bassler, Eds. Washington, DC, United States of America: ASM Press, ch. 11, pp. 161-184.

[92] Novick, R.P., 1999, "Regulation of Pathogenicity in Staphylococcus Aureus ," in *Cell-Cell Signalling in Bacteria*, G.M. Dunny and S.C. Winans, Eds. Washington, DC, United States of America: ASM Press, ch. 9, pp. 129-146.

[93] Zimmerli, W., and Moser, C., 2012, "Pathogenesis and treatment concepts of othopaedic biofilm infections," *FEMS Immunol Med Microbiol*, vol. 65, pp. 158-168.

[94] Darouiche, R.O., 2001, "Device-Associated Infections: A Macroproblem that Starts with Microadherence," *Clinical Infectious Diseases*, vol. 33, pp. 1567-1572.

[95] An, Y.H., and Friedman, R.J., 1996, "Prevention of sepsis in total joint arthroplasty," *Journal of Hospital Infection*, vol. 33, pp. 93-108.

[96] Berbari, E.F., Hanssen, A.D., Duffy, M.C., Steckelberg, J.M., Ilstrup, D.M., Harmsen, W.S., and Osmon, D.R., 1998, "Risk Factors for Prosthetic Joint Infection: Case-Control Study," *Clinical Infectious Diseases*, vol. 27, no. 5, pp. 1247-1254.

[97] Pulido, L., Ghanem, E., Joshi, A., Purtill, J.J., and Parvizi, J., 2008, "Periprosthetic Joint Infection: The Incidence, Timing, and Predisposing Factors," *Clin Orthop Relat Res*, vol. 466, pp. 1710-1715.

[98] Montanaro, L., Speziale, P., Campoccia, D., Ravaioli, S., Cangini, I., Pietrocola, G., Giannini, S., and Arciola, C.R., 2011, "Scenery of Staphylococcus implant infections in orthopedics," *Future Microbiology*, vol. 6, no. 11, pp. 1329-1349.

[99] Kiederowski, M.R., and Horswill, A.R., 2011, "New approaches in treating staphylococcal biofilm infections," *Annals of the New York Academy of Sciences*, vol. 1241, pp. 104-121.

[100] Fernebro, J., 2011, "Fighting bacterial infections - Future treatment options," *Drug Resistance Updates*, vol. 14, pp. 125-139.

[101] Sharma, H., De Leeuw, J., and Rowley, D.I., 2005, "Girdlestone resection arthroplasty following failed surgical procedures," *International Orthopaedics (SICOT)*, vol. 29, pp. 92-95.

[102] Masri, B.A., and Salvati, E.A., 1998, "Sepsis: Two-Stage Exchange," in *The Adult Hip: Volume II*, Callaghan, J.J, Rosenberg, A.G., and Rubash, H.E., Eds. Philadelphia, United States of America: Lippincott-Raven, ch. 81, pp. 1317-1330.

[103] Scharfenberger, A., Clark, M., Lavoie, G., O'Connor, G., Masson, E., and Beaupre, L.A., 2007, "Treatment of an infected total hip replacement with the PROSTALAC system," *Canadian Journal of Surgery*, vol. 50, no. 1, pp. 24-28.

[104] Sigma_Aldrich, 2014, 48760 Gentamicin sulfate from Micromonospora. [Online]. http://www.sigmaaldrich.com/content/dam/sigma-aldrich/docs/Sigma/Datasheet/6/48760dat.pdf

[105] Veyssier, P., and Bryskier, A., 2005, "Aminocyclitol Aminoglycosides," in *Antimicrobial Agents: Antibacterials and Antifungals*, A. Bryskier, Ed. Washington, District of Columbia, United States of America: ASM Press, ch. 16, pp. 453-469.

[106] Mascaretti, O.A., 2003, "Inhibitors of the 30S Ribosomal Subunit - Aminoglycosides and Tetracyclines," in *Bacteria versus Antimicrobial Agents - An Integrated Approach*, 1st ed., ASM_Press, Ed. Washington, District of Columbia, United States of America: ASM Press, ch. 17, pp. 229-246.

[107] Benveniste, R., and Davies, J., 1973, "Structure-Activity Relationships Among the Aminoglycoside Antibiotics: Role of Hydroxyl and Amino Groups," *Antimicrobial Agents and Chemotherapy*, vol. 4, no. 4, pp. 402-409.

[108] Ensing, G.T., Van Horn, J.R., Van der Mei, H.C., Busscher, H.J., and Neut, D., 2008, "Copal Bone Cement Is More Effective in Preventing Biofilm Formation than Palacos R-G," *Clin Orthop Relat Res*, vol. 466, pp. 1492-1498.

[109] Drew, D.A., 2001, "A Mathematical Model for Prokaryotic Protein Synthesis," *Bulletin of Mathematical Biology*, vol. 63, pp. 329-351.

[110] Cabanillas, P.F., Peña, E.D., Barrales-Rienda, J.M., and Frutos, G., 2000, "Validation and in vitro characterization of antibiotic-loaded bone cement release," *International Journal of Pharmaceutics*, vol. 209, pp. 15-26.

[111] Elson, R.A., Jephcott, A.E., McGechie, D.B., and Verettas, D., 1977, "Antibiotic-loaded Acrylic Cement," *The Journal of Bone and Joint Surgery*, vol. 59-B, no. 2, pp. 200-205.

[112] Hill, J., Klenerman, L., Trustey, S., and Blowers, R., 1977, "Diffusion of Antibiotics from Acrylic Bone-Cement - In Vitro," *The Journal of Bone and Joint Surgery*, vol. 59-B, no. 2, pp. 197-199.

[113] Lewis, G., 2008, "Properties of Antibiotic-Loaded Acrylic Bone Cements for Use in Cemented Arthroplasties: A State-of-the-Art Review," *Journal Biomedical Material Research Part: Applied Biomaterials*, pp. 558-574.

[114] Neut, D., Kluin, O.S., Thompson, J., Van der Mei, H.C., and Busscher, H.J., 2010, "Gentamicin release from commercially-available gentamicin-loaded PMMA bone cements in a prosthesis-related interfacial gap model and their antibacterial efficacy," *BMC Musculoskeletal Disorders*, vol. 11, no. 258.

[115] Torrado, S., Frutos, P., and Frutos, G., 2001, "Gentamicin bone cements: characterisation and release (in vitro and in vivo assays)," *International Journal of Pharmaceutics*, vol. 217, pp. 57-69.

[116] Dunne, N., Hill, J., McAfee, P., Todd, K., Kirkpatrick, R., Tunney, M., and Patrick, S., 2007, "In vitro study of the efficacy of acrylic bone cement loaded with supplementary amounts of gentamicin: Effect on mechanical properties, antibiotic release, and biofilm formation," *Acta Orthopaedica*, vol. 78, no. 6, pp. 774-785.

[117] Bryskier, A., and Veyssier, P., 2005, "Glycopeptides and Lipoglycopeptides," in *Antimicrobial Agents - Antibacterials and Antifungals*, A. Bryskier, Ed. Washington, District of Columbia, United States of America: ASM Press, ch. 31, pp. 880-903.

[118] Mascaretti, O.A., 2003, "Inhibitors of Peptidoglycan Biosynthesis - Bacitracin and Glycopeptides," in *Bacteria versus Antibacterial Agents - An Integrated Approach*. Washington, District of Columbia, United States of America: ASM Press, ch. 14, pp. 203-214.

[119] Ross, G.H., Wright, D.H., Rotschafer, J.C., and Ibrahim, K.H., 2002, "Glycopeptide Pharmacodynamics," in *Antimicrobial Pharmacodynamics in Theory and Clinical Practice*, C.H. Nightingale, T. Murakawa, and P.G. Ambrose, Eds. New York, New York, United States of America: Marcel Dekker Inc, ch. 8, pp. 177-204.

[120] Sigma_Aldrich, 2011, Vancomycin hydrochloride from Streptomyces orientalis - Product Specification. [Online]. http://www.sigmaaldrich.com/Graphics/COfAInfo/SigmaSAPQM/SPEC/V8/V8138/V8138-BULK SIAL .pdf

[121] Schäfer, M., Schneider, T.R., and Sheldrick, G.M., 1996 "Crystal structure of vancomycin," *Structure*, vol. 4, no. 12, pp. 1509-1515.

[122] Van Bambeke, F., 2006, "Glycopeptides and glycodepsipeptides in clinical development: A comparative review of their antibacterial spectrum, pharmacokinetics and clinical efficacy," *Current Opinion in Investigational Drugs*, vol. 7, no. 8, pp. 740-749.

[123] Nelson, R.R.S., 1999, "Intrinsically vancomycin-resistant Gram-positive organisms: clinical relevance and implications for infection control," *Journal of Hospital Infection*, vol. 42, pp. 275-282.

[124] Gultepe, E., Nagesha, D., Sridhar, S., and Amiji, M., 2010, "Nanoporous inorganic membranes or coatings for sustained drug delivery in implantable devices," *Advanced Drug Delivery Reviews*, vol. 62, pp. 305-315.

[125] Baker, R.W., 2012, "Controlled Drug Delivery," in *Membrane Technology and Applications - eBook*, 3rd ed. Chichester, West Sussex, United Kingdom: Wiley, ch. 12, pp. 501-519.

[126] Young, S.E., Zhang, M., Freeman, J.T., Mutu-Grigg, J., Pavlou, P., and Moore, G.A., 2014, "Higher Tissue Concentrations of Vancomycin with Low-dose Intraosseous Regional Versus Systemic Prophylaxis in TKA," *Clinical Orthopaedics and Related Research*, vol. 472, no. 1, pp. 57-65.

[127] Jeon, G., Yang, S.Y., and Kim, J.K., 2012, "Functional nanoporous membrances for drug delivery," *Journal of Materials Chemistry*, vol. 22, pp. 14814-14834.

[128] Yang, S.Y., Yang, J., Kim, E-.S., Jeon, G., Oh, E.J., Choi; K.Y., Hahn, S.K., and Kim, J.K., 2010, "Single-File Diffusion of Protein Drugs through Cylindrical Nanochannels," *ACSNano*, vol. 4, no. 7, pp. 3817-3822.

[129] Korsmeyer, R.W., Gurny, R., Doelker, E., Buri, P., and Peppas, N.A., 1983, "Mechanisms of solute release from porous hydrophilic polymers," *International Journal of Pharmaceutics*, vol. 15, pp. 25-35.

[130] Costa, P., Lobo, J.M.S., 2001, "Modeling and comparison of dissolution profiles," *European Journal of Pharmaceutical Sciences*, vol. 13, pp. 123-133.

[131] Siepmann, J., and Siepmann, F., 2008, "Mathematical modeling of drug delivery," *International Journal of Pharmaceutics*, vol. 364, pp. 328-343.

[132] British_Pharmacopoeia, 2013, Vancomycin Hydrochloride Monograph. [Online]. http://www.pharmacopoeia.co.uk.ez.sun.ac.za/bp2014/ixbin/bp.cgi?a=display&r=aH6VamZqUJx&id=6667&tab=search

[133] Farin, D., Guillermo, A.P., Gozlan, I., and Kitzes-Cohen, R., 1998, "A modified HPLC method for the determination of vancomycin in plasma and tissues and comparison to FPIA (TDX)," *Journal of Pharmaceutical and Biomedical Analysis*, vol. 18, pp. 367-372.

[134] Meyer, V.R., 2010, *Practical High-Performance Liquid Chromatography*, 5th ed. Chichester, West Sussex, United Kingdom: John Wiley and Sons.

[135] Unger, K.K., Lamotte, S., and Machtejevas, E., 2013, "Column Technology in Liquid Chromatography," in *Liquid Chromatography: Fundamentals and Instrumentation*, Fanali, S., Haddad, P.R., Poole, C.F., Schoenmakers, P., Lloyd, D., Eds. Waltham, Massachusetts, United States of America: Elsevier, ch. 3, pp. 41-86.

[136] Aguilar, M.-I., 2004, "Reversed-Phase High-Performance Liquid Chromatography," in *Methods in Molecular Biology Volume 251: HPLC of Peptides and Proteins - Methods and Protocols*, Aguilar, M.-I., Ed. Totowa, New Jersey, United States of America: Humana Press Inc., ch. 2, pp. 9-22.

[137] Aguilar, M.-I., 2004, "HPLC of Peptides and Proteins," in *Methods in Molecular Biology Volume 251: HPLC of Peptides and Proteins - Methods and Protocols*, Aguilar, M.-I., Ed. Totowa, New Jersey, United States of America: Humana Press Inc., ch. 1, pp. 3-8.

[138] Levy, G.N., Schindel, R., and Kruth, J.P., 2003, "Rapid manufacturing and rapid tooling with layer manufacturing (LM) technologies, state of the art and future perspectives," *CIRP Annals - Manufacturing Technology*, vol. 52, no. 2, pp. 589-609.

[139] Hopkinson, N., Hague, R.J.M., and Dickens, P.M., 2006, *Rapid Manufacturing: An Industrial Revolution for the Digital Age*, 1st ed., Hopkinson, N., Hague, R.J.M., and Dickens P.M., Eds. Chichester, West Sussex, England: John Wiley & Sons, Ltd.

[140] Horn, T.J., and Harrysson, O.L.A., 2012, "Overview of current additive manufacturing technologies and selected applications," *Science Progress*, vol. 95, no. 3, pp. 255-282.

[141] Petrovic, V., Gonzalez, J.V.H., Ferrando, O.J., Gordillo, J.D., Puchades, J.R.B., and Griñan, L.P., 2011, "Additive layered manufaturing: sectors of industrial application shown through case studies," *International Journal of Production Research*, vol. 49, no. 4, pp. 1061-1079.

[142] Murr, L.E., Quinones, S.A., Gaytan, S.M., Lopez, M.I., Rodela, A., Martinez, E.Y., Hernandez, D.H., Martinez, E., Medina, F., and Wicker, R.B., 2009, "Microstructure and mechanical behavior of Ti-6Al-4V produced by rapid-layer manufacturing, for biomedical applications," *Journal of the Mechanical Behavior of Biomedical Materials*, vol. 2, pp. 20-32.

[143] Cronskär, M., Bäckström, M., and Rännar, L.-E., 2013, "Production of Customized Hip Stem Prostheses - A comparison between conventional Machining and Electron Beam Melting (EBM)," *Pre-print paper (Emerald Group Publishing Limited)*, pp. 1-16.

[144] Dehoff, R., Duty, C., Peter, W., Yamamoto, Y., Chen, W., Blue, C., and Tallman, C., 2013, "Case Study: Additive Manufacturing of Aerospace Brackets," *Advanced Materials & Processes*, vol. 171, no. 3, pp. 19-22.

[145] Grimm, T., 2004, *User's Guide to Rapid Prototyping*, 1st ed., R. Csizmadia, Ed. Dearborn, Michigan, United States of America: Society of Manufacturing Engineers.

[146] Vandenbroucke, B., and Kruth, J-P., 2007, "Selective laser melting of biocompatible metals for rapid manufacturing of medical parts," *Rapid Prototyping Journal*, vol. 13, no. 4, pp. 196-203.

[147] Song, B., Dong, S., Zhang, B., Liao, H., and Coddet, C., 2012, "Effects of processing parameters on microstructure and mechanical property of selective laser melted Ti6Al4V," *Materials and Design*, vol. 35, pp. 120-125.

[148] Cooke, M.N., Fisher, J.P., Dean, D., Rimnac, C., and Mikos, A.G., 2002, "Use of Stereolithography to Manufacture Critical-Sized 3D Biodegradable Scaffolds for Bone Ingrowth," *Journal of Biomedical Materials Research Part B: Applied Biomaterials*, vol. 64B, no. 2, pp. 65-69.

[149] Sachs, E., Cima, M., and Cornie, J., 1990, "Three-Dimensional Printing: Rapid Tooling and Prototypes Directly from a CAD Model," *CIRP Annals - Manufacturing Technology*, vol. 39, no. 1, pp. 201-204.

[150] Upcraft, S., and Fletcher, R., 2003, "The rapid prototyping technologies," *Assembly Automation*, vol. 23, no. 4, pp. 318-330.

[151] Dimitrov, D., Schreve, K., Taylor, A., and Vincent, B., 2007, "Rapid prototyping driven desigins and realisation of large components," *Rapid Prototyping Journal*, vol. 13, no. 2, pp. 85-91.

[152] Kruth, J-P., Mercelis, P., Van Vaerenberg, J., Froyen, L., and Rombouts, M., 2005, "Binding mechanisms in selective laser sintering and selective laser melting," *Rapid Prototyping Journal*, vol. 11, no. 1, pp. 26-36.

[153] Rännar, L-E., Glad, A., and Gustafson, C-G., 2007, "Efficient cooling with tool inserts manufactured by electron beam melting," *Rapid Prototyping Journal*, vol. 13, no. 3, pp. 128-135.

[154] Palmquist, A., Snis, A., Emanualsson, L., Browne, M., and Thomsen, P., 2013, "Long-term biocompatibility and osseointegration of electron beam melted, free-form-fabricated solid and porous titanium alloy: Experimental studies in sheep," *Journal of Biomaterials Applications*, vol. 27, no. 8, pp. 1003-1016.

[155] Cormier, D., Harryson, O., and West, H., 2004, "Characterization of H13 steel produced via electron beam melting," *Rapid Prototyping Journal*, vol. 10, no. 1, pp. 35-41.

[156] Arcam_AB, 2013, www.arcam.com. [Online]. http://www.arcam.com/wp-content/uploads/Arcam-Ti6Al4V-ELI-Titanium-Alloy.pdf

[157] Rombouts, M., Kruth, J.P., Froyen, L., and Mercelis, P., 2006, "Fundamentals of Selective Laser Melting of alloyed steel powders," *CIRP Annals - Manufacturing*, vol. 55, no. 1, pp. 187-192.

[158] Kruth, J-P., Vandenbroucke, B., Van Vaerenberg, J., and Mercelis, P., 2005, "Benchmarking of Different SLS/SLM Processes as Rapid Manufacturing Techniques," in *Int. Conf. Polymers & Moulds Innovations (PMI)*, Gent, [Online]. http://doc.utwente.nl/52902/1/Wa1021.pdf

[159] Spierings, A.B., Scheider, M., and Eggenberger, R., 2011, "Comparison of density measurement techniques for additive manufactured metallic parts," *Rapid Prototyping Journal*, vol. 17, no. 5, pp. 380-386.

[160] Van Rooyen, M., 2013, "Material Characterisation of LaserCusing Manufactured Ti-6Al-4V," Stellenbosch University, Stellenbosch, Bachelor Thesis.

[161] Yasa, E., and Kruth, J., 2011, "Application of Laser Re-Melting on Selective Laser Melting Parts," *Advances in Production Engineering and Management*, vol. 6, no. 4, pp. 259-270.

[162] Qiu, C., Adkins, N.J.E., and Attallah, M.M., 2013, "Microstructure and tensile properties of selective laser-melted and HIPed laser-melted Ti-6Al-4V," *Materials Science & Engineering A*, vol. 578, pp. 230-239.

[163] Leuders, S., Thöne, M., Riemer, A., Niendorf, T., Tröster, T., Richard, H.A., and Maier, H.J., 2013, "On the mechanical behaviour of titanium alloy TiAl6V4 manufactured by selective laser melting: Fatigue resistance and crack growth performance," *International Journal of Fatigue*, vol. 48, pp. 300-307.

[164] Concept_Laser, 2013, Concept-Laser. [Online]. http://www.concept-laser.de/en/technology/lasercusingr.html

[165] ASTM_International, 2013, F3001 - 13: Standard Specification for Additive Manufacturing of Titanium-6 Aluminium -4 Vanadium ELI (Extra Low Interstitial) with Powder Bed Fusion.

[166] Meyer, J., Piller, G., Spiegel, C.A., Hetzel, S., and Squire, M., 2011, "Vacuum-Mixing Significantly Changes Antibiotic Elution Characteristics of Commercially Available Antibiotic-Impregnated Bone Cements," *The Journal of Bone and Joint Surgery, Inc*, vol. 93, pp. 2049-2056.

[167] Miola, M., Bistolfi, A., Valsania, M.C., Bianco, C., Fucale, G., and Verné, E., 2013, "Antibiotic-loaded acrylic bone cements: An in vitro study on the release mechanism and its efficacy," *Materials Science and Engineering C*, vol. 33, pp. 3025-3032.

[168] Thompson, J.R., Ludwig, B.J., Jagodzinski, J.E., Andes, D.R., and Squire, M.W., 2007, "In Vitro Comparison of Comercially Available Antibiotic Impregnated Bone Cements," *53rd Annual Meeting of the Orthopaedic Research Society*, p. Poster No: 1866.

[169] Ferraris, S., Miola, M., Bistolfi, A., Fucale, G., Crova, M., Massé, A., and Verné, E., 2010, "In vitro comparison between commercially and manually mixed antibiotic-loaded cements," *Journal of Applied Biomaterials & Functional Materials*, vol. 8, no. 3, pp. 166-174.

[170] Heraeus_Medical_GmbH, 2014,. Palacos R+G High viscosity, radiopaque bone cement containing Gentamicin. [Online]. http://heraeus-medical.com/media/webmedia_local/dc/instructions/ifu_Palacos_RG_INT.pdf

[171] Jorgensen, J.H., and Ferraro, M.J., 2009, "Antimicrobial Susceptibility Testing: A Review of General Principles and Contemporary Practices," *Clinical Infectious Diseases*, vol. 49, no. 11, pp. 1749-1755.

[172] Squire, M.W., Ludwig, B.J., Thompson, J.R., Jagodzinski, J., Hall, D., and Andes, D., 2008, "Premixed Antibiotic Bone Cement - An In Vitro Comparison of Antimicrobial Efficacy," *The Journal of Arthroplasty*, vol. 23, no. 6 Suppl. 1, pp. 110-114.

[173] Boyle, V.J., Fancher, M.E., and Ross, R.W. Jr., 1973, "Rapid, Modified Kirby-Bauer Susceptitbility Test with Single, High-Concentration Antimicrobial Disks," *Antimicrobial Agents and Chemotherapy*, vol. 3, no. 3, pp. 417-424.

[174] Montgomery, D.C., and Runger, G.C., 2007, *Applied Statistics and Probability for Engineers*, 4th ed., N. Repasky, Ed. Hoboken, New Jersey, United States of America: John Wiley & Sons, Inc.

[175] Poelstra, K.A., Barekzi, N.A., Rediske, A.M., Felts, A.G., Lunt, J.B., and Grainger, D.W., 2002, "Prophylactic treatment of gram-positive and gram-negative abdominal implant infections using locally delivered polyclonal antibodies," *Journal of Biomedical Materials Research*, vol. 60, no. 1, pp. 206-215.

[176] Jiranek, W.A., Hanssen, A.D., and Greenwald, S., 2006, "Antibiotic-Loaded Bone Cement for Infection Prophylaxis in Total Joint Replacement ," *The Journal of Bone and Joint Surgery*, vol. 88-A, no. 11, pp. 2487-2500.

Appendix A: t-Test Statistics

Each random variable, $X_1, X_2, \ldots, X_n$ for a sample size of *n* has the arithmetic sample mean $\bar{x}$,

$$\bar{x} = \frac{1}{n}\sum_{i=1}^{n} x_i \tag{A.1}$$

and sample variance,

$$s^2 = \left(\sum_{i=1}^{n}(x_i - \bar{x})^2\right) \Big/ (n-1) \tag{A.2}$$

where the sample standard deviation is the square root of the sample variance.

The two sample variances S_1^2 and S_2^2 are combined to create an estimator of σ^2. This is called the pooled estimator, S_p^2.

$$S_p^2 = \frac{(n_1 - 1)S_1^2 + (n_2 - 1)S_2^2}{n_1 + n_2 - 2} \tag{A.3}$$

The Test *T-statistic* is then calculated by,

$$T = \frac{\bar{X}_1 - \bar{X}_2 - (\mu_1 - \mu_2)}{S_p\sqrt{\frac{1}{n_1} + \frac{1}{n_2}}} \tag{A.4}$$

which has a *t* distribution with $n_1 + n_2 - 2$ degrees of freedom.

Once the *T-statistic* has been calculated, the hypothesis test can proceed in two ways, since one implies the other. The calculated *T-statistic* can be compared to *Tcrit* where *Tcrit* is read from the standard *t-table*, or the P-values can be used. H_0 should be rejected if the calculated *T-statistic* is greater than *Tcrit* or if the P-value accompanying the calculated *T-statistic* is smaller than the level of significance α (0.05 in this study). The porosities from the CT-scans are presented below in Figure A.1

Porosities for bone cement samples			
	Ratio		
Sample	1 to 2	1 to 1.5	1 to 1
1	1.37	5.37	3.73
2	2.29	2.35	2.74
3	4.18	1.31	2
Mean	2.61	3.01	2.82
StdDev	1.43	2.11	0.87
Var	2.05	4.45	0.75

Figure A.1: Summary of porosities of bone cement samples

The following figures reveal both the t-test calculations for each of the three combinations, done both with the *MSExcel* built in function and by manually entering the formulas. The alternative hypothesis stated that the means are unequal. Therefore, the two-tailed P-values from the *MSExcel* function were used for comparison to the manual calculations.

t-TEST EXCEL BLACK BOX			t-TEST MANUAL CALCULATIONS		
1:2 and 1:1.5 (alpha 0.05)			**1:2 and 1:1.5 (alpha 0.05)**		
t-Test: Two-Sample Assuming Equal Variances			t-Test: Two-Sample Assuming Equal Variances		
	Variable 1	*Variable 2*		1 to 2	1 to 1.5
Mean	2.613333333	3.01	sample mean	2.613333333	3.01
Variance	2.052433333	4.4476	sample variance	2.052433333	4.4476
Observations	3	3	Estimator Sp^2	3.250016667	
Pooled Variance	3.250016667		Estimator Sp	1.80278026	
Hypothesized Mean Difference	0		t-statistic	-0.269481243	
df	4		T(α/2),n1+n2-2 (from t-table)	2.776	
t Stat	-0.269481243		(-)T(α/2),n1+n2-2	-2.776	
P(T<=t) one-tail	0.400444833		**P-Value (from t-table)**	**0.8**	
t Critical one-tail	2.131846782				
P(T<=t) two-tail	**0.800889666**				
t Critical two-tail	2.776445105				

Figure A.2: *MSExcel* and manually calculated t-Test results for ratios 1:2 and 1:1.5

t-TEST EXCEL BLACK BOX			t-TEST MANUAL CALCULATIONS		
1:2 and 1:1 (alpha 0.05)			**1:2 and 1:1 (alpha 0.05)**		
t-Test: Two-Sample Assuming Equal Variances			t-Test: Two-Sample Assuming Equal Variances		
	Variable 1	*Variable 2*		1 to 2	1 to 1
Mean	2.613333333	2.823333	sample mean	2.613333333	2.823333
Variance	2.052433333	0.753433	sample variance	2.052433333	0.753433
Observations	3	3	Estimator Sp^2	1.402933333	
Pooled Variance	1.402933333		Estimator Sp	1.184454868	
Hypothesized Mean Difference	0		t-statistic	-0.217143287	
df	4		T(α/2),n1+n2-2 (from t-table)	2.776	
t Stat	-0.217143287		(-)T(α/2),n1+n2-2	-2.776	
P(T<=t) one-tail	0.419361379		**P-Value (from t-table)**	**> 0.8**	
t Critical one-tail	2.131846782				
P(T<=t) two-tail	**0.838722757**				
t Critical two-tail	2.776445105				

Figure A.3: *MSExcel* and manually calculated t-Test results for ratios 1:2 and 1:1

t-TEST EXCEL BLACK BOX			t-TEST MANUAL CALCULATIONS		
1:1.5 and 1:1 (alpha 0.05)			**1:1.5 and 1:1 (alpha 0.05)**		
t-Test: Two-Sample Assuming Equal Variances			t-Test: Two-Sample Assuming Equal Variances		
	Variable 1	*Variable 2*		1 to 1.5	1 to 1
Mean	3.01	2.823333	sample mean	3.01	2.823333
Variance	4.4476	0.753433	sample variance	4.4476	0.753433
Observations	3	3	Estimator Sp^2	2.600516667	
Pooled Variance	2.600516667		Estimator Sp	1.612611753	
Hypothesized Mean Difference	0		t-statistic	0.141769426	
df	4		T(α/2),n1+n2-2 (from t-table)	2.776	
t Stat	0.141769426		(-)T(α/2),n1+n2-2	-2.776	
P(T<=t) one-tail	0.447057904		**P-Value (from t-table)**	**>> 0.8**	
t Critical one-tail	2.131846782				
P(T<=t) two-tail	**0.894115807**				
t Critical two-tail	2.776445105				

Figure A.4: *MSExcel* and manually calculated t-Test results for ratios 1:1.5 and 1:1

Based on the above comparisons, it was deemed valid to only utilise the *MSExcel* function for the remainder of the t-Tests carried out during the study. Screen shots of these are shown below.

Obs	Time Interval	Concentration [μg/ml] @ Wavelength [nm]	
		254	**280**
1	1	3.03	3.96
2	3	6.55	7.45
3	5	8.21	9.19
4	8	9.8	10.59
5	16	10.9	11.71
6	24	42.04	41.52
7	43	69.82	68.66

t-Test: Two-Sample Assuming Equal Variances		
	Variable 1	*Variable 2*
Mean	21.47857143	21.8685714
Variance	624.5380476	582.562914
Observations	7	7
Pooled Variance	603.550481	
Hypothesized Mean Difference	0	
df	12	
t Stat	-0.029699	
P(T<=t) one-tail	0.488397667	
t Critical one-tail	1.782287548	
P(T<=t) two-tail	0.976795334	
t Critical two-tail	2.178812827	

Figure A.5: *MSExcel* t-Test results comparing interval concentrations at different wavelengths

Obs	Time Cumul	Concentration [μg/ml] @ Wavelength [nm]	
		254	**280**
1	1	3.03	3.96
2	4	9.57	11.41
3	9	17.78	20.6
4	17	27.58	31.19
5	33	38.47	42.9
6	57	80.51	84.42
7	100	150.32	153.08

t-Test: Two-Sample Assuming Equal Variances		
	Variable 1	*Variable 2*
Mean	46.75142857	49.6514286
Variance	2739.263581	2781.13801
Observations	7	7
Pooled Variance	2760.200798	
Hypothesized Mean Difference	0	
df	12	
t Stat	-0.103267029	
P(T<=t) one-tail	0.459728391	
t Critical one-tail	1.782287548	
P(T<=t) two-tail	0.919456782	
t Critical two-tail	2.178812827	

Figure A.6: *MSExcel* t-Test for comparing cumulative concentrations at different wavelengths

Obs	Time Interval	Mass [μg] @ Wavelength [nm]	
		254	**280**
1	1	48.46	63.42
2	3	104.73	119.19
3	5	131.31	146.97
4	8	156.74	169.45
5	16	174.32	187.35
6	24	672.56	664.3
7	43	1117.07	1098.63

t-Test: Two-Sample Assuming Equal Variances		
	Variable 1	*Variable 2*
Mean	343.5985714	349.90143
Variance	159879.4068	149151.19
Observations	7	7
Pooled Variance	154515.2999	
Hypothesized Mean Difference	0	
df	12	
t Stat	-0.029997547	
P(T<=t) one-tail	0.488281073	
t Critical one-tail	1.782287548	
P(T<=t) two-tail	0.976562147	
t Critical two-tail	2.178812827	

Figure A.7: *MSExcel* t-Test results comparing interval mass release at different wavelengths

Obs	Time Cumul	Mass [μg] @ Wavelength [nm]	
		254	**280**
1	1	48.46	63.42
2	4	153.19	182.61
3	9	284.5	329.58
4	17	441.24	499.04
5	33	615.56	686.38
6	57	1288.13	1350.69
7	100	2405.19	2449.31

t-Test: Two-Sample Assuming Equal Variances		
	Variable 1	*Variable 2*
Mean	748.0385714	794.43286
Variance	701274.7586	711961.32
Observations	7	7
Pooled Variance	706618.0386	
Hypothesized Mean Difference	0	
df	12	
t Stat	-0.103253826	
P(T<=t) one-tail	0.45973352	
t Critical one-tail	1.782287548	
P(T<=t) two-tail	0.91946704	
t Critical two-tail	2.178812827	

Figure A.8: *MSExcel* t-Test results comparing cumulative mass release at different wavelengths

Time	Observed	K-P Estimate
1	6.342	6.455
4	18.261	17.67
9	32.958	31.847
17	49.904	50.548

t-Test: Two-Sample Assuming Equal Variances		
	Variable 1	*Variable 2*
Mean	26.62996752	26.86637832
Variance	362.1923069	354.368227
Observations	4	4
Pooled Variance	358.280267	
Hypothesized Mean Difference	0	
df	6	
t Stat	-0.01766326	
P(T<=t) one-tail	0.493240102	
t Critical one-tail	1.943180274	
P(T<=t) two-tail	0.986480203	
t Critical two-tail	2.446911846	

Figure A.9: *MSExcel* t-Test results for evaluating Korsmeyer-and-Peppas estimates to observed values

Appendix B: ZOI Measurement Data

ZOI data after 24 Hours for Sample 17

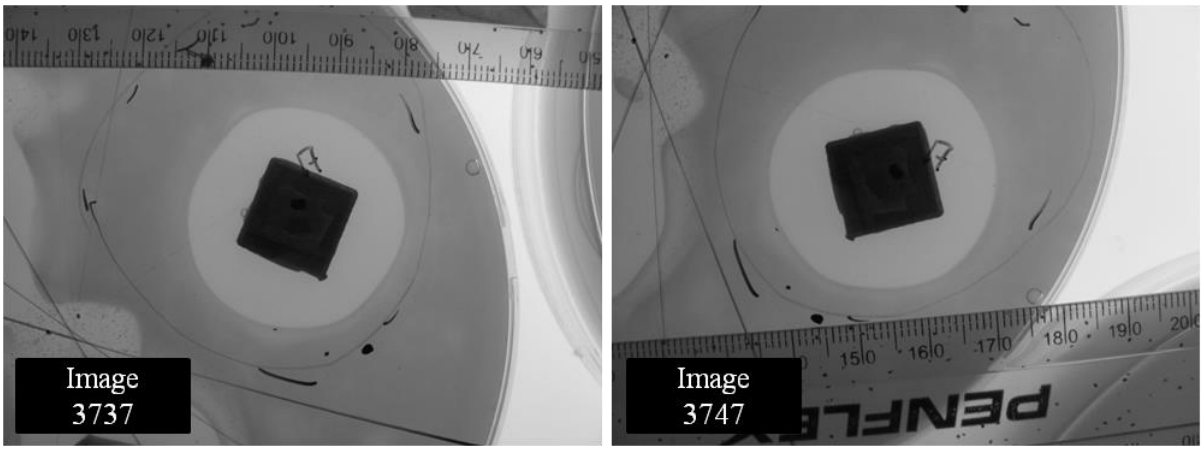

Figure B.1: 24 Hour photographs for Sample 17

Table B.1: 24 Hour ZOI measurements for Sample 17

	Image 3737	**Image 3747**
Measurement Number	**ZOI without Sample Surface [mm^2]**	**ZOI without Sample Surface [mm^2]**
1	701.60	683.29
2	700.90	686.03
3	704.84	685.14
4	699.40	686.40
5	699.85	682.99
6	701.08	685.73
7	697.14	689.36
8	701.15	686.17
9	700.03	689.10
10	701.88	680.95
Average	**700.79**	**685.517**
Sample Average ± Standard Deviation	**693.15 ± 8.15**	

ZOI data after 24 Hours for Sample 23

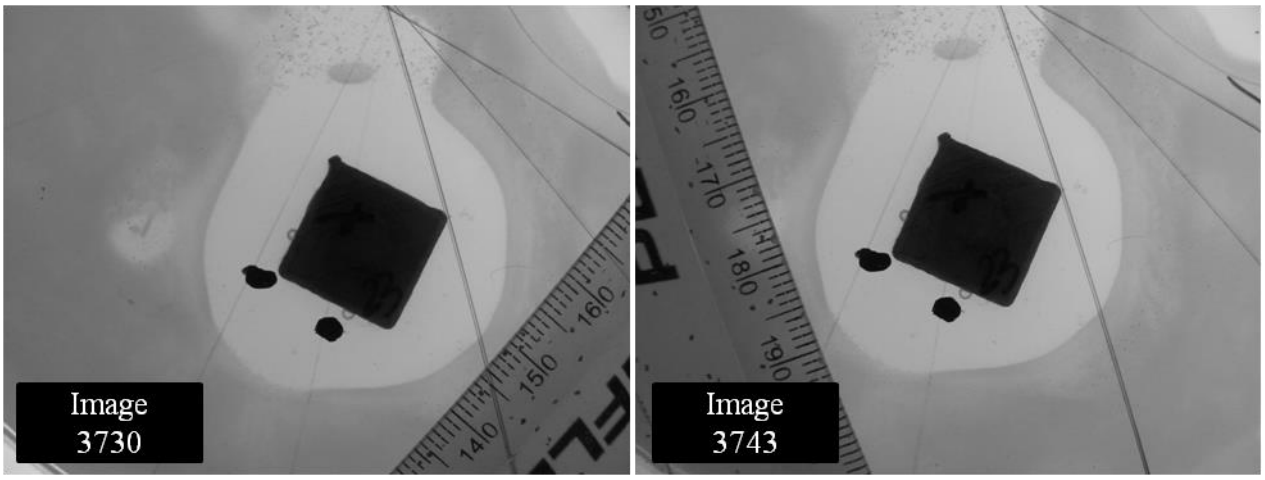

Figure B.2: 24 Hour photographs for Sample 23

Table B.2: 24 Hour ZOI measurements for Sample 23

	Image 3730	**Image 3743**
Measurement Number	**ZOI without Sample Surface [mm^2]**	**ZOI without Sample Surface [mm^2]**
1	789.73	782.48
2	783.58	787.60
3	791.17	786.14
4	775.72	787.62
5	782.61	784.30
6	786.58	778.59
7	782.42	780.03
8	784.07	781.66
9	783.10	785.82
10	783.77	783.73
Average	**784.27**	**783.80**
Sample Average ± Standard Deviation	**784.04 ± 3.64**	

ZOI data after 24 Hours for Sample 25

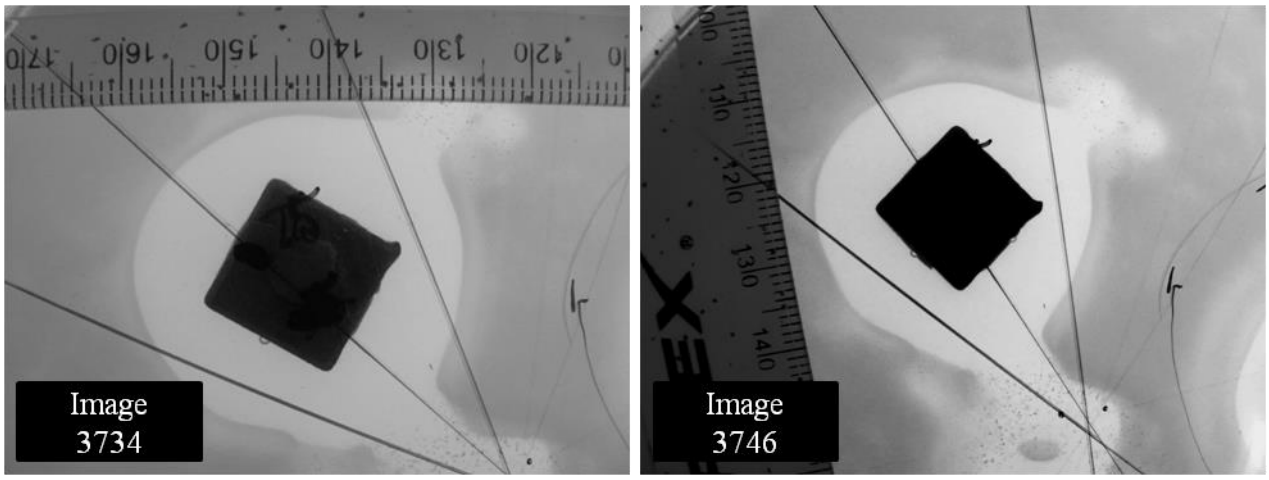

Figure B.3: 24 Hour photographs for Sample 25

Table B.3: 24 Hour ZOI measurements for Sample 23

	Image 3734	**Image 3746**
Measurement Number	**ZOI without Sample Surface [mm^2]**	**ZOI without Sample Surface [mm^2]**
1	694.57	699.75
2	692.68	697.81
3	696.65	696.03
4	699.36	698.01
5	698.81	697.31
6	694.94	694.67
7	691.75	694.82
8	687.60	699.59
9	691.65	697.50
10	690.38	695.75
Average	**693.84**	**697.12**
Sample Average ± Standard Deviation	**695.48 ± 3.32**	

ZOI data after 48 Hours for Sample 17

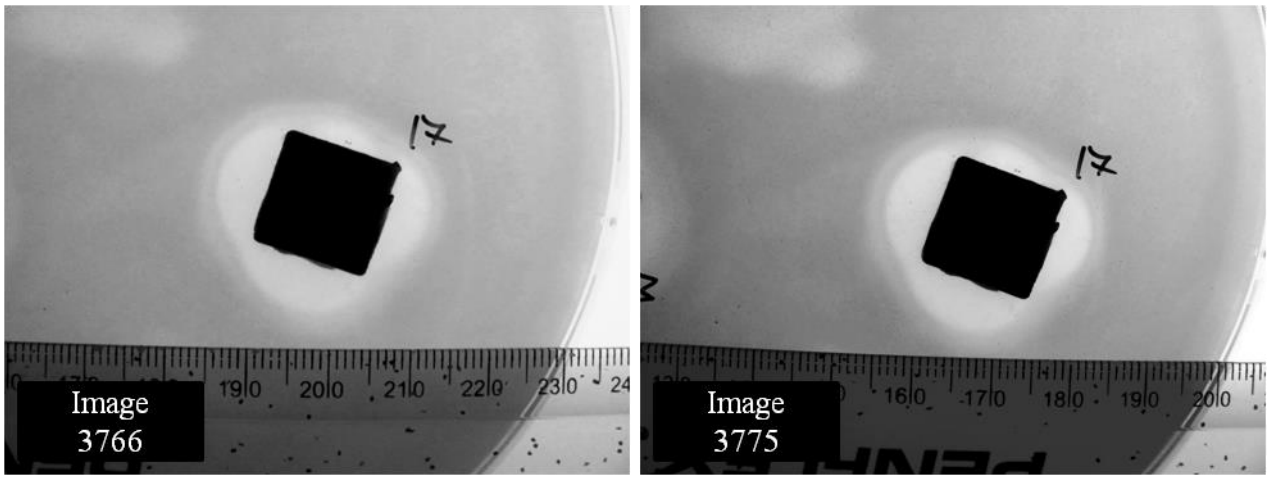

Figure B.4: 48 Hour photographs for Sample 17

Table B.4: 48 Hour ZOI measurements for Sample 17

	Image 3766	**Image 3775**
Measurement Number	**ZOI without Sample Surface [mm^2]**	**ZOI without Sample Surface [mm^2]**
1	271.36	266.29
2	269.54	263.84
3	253.69	259.57
4	256.41	254.52
5	265.94	258.07
6	258.84	256.16
7	256.68	254.65
8	253.61	254.01
9	255.33	253.38
10	256.61	255.42
Average	**259.80**	**257.59**
Sample Average ± Standard Deviation	**258.70 ± 5.59**	

ZOI data after 48 Hours for Sample 23

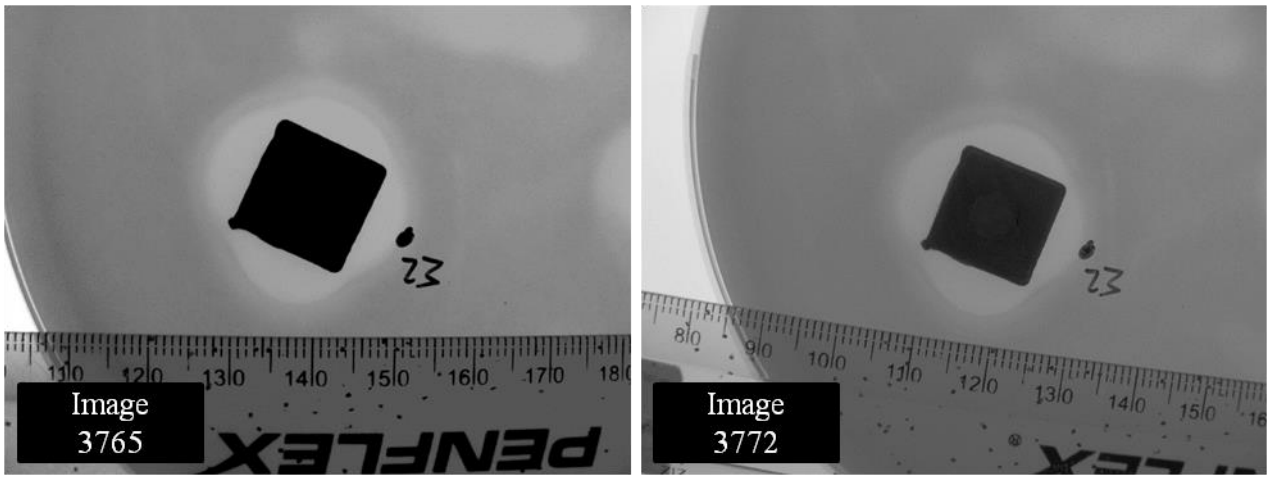

Figure B.5: 48 Hour photographs for Sample 23

Table B.5: 48 Hour ZOI measurements for Sample 23

	Image 3765	**Image 3772**
Measurement Number	**ZOI without Sample Surface [mm^2]**	**ZOI without Sample Surface [mm^2]**
1	250.94	254.84
2	252.90	253.62
3	252.70	255.78
4	254.28	256.64
5	256.31	254.64
6	254.78	255.54
7	252.18	253.51
8	252.42	252.53
9	254.32	255.64
10	253.25	254.65
Average	**253.41**	**254.75**
Sample Average ± Standard Deviation	**254.07 ± 1.52**	

ZOI data after 48 Hours for Sample 25

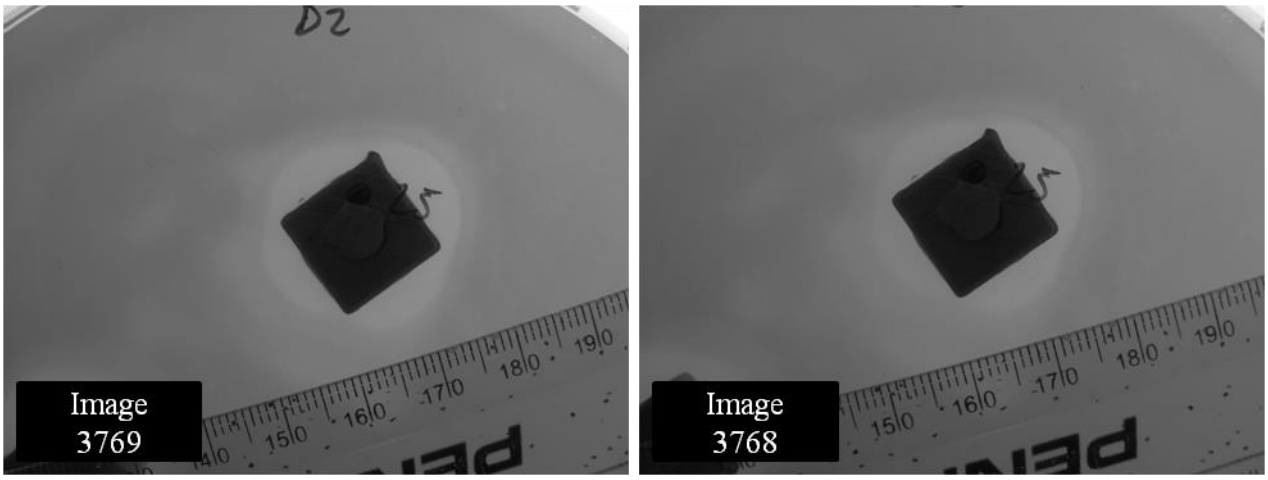

Figure B.6: 48 Hour photographs for Sample 25

Table B.6: 48 Hour ZOI measurements for Sample 25

	Image 3766	**Image 3775**
Measurement Number	**ZOI without Sample Surface [mm^2]**	**ZOI without Sample Surface [mm^2]**
1	245.41	235.38
2	246.15	238.34
3	243.48	237.14
4	246.05	238.62
5	238.04	235.01
6	239.51	237.11
7	241.65	240.11
8	242.27	238.39
9	243.26	237.40
10	240.95	235.82
Average	**242.68**	**237.33**
Sample Average ± Standard Deviation	**240.00 ± 3.51**	

ZOI data after 72 Hours for Sample 17

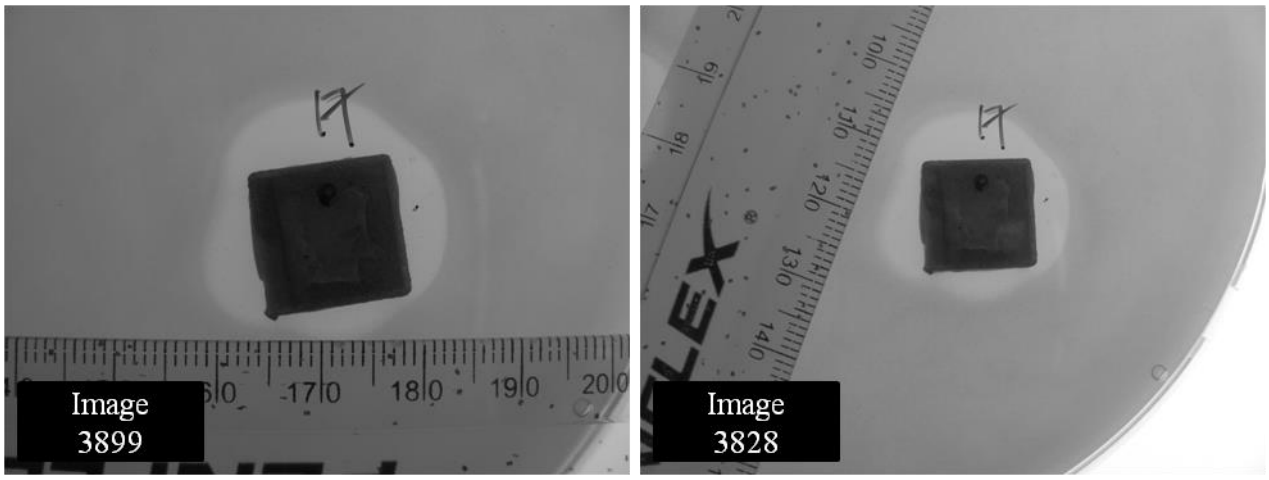

Figure B.7: 72 Hour photographs for Sample 17

Table B.7: 72 Hour ZOI measurements for Sample 17

	Image 3899	**Image 3828**
Measurement Number	**ZOI without Sample Surface [mm^2]**	**ZOI without Sample Surface [mm^2]**
1	243.87	243.16
2	241.57	239.47
3	237.96	238.05
4	247.61	238.55
5	241.84	239.74
6	242.59	239.88
7	240.32	237.84
8	239.69	235.84
9	234.36	238.02
10	238.94	237.36
Average	**240.88**	**238.79**
Sample Average ± Standard Deviation	**239.83 ± 3.00**	

ZOI data after 72 Hours for Sample 23

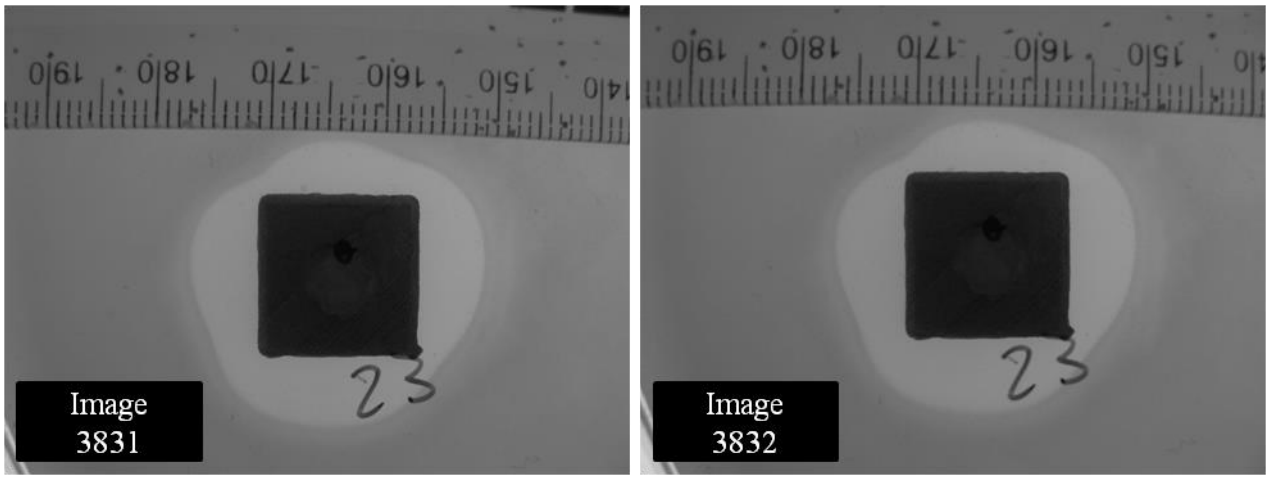

Figure B.8: 72 Hour photographs for Sample 23

Table B.8: 72 Hour ZOI measurements for Sample 23

	Image 3831	**Image 3832**
Measurement Number	**ZOI without Sample Surface [mm^2]**	**ZOI without Sample Surface [mm^2]**
1	330.52	329.31
2	329.26	327.97
3	330.69	331.78
4	332.28	330.52
5	331.81	329.36
6	331.32	331.12
7	330.38	330.41
8	329.89	331.34
9	330.53	331.01
10	330.13	330.03
Average	**330.68**	**330.28**
Sample Average ± Standard Deviation	**330.48 ± 1.03**	

ZOI data after 72 Hours for Sample 25

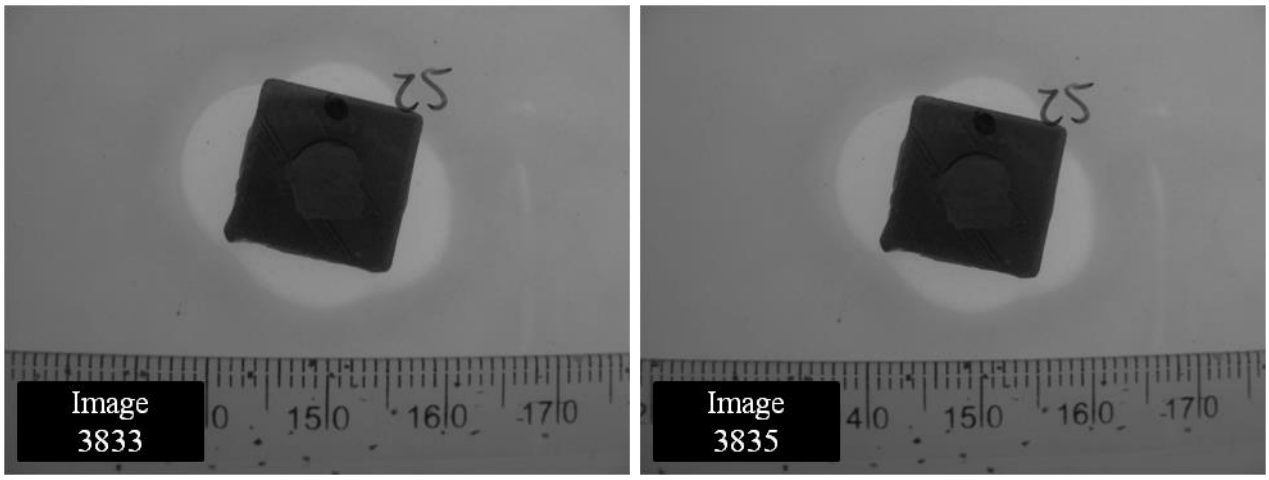

Figure B.9: 72 Hour photographs for Sample 25

Table B.9: 72 Hour ZOI measurements for Sample 25

	Image 3833	**Image 3835**
Measurement Number	**ZOI without Sample Surface [mm^2]**	**ZOI without Sample Surface [mm^2]**
1	169.88	169.58
2	172.07	170.13
3	174.53	169.02
4	172.61	170.78
5	172.14	171.40
6	167.48	170.02
7	165.48	167.79
8	167.37	168.09
9	167.92	167.83
10	166.97	168.99
Average	**169.65**	**169.36**
Sample Average ± Standard Deviation	**169.50 ± 2.25 *REACHED***	

ZOI data after 96 Hours for Sample 17

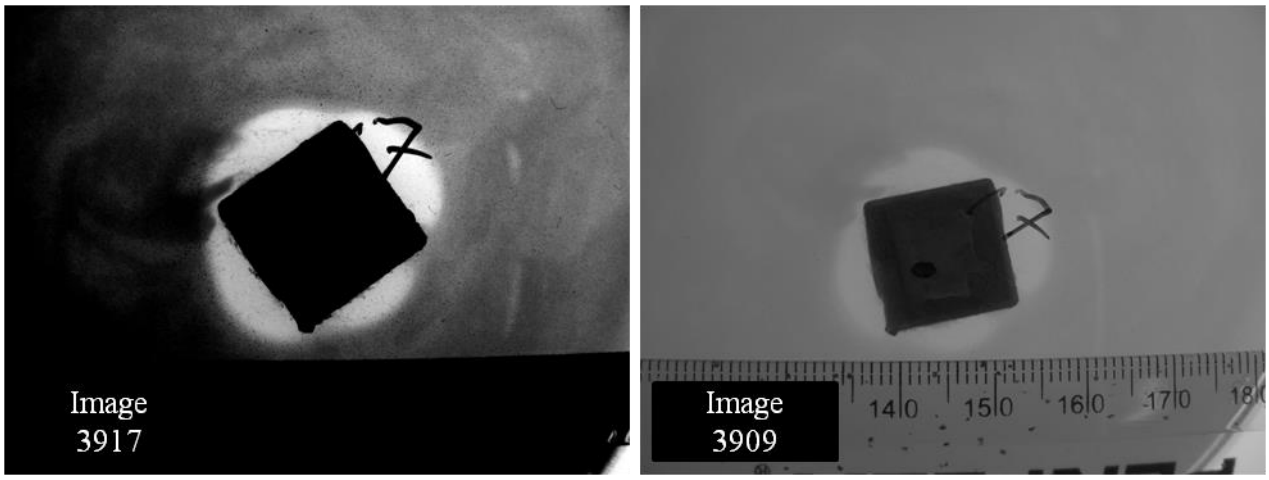

Figure B.10: 96 Hour photographs for Sample 17

Table B.10: 96 Hour ZOI measurements for Sample 17

	Image 3917	**Image 3909**
Measurement Number	**ZOI without Sample Surface [mm^2]**	**ZOI without Sample Surface [mm^2]**
1	164.12	165.85
2	162.99	165.21
3	162.27	164.25
4	162.94	156.56
5	163.28	157.91
6	162.78	158.27
7	162.22	158.20
8	162.80	159.01
9	160.73	158.73
10	159.32	158.46
Average	**162.34**	**160.24**
Sample Average ± Standard Deviation	**161.30 ± 2.76 *REACHED***	

ZOI data after 96 Hours for Sample 23

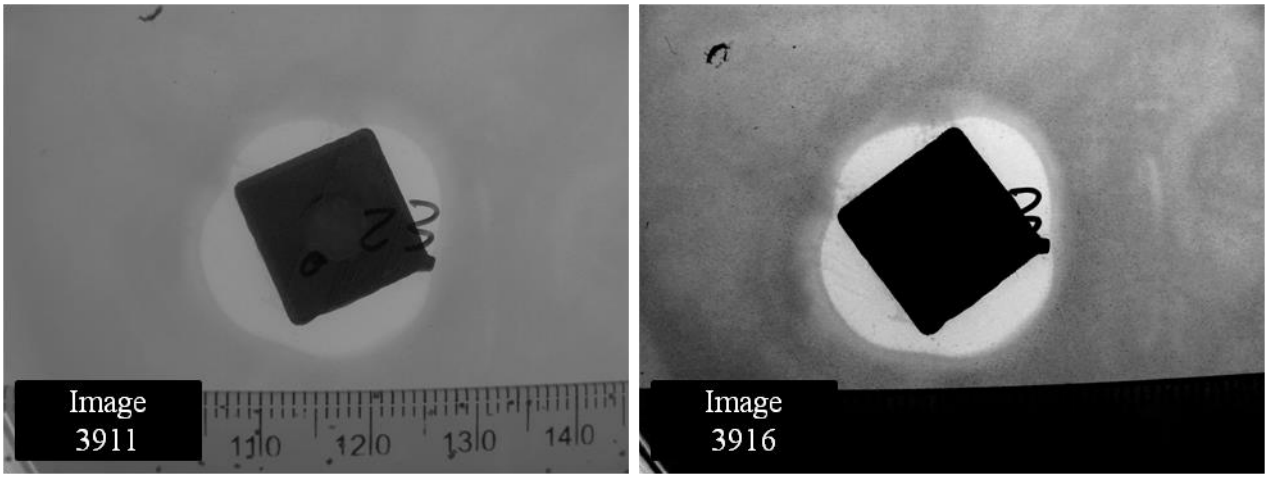

Figure B.10: 96 Hour photographs for Sample 17

Table B.10: 96 Hour ZOI measurements for Sample 17

	Image 3911	**Image 3916**
Measurement Number	**ZOI without Sample Surface [mm^2]**	**ZOI without Sample Surface [mm^2]**
1	202.27	200.68
2	200.88	201.62
3	200.78	202.19
4	202.82	201.82
5	202.46	201.45
6	202.82	200.84
7	201.42	200.35
8	200.56	201.30
9	201.25	200.52
10	200.68	201.56
Average	**201.59**	**201.23**
Sample Average ± Standard Deviation	**201.41 ± 0.77 *REACHED***	

Appendix C: Antibiotics in Clinical Use

Table C.1: Summary of antibiotic properties (from reference [85])

Class/Drug	***Molecular Weight [g/mol]***	***Water Solubility [mg/ml]***	***pH induced in Surrounding***	***Solubility in Organic Solvents***	***Melting Temperature [°C]***	***Antibacterial Spectrum***
Aminoglycosides						Broad spectrum, many Gram-positive and Gram-negative bacteria
Amikacin	585.6	185 (highly soluble)	Base	Insoluble	220-230 (decomposes)	
Gentamicin	477.6	100 (highly soluble)	Base	DMF, MeOH, Ether, $CHCl_3$, Acetone. Low solubility: DMSO	102-108 (Hydrochloride 194-209)	
Tobramycin	467.5	538 (highly soluble)	Base	Low: EtOH	168	
Cefalosporins						Gram-positive, with increased activity against Gram-negative bacteria
Cefazolin	454.5	0.487 (slightly soluble)	Weak acid	DMF, Pyridine, Acetone. Low: EtOH, MeOH	198-200 (decomposes)	
Cefoperazone	645.7	0.286 (slightly soluble)	Weak acid	MeOH	169-171	
Glycopeptides						Mainly Gram-positive bacteria. Mycobacteria
Vancomycin	1449.3	>100 (highly soluble)	Amphoteric	DMSO	185-188	
Macrolides						Gram-positive and fastidious Gram-negative bacteria
Erythromycin	733.9	1.44 (slightly soluble)	Weak base	High: MeOH, EtOH, Acetone, ACN, $CHCl_3$, EtOAc, Ether, DMF, DMSO. Low: hexane, toluene	191	
Nitromidazoles						Most anaerobes
Metronidazole	171.2	10 (soluble)	Lipophilic, low ionisation	High: EtOH. Low: Ether,	158-190	

				$CHCl_3$		
Penicillins						Gram-positive and
Ampicillin	349.4	10.1 (soluble)	Acid	High: MeOH, DMF. EtOH, Acetone, DMSO. Low: $CHCl_3$	199-202 (decomposes)	some Gram-negative bacteria. Broader spectrum than most penicillins.
Polypeptides						Mainly Gram-negative bacteria
Colistin (polymyxin E)	1155.4	564 (highly soluble)	Base	MeOH, DMF, DMSO. Low: Dioxane	200-220	
Quinolones						Broad spectrum.
Ciprofloxacin	331.4	0.001 (insoluble)	Amphoteric	High: MeOH, DMF, DMSO. Low: Dioxane	255-257 (decomposes)	More effective against Gram-negative than Gram-positive bacteria
Ofloxacin	361.4	28.3 (soluble)	Amphoteric	$CHCl_3$. Low: EtOH, MeOH	250-257 (decomposes)	
Rifamycins						Gram-positive and
Rifampin/ Rifampicin	823.0	1.4 (slightly soluble)	Lipophilic, low ionisation	DMSO, $CHCl_3$, EtOAc, MeOH, THF. Low: Acetone	183-188	fastidious Gram-negative bacteria. Mycobacteria
Tetracyclines						Broad spectrum,
Doxycycline	444.5	0.63 (slightly soluble)	Amphoteric	High: MeOH, Dioxane, DMF	201	many Gram-positive and Gram-negative bacteria,
Minocycline	457.5	52 (soluble)	Amphoteric	Low: EtOH	N.A.	mycoplasma.
Tetracycline	444.5	0.23 (slightly soluble)	Amphoteric	High: Toluene, Ether, EtOAc, Acetone. Low: MeOH, EtOH, $CHCl_3$, DMF, Dioxane	165	

Table C.2: Clarification of organic solvents listed in Table C.1

Abbreviation	***Name***	***Formula***
DMF	Dimethylformamide	C_3H_7NO
MeOH	Methanol	CH_3OH
EtOH	Ethanol	C_2H_5OH
Ether	Diethyl ether	$C_4H_{10}O$
	Chloroform	$CHCl_3$
	Acetone	C_3H_6O
DMSO	Dimethyl sulfoxide	C_2H_6OS
	Pyridine	C_5H_5
AcN	Acetonitrile	C_2H_3N
EtOAc	Ethyl Acetate	$C_4H_8O_2$
	Hexane	C_6H_{14}
	Toluene	C_7H_8
	Dioxane	$C_4H_8O_2$
THF	Tetrahydrofuran	C_4H_8O

Appendix D: Vancomycin Liquid Chromatography-Mass Spectrometry

The chromatographic method as applied at CAF is shown in the figure D.1 below.

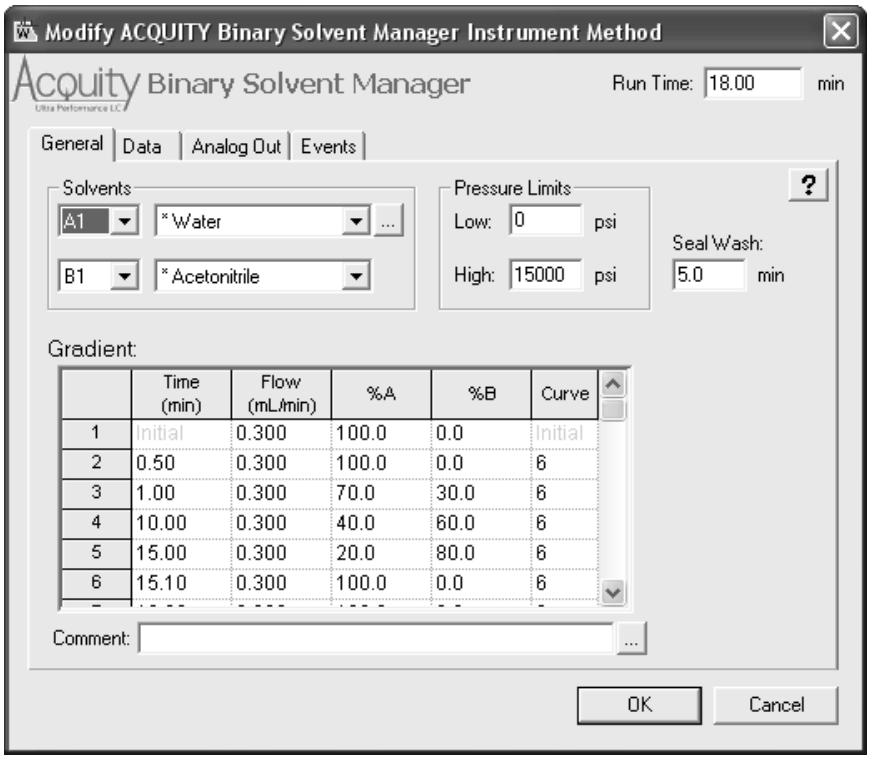

Figure D.1: Chromatographic gradient elution profile

The equipment and setup information is reproduced directly from their report and is as follows: "*Column: Waters UPLC HSS C18, 2.1x150mm, solvent A contained 1% formic acid and solvent B: acetonitrile. Source: Electrospray positive, Capillary voltage 3 kV, Cone Voltage 15V, mass spectra were obtained by scanning from m/z 200-2000*"

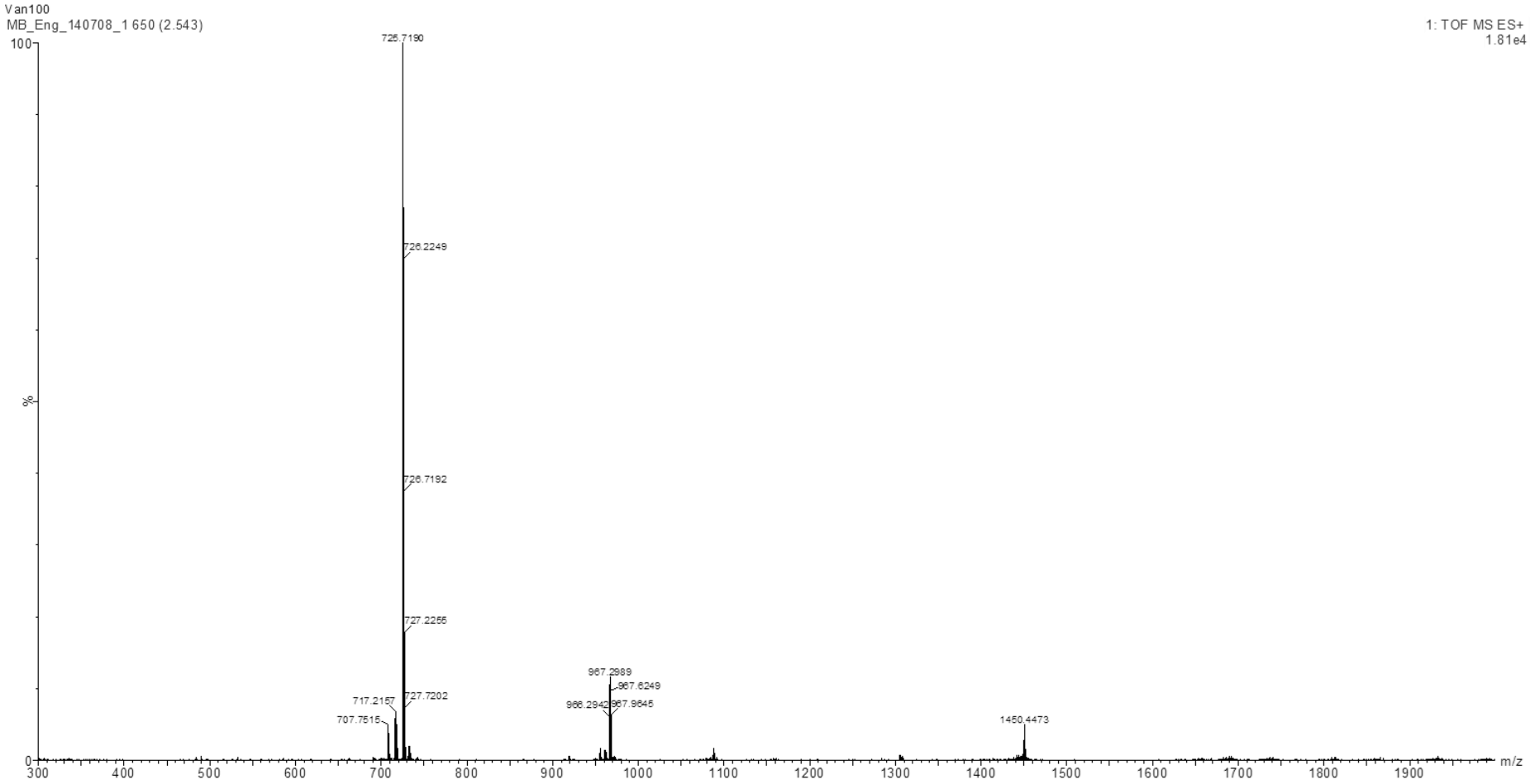

Figure D.2: Mass spectrum of vancomycin hydrochloride

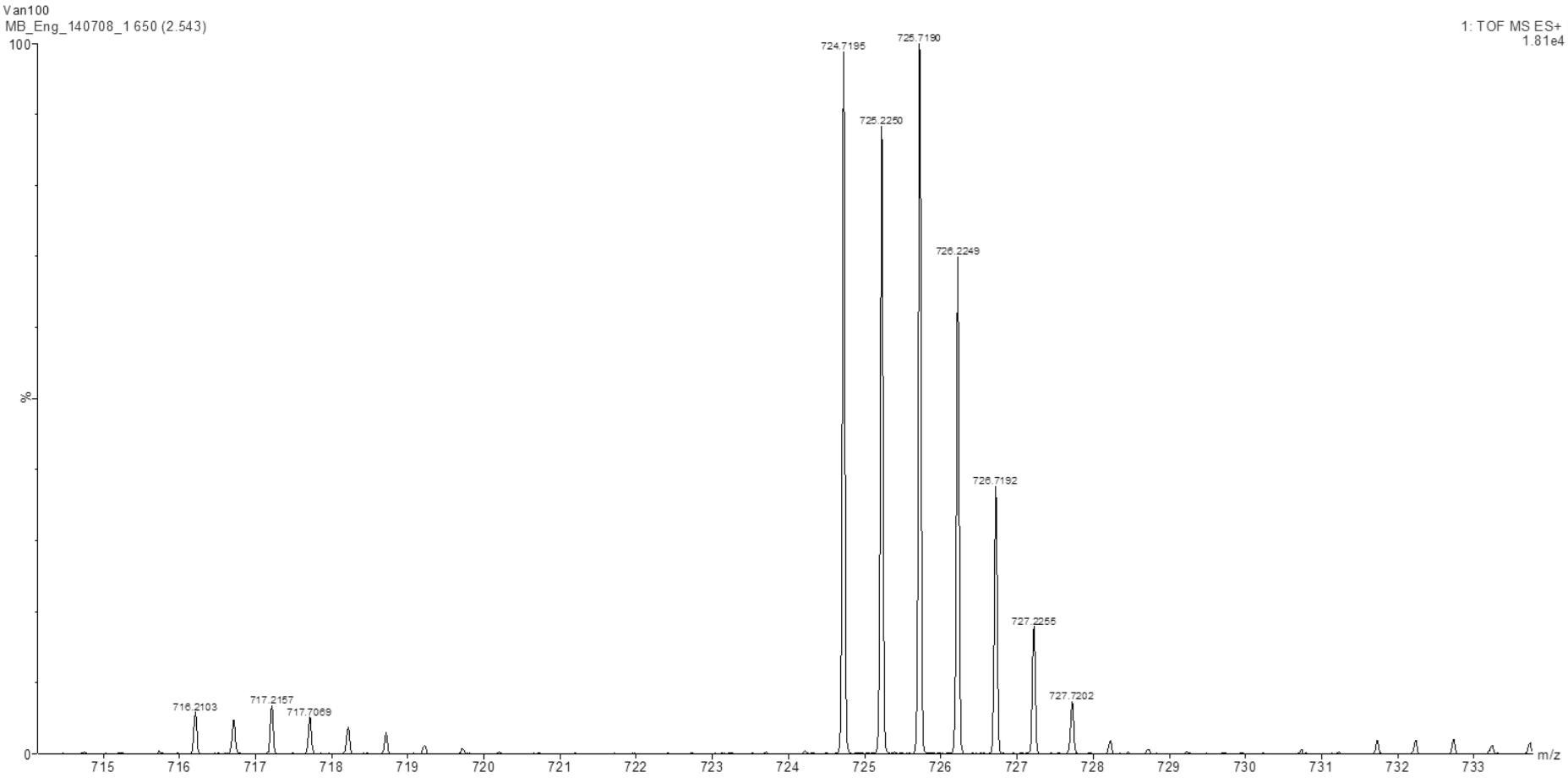

Figure D.3: Resolved isotope mass spectrum within isotopic cluster at 2 charges

Appendix E: Simple Linear Regression for RP-HPLC Calibration Curves

Consider the regressor and response variables *x* and *Y*, and let their relationship be linear with the response, *Y*, a random variable for each respective value of *x*. The assumption is that the response is described by the straight line model,

$$Y = \beta_0 + \beta_1 x + \epsilon \tag{E.1}$$

where β_0, the intercept, and β_1, the slope, are unknown regression coefficients. The random error, $\boldsymbol{\epsilon}$, has a mean of zero and an unknown variance, σ^2.

The method of least squares is used for estimation of the regression coefficients.

If there are *n* observations within the sample, it can be written as,

$$y_i = \beta_0 + \beta_1 x_i + \epsilon_i, \qquad i = 1, 2, \ldots, n \tag{E.2}$$

with sum of the squares of any errors from the true linear relationship expressed as,

$$L = \sum_{i=1}^{n} \epsilon_i^2 = \sum_{i=1}^{n} (y_i - \beta_0 - \beta_1 x_i)^2 \tag{E.3}$$

The intercept, β_0, and the slope, β_1, are estimated each with their respective least squares estimator, $\hat{\beta}_0$ and $\hat{\beta}_1$, which have to meet the criteria,

$$\begin{aligned} \frac{\partial L}{\partial \beta_0}\Big| \hat{\beta}_0, \hat{\beta}_1 &= -2 \sum_{i=1}^{n} \left(y_i - \hat{\beta}_0 - \hat{\beta}_1 x_i\right) = 0 \\ \frac{\partial L}{\partial \beta_1}\Big| \hat{\beta}_0, \hat{\beta}_1 &= -2 \sum_{i=1}^{n} \left(y_i - \hat{\beta}_0 - \hat{\beta}_1 x_i\right) x_i = 0 \end{aligned} \tag{E.4}$$

when simplified leads to,

$$\begin{aligned} n\hat{\beta}_0 + \hat{\beta}_1 \sum_{i=1}^{n} x_i &= \sum_{i=1}^{n} y_i \\ \hat{\beta}_0 \sum_{i=1}^{n} x_i + \hat{\beta}_1 \sum_{i=1}^{n} x_i^2 &= \sum_{i=1}^{n} y_i x_i \end{aligned} \tag{E.5}$$

which are also referred to as the least squares normal equations. The least squares estimators $\hat{\beta}_0$ and $\hat{\beta}_1$ are obtained by solving the least squares normal equations.

$$\hat{\beta}_0 = \bar{y} - \hat{\beta}_1 \bar{x} \tag{E.6}$$

$$\hat{\beta}_1 = \frac{\sum_{i=1}^{n} y_i x_i - \frac{(\sum_{i=1}^{n} y_i)(\sum_{i=1}^{n} x_i)}{n}}{\sum_{i=1}^{n} x_i^2 - \frac{\left(\sum_{i=1}^{n} x_i\right)^2}{n}} = \frac{SS_{xy}}{SS_{xx}} = \frac{\sum_{i=1}^{n}(y_i - \bar{y})(x_i - \bar{x})}{\sum_{i=1}^{n}(x_i - \bar{x})^2} \tag{E.7}$$

where $\bar{y} = \frac{1}{n}\sum_{i=1}^{n} y_i$ and $\bar{x} = \frac{1}{n}\sum_{i=1}^{n} x_i$

SS_{xy} and SS_{xx} are the respective sums of squares as denoted in the subscript of the notation.

The regression line then becomes,

$$\hat{y} = \hat{\beta}_0 + \hat{\beta}_1 x \tag{E.8}$$

Each pair of observations satisfies,

$$y_i = \hat{\beta}_0 + \hat{\beta}_1 x_i + e_i \qquad i = 1,2, \ldots, n$$

where $e_i = y_i - \hat{y}_i$ is known as the residual.

The sum of squares of the residuals, also known as the error sum of squares, is

$$SS_E = \sum_{i=1}^{n} e_i^2 = \sum_{i=1}^{n} (y_i - \hat{y}_i)^2 \tag{E.9}$$

The regression sum of squares for *Y* is,

$$SS_R = \sum_{i=1}^{n} (\hat{y}_i - \bar{y})^2 \tag{E.10}$$

The total sum of squares with regard to the response variably *Y* is,

$$SS_T = \sum_{i=1}^{n} (y_i - \bar{y})^2 \tag{E.11}$$

which is also the sum of the regression and error sums of squares,

$$SS_T = SS_E + SS_R \tag{E.12}$$

The sums of squares are used in determining the ratio R^2, the coefficient of determination,

$$R^2 = \frac{SS_R}{SS_T} = 1 - \frac{SS_E}{SS_T} \tag{E.13}$$

It is typically utilised as a measure of adequacy of a regression model. It is an indication of the regression model's ability to account for variability in the observations, where 1 represents a 100% fit. Therefore, the closer the coefficient of determination is to one, the better the fit of the regression model.

A series of screen shots from *MSExcel* follows which represents the application of the above process to determine the calibration curves for the RP-HPLC procedure.

- **First standard series injection with 254 nm detection:**

n = 7							
Obs# oi	**x**	**y**	**xy**	**y^2**	**x^2**	**xbar**	**ybar**
1	0	178681	0	31926899761.0000	0.00	66.7857	1385662.4286
2	5	244618	1223090	59837965924.0000	25.00		
3	12.5	395502	4943775	156421832004.0000	156.25		
4	25	652763	16319075	426099534169.0000	625.00		
5	50	1119492	55974600	1253262338064.0000	2500.00		
6	125	2497347	3.12E+08	6236742038409.0000	15625.00		
7	250	4611234	1.15E+09	21263479002756.0000	62500.00		

Figure E.1: Response data for first standard series injection with 254 nm detection

SUMMARY OUTPUT								
Regression Statistics								
Multiple R	0.999665984							
R Square	0.999332079							
Adjusted R Square	0.999198495							
Standard Error	46213.16251							
Observations	7							
ANOVA								
	df	*SS*	*MS*	*F*	*Significance F*			
Regression	1	1.59767E+13	1.59767E+13	7480.917271	3.91557E-09			
Residual	5	10678281947	2135656389					
Total	6	1.59873E+13						
	Coefficients	*Standard Error*	*t Stat*	*P-value*	*Lower 95%*	*Upper 95%*	*Lower 95.0%*	*Upper 95.0%*
Intercept	194321.0839	22244.45365	8.735709446	0.000325606	137139.8954	251502.2724	137139.8954	251502.2724
X Variable 1	17838.26612	206.2410983	86.49229602	3.91557E-09	17308.1065	18368.42574	17308.1065	18368.42574

Figure E.2: *MSExcel* regression function output for linear estimation of calibration curve

Sum x	467.5000
Sum y	9699637.0000
Sum x^2	81431.2500
Sum y^2	29427769611087.0000
Sum xy	1543437415
ß_hat_1	17838.2661236974
ß_hat_0	194321.08388
SSR	1.59767E+13
SSE	10678281947
SSR	1.59873E+13
R^2	0.999332079

Figure E.3: Manual calculation results for regression parameters

- **First standard series injection with 280 nm detection:**

n = 7							
Obs# oi	**x**	**y**	**xy**	**y^2**	**x^2**	**xbar**	**ybar**
1	0	36356	0	1321758736.0000	0.00	66.786	1264450.286
2	5	93726	468630	8784563076.0000	25.00		
3	12.5	235294	2941175	55363266436.0000	156.25		
4	25	484550	12113750	234788702500.0000	625.00		
5	50	948790	47439500	900202464100.0000	2500.00		
6	125	2360237	2.95E+08	5570718696169.0000	15625.00		
7	250	4692199	1.17E+09	22016731455601.0000	62500.00		

Figure E.4: Response data for first standard series injection with 280 nm detection

SUMMARY OUTPUT								
Regression Statistics								
Multiple R	0.999974327							
R Square	0.999948654							
Adjusted R Square	0.999938385							
Standard Error	13442.37557							
Observations	7							
ANOVA								
	df	*SS*	*MS*	*F*	*Significance F*			
Regression	1	1.75952E+13	1.76E+13	97373.61909	6.41435E-12			
Residual	5	903487305.4	1.81E+08					
Total	6	1.75961E+13						
	Coefficients	*Standard Error*	*t Stat*	*P-value*	*Lower 95%*	*Upper 95%*	*Lower 95.0%*	*Upper 95.0%*
Intercept	14220.67866	6470.414145	2.1978	0.079313318	-2412.0504	30853.40773	-2412.0504	30853.40773
X Variable 1	18720.01551	59.99092361	312.0475	6.41435E-12	18565.80393	18874.22709	18565.80393	18874.22709

Figure E.5: *MSExcel* regression function output for linear estimation of calibration curve

Sum x	467.50
Sum y	8851152.00
Sum x^2	81431.25
Sum y^2	2.8788E+13
Sum xy	1531042430.00
ß_hat_1	18720.02
ß_hat_0	14220.68
SSR	1.76E+13
SSE	9.0349E+08
SST	1.75961E+13
R^2	0.999949

Figure E.6: Manual calculation results for regression parameters

- **Second standard series injection with 254 nm detection**

n = 7							
Obs# oi	**x**	**y**	**xy**	**y^2**	**x^2**	**xbar**	**ybar**
1	0	178681	0	31926899761.0000	0.00	66.7857	1383306.4286
2	5	243882	1219410	59478429924.0000	25.00		
3	12.5	391505	4893813	153276165025.0000	156.25		
4	25	652588	16314700	425871097744.0000	625.00		
5	50	1120264	56013200	1254991429696.0000	2500.00		
6	125	2509887	3.14E+08	6299532752769.0000	15625.00		
7	250	4586338	1.15E+09	21034496250244.0000	62500.00		

Figure E.7: Response data for second standard series injection with 254 nm detection

SUMMARY OUTPUT								
Regression Statistics								
Multiple R	0.999513952							
R Square	0.99902814							
Adjusted R Square	0.998833769							
Standard Error	55530.84387							
Observations	7							
ANOVA								
	df	*SS*	*MS*	*F*	*Significance F*			
Regression	1	1.58494E+13	1.58494E+13	5139.776362	1.00009E-08			
Residual	5	15418373104	3083674621					
Total	6	1.58648E+13						
	Coefficients	*Standard Error*	*t Stat*	*P-value*	*Lower 95%*	*Upper 95%*	*Lower 95.0%*	*Upper 95.0%*
Intercept	196719.7104	26729.46874	7.359656576	0.000727326	128009.4236	265429.9971	128009.4236	265429.9971
X Variable 1	17767.07386	247.8242476	71.69223362	1.00009E-08	17130.02135	18404.12636	17130.02135	18404.12636

Figure E.8: *MSExcel* regression function output for linear estimation of calibration curve

Sum x	467.5000
Sum y	9683145.0000
Sum x^2	81431.2500
Sum y^2	29259573025163.0000
Sum xy	1538761498
ß_hat_1	17767.0738556745
ß_hat_0	196719.71035
SSR	1.58494E+13
SSE	15418373104
SST	1.58648E+13
R^2	0.99902814

Figure E.9: Manual calculation results for regression parameters

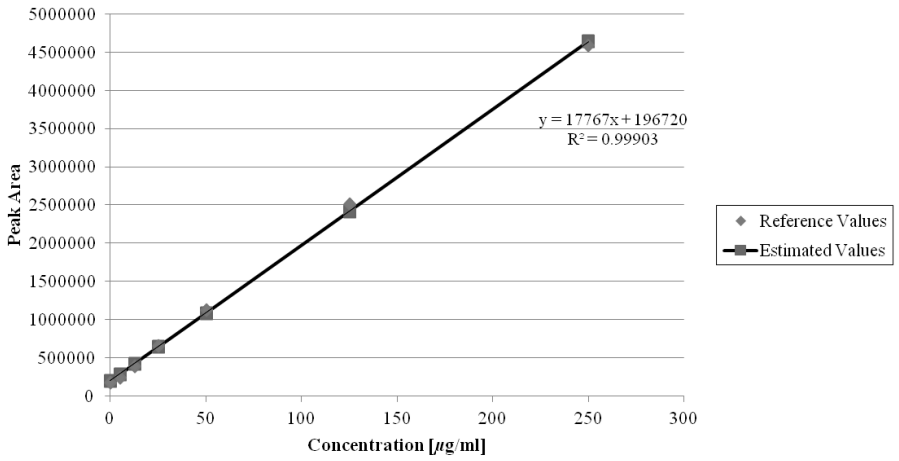

Figure E.10: Calibration curve for second standard series injection at 254 nm detection

- **Second standard series injection with 280 nm detection**

n = 7							
Obs# oi	**x**	**y**	**xy**	**y^2**	**x^2**	**xbar**	**ybar**
1	0	36356	0	1321758736.0000	0.00	66.7857	1267355.1429
2	5	89054	445270	7930614916.0000	25.00		
3	12.5	259945	3249313	67571403025.0000	156.25		
4	25	487392	12184800	237550961664.0000	625.00		
5	50	958742	47937100	919186222564.0000	2500.00		
6	125	2379099	2.97E+08	5660112051801.0000	15625.00		
7	250	4660898	1.17E+09	21723970166404.0000	62500.00		

Figure E.11: Response data for second standard series injection with 280 nm detection

SUMMARY OUTPUT								
Regression Statistics								
Multiple R	0.999941319							
R Square	0.999882641							
Adjusted R Square	0.999859169							
Standard Error	20194.22526							
Observations	7							
ANOVA								
	df	*SS*	*MS*	*F*	*Significance F*			
Regression	1	1.73723E+13	1.73723E+13	42599.3	5.06627E-11			
Residual	5	2039033670	407806733.9					
Total	6	1.73743E+13						
	Coefficients	*Standard Error*	*t Stat*	*P-value*	*Lower 95%*	*Upper 95%*	*Lower 95.0%*	*Upper 95.0%*
Intercept	25069.35222	9720.380156	2.579050595	0.049489	82.31956937	50056.38488	82.31956937	50056.38488
X Variable 1	18601.07066	90.123224	206.3959747	5.07E-11	18369.40154	18832.73978	18369.40154	18832.73978

Figure E.12: *MSExcel* regression function output for linear estimation of calibration curve

Sum x	467.5000
Sum y	8871486.0000
Sum x^2	81431.2500
Sum y^2	28617643179110.0000
Sum xy	1526428358
ß_hat_1	18601.0706618772
ß_hat_0	25069.35222
SSR	1.73723E+13
SSE	2039033670
SST	1.73743E+13
R^2	0.999882641

Figure E.13: Manual calculation results for regression parameters

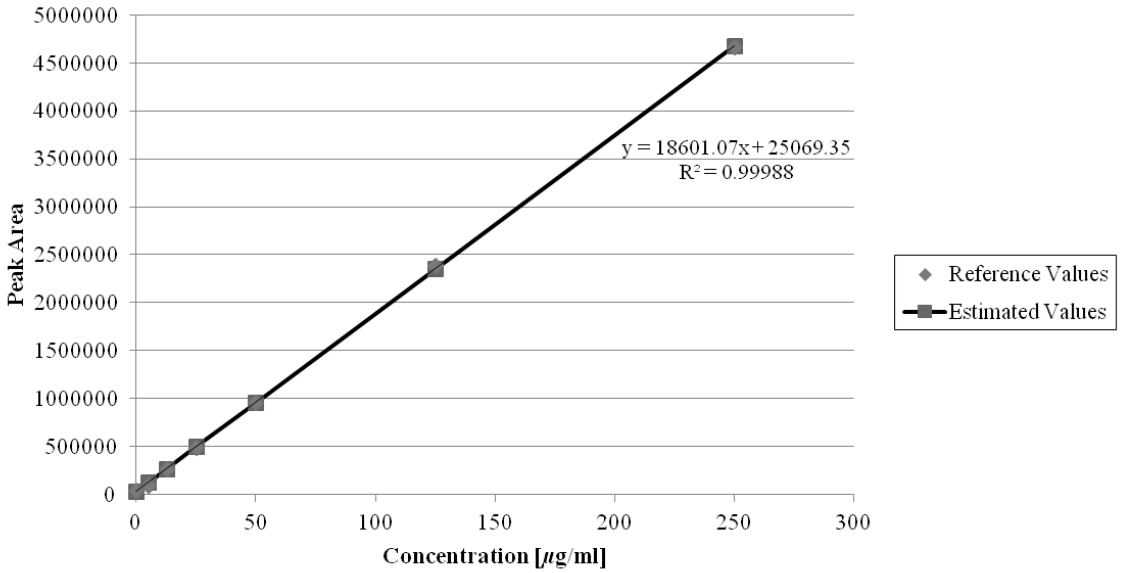

Figure E.14: Calibration curve for second standard series injection at 280 nm detection